# *IN SILICO* IDENTIFICATION OF NATURAL ANTICANCER PRODUCT AND THEIR EFFICACY IN BREAST CANCER CELLS AND CANCER STEM LIKE CELLS

Thesis submitted to the Central University of Punjab

For the award of

Doctor of Philosophy

In

Biochemistry and Microbial Sciences

BY

PREM PRAKASH KUSHWAHA

Supervisor
Dr. Shashank Kumar


Department of Biochemistry and Microbial Sciences
School of Basic and Applied Sciences
Central University of Punjab, Bathinda

July 2020

# DECLARATION

I declare that the thesis entitled **"*In silico* Identification of natural anticancer product and their efficacy in breast cancer cells and cancer stem like cells"** has been prepared by me under the guidance of Dr. Shashank Kumar, Assistant Professor, Department of Biochemistry, School of Basic and Applied Sciences, Central University of Punjab. No part of this thesis has formed the basis for the award of any degree or fellowship previously.

Prem Prakash Kushwaha
Department of Biochemistry and Microbial Sciences
School of Basic and Applied Sciences
Central University of Punjab, Bathinda - 151001
Date:

# CERTIFICATE

I certify that **Prem Prakash Kushwaha** has prepared his thesis entitled **"*In silico* Identification of natural anticancer product and their efficacy in breast cancer cells and cancer stem like cells"** for the award of PhD degree of the Central University of Punjab, under my guidance. He has carried out this work at Department of Biochemistry and Microbial Sciences, School of Basic and Applied Sciences, Central University of Punjab, Bathinda.

Dr. Shashank Kumar
Assistant Professor
Department of Biochemistry
School of Basic and Applied Sciences
Central University of Punjab, Bathinda - 151001
Date:

## ABSTRACT

### *In silico* Identification of natural anticancer product and their efficacy in breast cancer cells and cancer stem like cells

Name of student : Prem Prakash Kushwaha

Registration Number : 15phdbms03

Degree for which submitted : Doctor of Philosophy (Biochemistry and Microbial Sciences)

Name of supervisor : Dr. Shashank Kumar

Department : Biochemistry and Microbial Sciences

School of Studies : Basic and Applied Sciences

**Key words**

Breast cancer, Notch signaling, *Bulbine frutescens,* Kurarinone, 3-O-(E)-p-Coumaroylbetulinic acid, Phytochemicals, Breast cancer stem cells

Breast cancer is the most commonly diagnosed lethal cancer in women worldwide. Notch signaling pathway is directly linked to breast cancer recurrence and aggressiveness. Natural remedies are becoming a prime choice to overcome against cancer due to lesser side effect and cost-effectiveness. Literature survey and *in silico* study identified *Bulbine frutescens* (Asphodelaceae), Kurarinone (KU) and 3-O-(E)-p-coumaroylbetulinic acid (CB) as lead plant product/phytochemicals. Methanolic and hexane extract of *B. frutescens* (BME and BHE respectively), KU and CB were studied for their anticancer activity and notch signaling pathway inhibitory potential in breast cancer cells. Moreover, KU and CB were also studied for their effect in mammosphere. Literature-based identification of methanol soluble phytochemicals of *B. frutescens* and *in silico* docking study revealed Bulbineloneside D as a potent notch signaling inhibitor (ϒ-secretase). *In silico* docking potential of KU and CB were equal to standard gamma secretase inhibitor DAPT (-8.74 kcal/mol). KU-gamma secretase complex showed lower RMSD value, marginal fluctuation in Radius of gyration (Rg), more number of inter hydrogen bonding, and stable secondary structure of the protein which indicates KU as candidate gamma secretase inhibitor (GSI). *B. frutescens* extracts ($IC_{50}$ 4.8–28.4 µg/ml), Kurarinone ($IC_{50}$ 0.43-3.42 µM) and CB ($IC_{50}$ 0.99-5.88 µM) significantly decreased cell viability in MDA-MB-231 and T47D cells in time dependent manner. *B. frutescens*, KU and CB induced cell cycle arrest at G1 phase in MDA-MB-231 and T47D cells. RT-PCR analysis of cell cycle (cyclin D1, CDK4, and p21) and apoptosis modulating genes (caspase 3, Bcl2 and survivin) revealed upexpression of p21, and

caspase 3, and down expression of cyclin D1, CDK4, Bcl2 and survivin genes in test extract/phytochemicals treated breast cancer cells. Western Blot analysis showed reduced expression of cyclin D1 and increased procaspase 3 protein expression in extract/phytochemicals treated breast cancer cells in time dependent manner. Fluorescence spectrophotometry and confocal microscopy showed extract/phytochemicals induced nuclear morphology and mitochondrial integrity disruption, and increased reactive oxygen species production in MDA-MB-231 and T47D cells at $IC_{50}$ and sub $IC_{50}$ concentration. Flow cytometric apoptosis analysis of extract/phytochemicals treated MDA-MB-231 cells showed significant increase in early apoptotic population in comparison to non-treated cells at $IC_{50}$ and sub $IC_{50}$ (half of the $IC_{50}$) concentration. Dual-Luciferase Reporter assay confirmed notch promoter inhibitory activity of *B. frutescens,* Kurarinone and CB in HEK293 transfected cells at $IC_{50}$ concentration. Moreover, RT-PCR analysis showed down regulation of notch responsive genes (Hes1 and Hey1) at transcription levels in extract/phytochemical treated breast cancer cells in time dependent manner. Western Blot analysis showed reduced notch responsive protein (Hes1, Hey1 and E-cadherin) expression in extract/phytochemical treated breast cancer cells. KU and CB treatment decreased the mammosphere formation ability in MCF-7 cells at $IC_{50}$ concentration by lowering the notch signaling target proteins (Hes1, Hey1, and E-cadherin) and proteins involved in cancer cell self-renewal (c-Myc, SOX-2, CD44). In conclusion, extract/phytochemicals have cell cycle arrest, ROS production, apoptosis induction, and mitochondria membrane potential disruption efficacy in breast cancer cells. KU and CB have the ability to downregulate the notch signaling pathway in breast cancer and cancer stem like cells.

Prem Prakash Kushwaha
(Student)

Dr. Shashank Kumar
(Supervisor)

# *Acknowledgment*

*First and foremost, I am thankful to the almighty who has instilled in me the courage and determination. Unguided efforts unguided energies are all waste. No human efforts could climb the ladder of success without being given the right direction. It is my proud privilege to completed this thesis under the valuable guidance of* ***Dr. Shashank Kumar*** *without whose encouragement and help it would not have been possible for me to carry out this research. His vast knowledge, experience and undisputed expertise of the subject have been a constant source of inspiration for me.*

*I pay my sincere thanks to honorable* ***Vice-Chancellor*** *of CUPB, for providing me the necessary infrastructure and resources to accomplish this research work.*

*I also acknowledge* ***Dean****, School of Basic and Applied Sciences, and* ***Head of Department*** *for his beneficial suggestions and helping hands throughout my research.*

*I convey my sincere thanks to* ***Dr. Petrina Kapewangolo****, Senior Lecturer, Department of Chemistry and Biochemistry, Faculty of Science, University of Namibia, Namibia their help and support throughout my work.*

*My warmest thanks are due to my colleagues* ***Mr. Atul Kumar Singh****,* ***Ms. Kumari Sunita Prajapati****,* ***Mr. Mohd Shuaib****,* ***Mr. Pothabathula Seshu Vardhan*** *and all lab mates for their help and support throughout my work.*

*Above all, my sincere credit goes to my family members who made my dreams their own and bear by absence during the course of research work. I would like to express my deep gratitude to my mother "****Smt. Sumitra Kushwaha****" and my father "****Shri Shiv Ram Kushwaha****" for their sincere encouragement and inspiration through the course of my journey towards producing this thesis.*

*I pay my sincere thanks to University Grants Commission, India for providing financial support in form of Junior Research Fellowship (JRF) and Senior Research Fellowship (SRF).*

*A sincere thanks to the Department of Science and Technology, India and University Grants Commission, India for providing financial support in the form of DST-SERB Grant [EEQ/2016/000350] and UGC-BSR Research Start-Up-Grant [No. F.30–372/2017 (BSR)] respectively. A sincere thanks to the Central University of Punjab for providing the research grant in the form of Research Seed Money (GP:25) and infrastructure facilities to accomplish my research work.*

*Lastly, I want to pay sincere acknowledgment to the whole scientific community, without scientific literature support I cannot make this thesis possible. In due course, if some relevant citation is missed, I sincerely apologize for the inadvertent errors.*

***(Prem Prakash Kushwaha)***

# Table of Content

## LIST OF TABLES

## LIST OF FIGURES

## LIST OF APPENDICES

## LIST OF ABBREVIATIONS

| S. no. | Full form | Abbreviation |
|---|---|---|
| 1 | 3-(4,5-dimethylthiazol-2-yl)- 2,5- diphenyl tetrazolium bromide | MTT |
| 2 | 2′,7′-Dichlorodihydrofluorescein diacetate | H2-DCFDA |
| 3 | 3-O-(E)-p-Coumaroylbetulinic acid | CB |
| 4 | 5' adenosine monophosphate-activated protein kinase | AMPK |
| 5 | 5,5′,6,6′-tetrachloro-1,1′,3,3′-tetraethylbenzimi-dazolylcarbocyanine iodide | JC-1 |
| 6 | Absorption, Distribution, Metabolism, Excretion and Toxicity | ADME/T |
| 7 | Annexin V fluorescein Isothiocyanate | Annexin V FITC |
| 8 | Bicinchoninic acid assay | BCA |
| 9 | Blood brain barrier | BBB |
| 10 | Breast cancer cells | BCa |
| 11 | Breast cancer-1 | BRCA1 |
| 12 | Breast cancer-2 | BRCA2 |
| 13 | Breast tumor kinase | BRK |
| 14 | *Bulbine frutescens* hexane extract | BHE |
| 15 | *Bulbine frutescens* methanolic extract | BME |
| 16 | Bulbineloneside D | BD |
| 17 | Checkpoint kinase 2 | CHEK2 |
| 18 | Cyanidin-3-glucoside | C3G |
| 19 | Cyclin D1 | CD1 |
| 20 | Cyclin dependent kinase 4 | C4 |
| 21 | Dickkopf 1 | DKK1 |
| 22 | Dimethyl sulfoxide | DMSO |
| 23 | Domain cross-correlation matrix | DCCM |
| 24 | Dulbecco's modified eagle medium | DMEM |
| 25 | Epidermal growth factor receptor | EGFR |
| 26 | Epigallocatechin gallate | EGCG |
| 27 | Estrogen receptor | ER |
| 28 | Extracellular signal-regulated kinases | ERK |
| 29 | Fetal bovine serum | FBS |
| 30 | Frizzled-related protein 1 | FRP1 |
| 31 | Gallbladder cancer | GbC |
| 32 | Gas Chromatography-Mass Spectrometry | GC-MS |
| 33 | Glioma-associated oncogene-2 | GLI-2 |
| 34 | Histone deacetylase | HDAC |
| 35 | Human embryonic kidney 293 | HEK293 |
| 36 | Human Epidermal Growth Factor Receptor 2 | HER2 |
| 37 | Indian Medicinal Plants Database | IMPS |

| | | |
|---|---|---|
| 38 | Indian Medicinal Plants, Phytochemistry and Therapeutics | IMPPAT |
| 39 | Interleukin-6 | IL-6 |
| 40 | Interleukin-8 | IL-8 |
| 41 | International Agency for Research on Cancer | IARC |
| 42 | Kurarinone | KU |
| 43 | M.D. Anderson-Metastasis Breast Cancer 231 | MDA-MB-231 |
| 44 | Mammalian Target of Rapamycin | mTOR |
| 45 | Matrix metalloproteinase-9 | MMP-9 |
| 46 | Michigan Cancer Foundation-7 | MCF-7 |
| 47 | Mitochondrial membrane potential | MMP |
| 48 | Molecular Dynamics | MD |
| 49 | Molecular weight | MW |
| 50 | N-[(3,5-Difluorophenyl)acetyl]-L-alanyl-2-phenyl]glycine-1,1-dimethylethyl ester | DAPT |
| 51 | N-{(2R,4S,5S)-2-benzyl-5-[(tert-butoxycarbonyl)amino]-4-hydroxy-6-phenylhexanoyl}-L-leucyl-L-phenylalaninamide | 4B5 |
| 52 | Optimized potential for liquid simulations | OPLS |
| 53 | Patched homolog-1 | PTCH-1 |
| 54 | PhenethylIsothiocyanate | PEITC |
| 55 | Phosphoinositide-3-kinases | PI3K |
| 56 | Propidium iodide-height | PI-H |
| 57 | Protein design automation | PDA |
| 58 | Protein Kinase B | AKT |
| 59 | Radius of gyration | Rg |
| 60 | Reactive oxygen species | ROS |
| 61 | Root mean square deviations | RMSD |
| 62 | Signal transducer and activator of transcription 3 | STAT3 |
| 63 | Sonic hedgehog | SHH |
| 64 | Stem cell media | SCM |
| 65 | Stroma-derived factor-1 | SDF-1 |
| 66 | Triple-negative breast cancer | TNBC |
| 67 | Tumor protein p53 | TP53 |
| 68 | Vascular endothelial growth factor | VEGF |

# Chapter 1
# Introduction

# 1. Introduction

Breast cancer is the second most common cancer worldwide after lung cancer and the leading cause of cancer death in women. In 2019, around 271,270 new cases have been reported in the U.S. alone (American Cancer Society, 2019). In India, according to the Globocan 2018 data, 1,62,468 new cases registered and 87,090 deaths were reported (Globocan 2018). Some clinical trials have been established for prevention from some forms of breast cancer (Siegel et al. 2013). The occurrence of breast cancer may be genetic or non-genetic. Both breast cancer-1 (BRCA1) and breast cancer-2 (BRCA2) genes play a significant role in the development of breast cancer. Tumor protein p53 ($TP_{53}$) and checkpoint kinase 2 (CHEK2) genes are also allied with the development of breast cancer. Literature reveals that different signaling pathways are deregulated in cancer cells. Recent popular targets in breast cancer are the agents that target deregulated and proto-oncogenic signaling pathways such as Notch, Wnt, and Sonic hedgehog (SHH). Interaction of Notch signaling protein with the human epidermal growth factor receptor 2 (HER2) signaling pathway is known to involve in breast cancer pathogenesis (Osipo et al. 2008). Activation of Notch signaling and its connections with ERK (extracellular signal-regulated kinases) pathway endorse tumor angiogenesis and breast cancer development respectively (Zeng et al. 2005, Sridhar et al. 2005). Wnt signaling activation in an unregulated manner has been implicated in various solid cancers including breast cancer (Kamdje et al. 2014). The expression of β-catenin has been found to associate with poor prognosis of breast cancer (Kamdje et al. 2014). Interruption of Sonic Hedgehog (SHH) downstream transcriptional targets like Patched homolog-1 (PTCH-1) or glioma-associated oncogene-2 (GLI-2) genes leads to severe deformities in ductal morphogenesis like human breast ductal dysplasia (García-Zaragoza et al. 2012). Breast tumor kinase (BRK, a non-receptor tyrosine kinase) depletion in breast cancer cells diminished the activation of EGFR (epidermal growth factor receptor) regulated signaling proteins (Kamdje et al. 2014). Human epidermal growth factor receptor-2 (HER2/neu, cerbB2) is amplified in several human breast cancer cell lines (King et al. 1985). Amplification of the HER2 pathway leads to Her2 protein overexpression which is related to cancer cell proliferation and

progression (Kamdje et al. 2014). The PI3K/Akt/mTOR pathway tempers estrogen receptor (ER) therapy in a ligand-independent manner (Kim et al. 2011). The literature revealed that the target genes of various cancer signaling pathways are known to converge into some phenotypic phenomena such as decreased apoptosis, increased cell migration and uncontrolled cell cycle. Natural inhibitors might promote apoptosis, inhibit cancer cell migration, proliferation, and drug resistance by blocking different cancer signaling pathway proteins (Basu et al. 2014; Wang et al. 2016). Different studies showed that inhibitors (natural/synthetic) by targeting Hippo, TGF-β, Wnt, STAT, NFKB and PPARγ signaling pathways, induces apoptosis and inhibition of cell cycle cell migration, proliferation, and drug resistance were decreased in cancer cells *in vitro* (Sikander et al. 2016; Zhang and Wang, 2015).

Mammosphere are used as a model for culturing and sustaining or cancer stem cells (CSCs) *in vitro*. As mammosphere replicate the micro-niche of the tumor, they are a model for studying the characteristics of cancer stem cells (CSCs), and for mapping, isolating, and characterizing the CSC generated lineages (Lombardo et al. 2015). Cancer stem cells possess the properties of self-renewal and the capacity to generate all cell types. Notch and other signaling cascades play an important role in normal development, embryogenesis, and hemostasis. However, dysregulation of these cascades is reported to cause several tumor types and malignancies. Abnormal expression of these pathways is associated with the modulation of mammosphere formation and CSCs (Koury et al. 2017). Notch signaling is the most commonly hyperactivated signaling cascade in cancer cells, which is reported to contribute to self-renewal and stemness properties to the tumors. Notch signaling has a vital role in the connections between angiogenesis and CSCs properties. Due to this, CSCs are receiving attention as a target to eradicate CSCs population. Notch signaling inhibition may contribute to the therapeutic approaches to treat cancer by eliminating CSCs (Venkatesh et al. 2018). Various phytochemicals are reported to possess inhibitory activity against CSCs proliferation and repress the process of mammosphere formation *in vitro*. Montales et al. (2012) reported that the genistein represses mammosphere formation in MDA-MB-231 and MCF-7 cells. In another study by Seo et al. (2015) shikonin and artesunate are reported to inhibit mammosphere formation in MCF-7 cells.

Charpentier et al. (2014) reported the mammosphere inhibitory potential of curcumin in breast cancer cells *in vitro.*

People have been using plant-derived medicines for several centuries throughout the world. Various rewards are allied with using natural medicines in contrast to pharmaceutical products. First, natural compounds reduce the risk of side effects. Second, it is also effective with chronic conditions. Third, natural compounds comprise cost-effective drugs. Fourth, the advantage of the natural compounds is its widespread availability. Fifth, the advantage of the natural compounds is its synergistic multi-target effects. Natural products affect not only one target, but numerous targets and can co-operate in a synergistic and agonistic way (Essa et al. 2016). Few natural products such as curcumin and resveratrol may be used as mTOR pathway inhibitors. Lin et al. (2009) reported that resveratrol activated AMP-activated protein kinase (AMPK) in both ER-positive and ER-negative breast cancer cells. It also has excellent efficacy to inhibit mTOR and its downstream 4E-BP1 signaling (Lin et al. 2009). Curcumin exerts its anti-proliferative potential by obstructing the mTOR pathway. Curcumin also prevents proliferation of different types of cancer cells (Johnson et al. 2009). Phytoconstituents from *Withania somnifera* such as Withaferin A prevents interleukin-6 (IL-6)-mediated activation of STAT3, which promotes different malignancies including breast cancer (Lee et al. 2010). Resveratrol has been shown to cause apoptosis and inhibition of growth in cancer cells (Khan et al. 2013). Lycopene inhibits *in vitro* cell growth and induces apoptosis in breast cancer cells (Wang and Zhang, 2007; Fornelli et al. 2007). Pomegranate constituents such as delphinidin, cyanidin and petunidin repressed the breast cancer cells growth (Zhang et al. 2005). EGCG induces p53 expression and its targets BAX and p21 in breast cells (Hastak et al. 2005; Roy et al. 2005). EGCG suppressed STAT3 expression contributing to prevent cell growth and apoptosis induction and inhibits angiogenesis by suppressing the vascular endothelial growth factor (VEGF) expression and matrix metalloproteinase-9 (MMP-9) in breast cells (Leong et al. 2009). The polyphenols present in pomegranate also inhibits breast cancer cell proliferation (Kim et al. 2002).

*In silico* approaches can help in recognizing drug targets through bioinformatics tools. This approach has the potential to predict the target structures for possible binding,

generate candidate molecules, specific active sites detection, drug-likeness prediction, drug-protein docking etc. *In silico* study also provides novel targets and their particular functions of lead compounds with desired properties. Computational drug discovery involves de novo design, virtual screening, *in silico* ADME/T prediction and determines protein-ligand binding pattern (Wadood et al. 2013). Besides that *in silico* technique reduces the cost and time for drug discovery.

# Chapter 2
# Review of Literature

# 2. Review of literature

Breast cancer is the second most common cancer in female while its rates are continuously rising throughout the world. According to the International Agency for Research on Cancer (IARC) of the World Health Organization report, an estimated 2.09 million cancer cases diagnosed in 2018. In US, 271,270 new breast cancer cases (2,670 male and 268,600 female) and 42,260 deaths (500 male and 41,760 female) were reported in 2019 **(Figure 2.1)** (American Cancer Society, 2019). Based on the presence or absence of molecular receptors such as estrogen receptors (ER), progesterone receptors (PR) and human epidermal growth factor 2 (HER2), breast cancer is categorized into three major subtypes. Different subtypes of breast cancer show differential drug susceptibility, prognosis, and aggressiveness. Triple-negative breast cancer (TNBC) is more aggressive in nature, susceptible to chemotherapy and shows poor prognosis. On the other hand, luminal types of BCa cells are less drug-susceptible, show better prognosis and are comparatively less aggressive in nature. Studies show that 70% of the breast cancer patients comprise $ER^+/PR^+/HER2^-$ types of breast cancer, 15%-20% comprises $ER^+/PR^+/HER2^+$ type of breast cancer, and 15% comprises $ER^-/PR^-/HER2^-$ types of breast cancer. About >90% of breast tumors do not show metastatic properties at the time of diagnosis. The therapeutic approach for these type of cancer patients is the tumor abolition and inhibiting recurrence. Nonmetastatic breast cancer patients receive systemic therapy based on subtypes. Endocrine therapy with minor chemotherapy is being used for $ER^+/PR^+/HER2^-$ cancer patients. Cancer patients having $ER^+/PR^+/HER2^+$ subtypes of tumor receive HER2-targeted antibody/small molecule inhibitor therapy in combination with chemotherapy. Triple-negative cancer patients receive chemotherapy alone.

There are noteworthy parallels among normal cell growth and cancer proliferation at the molecular level (Macias and Hinck, 2012; Huebner and Ewald, 2014). Normal cellular growth regulated by complex cellular signaling pathways in a tight manner. This allows the cells to contact with the adjacent environment and other cells (Hunter, 2000; Hunter, 2007).

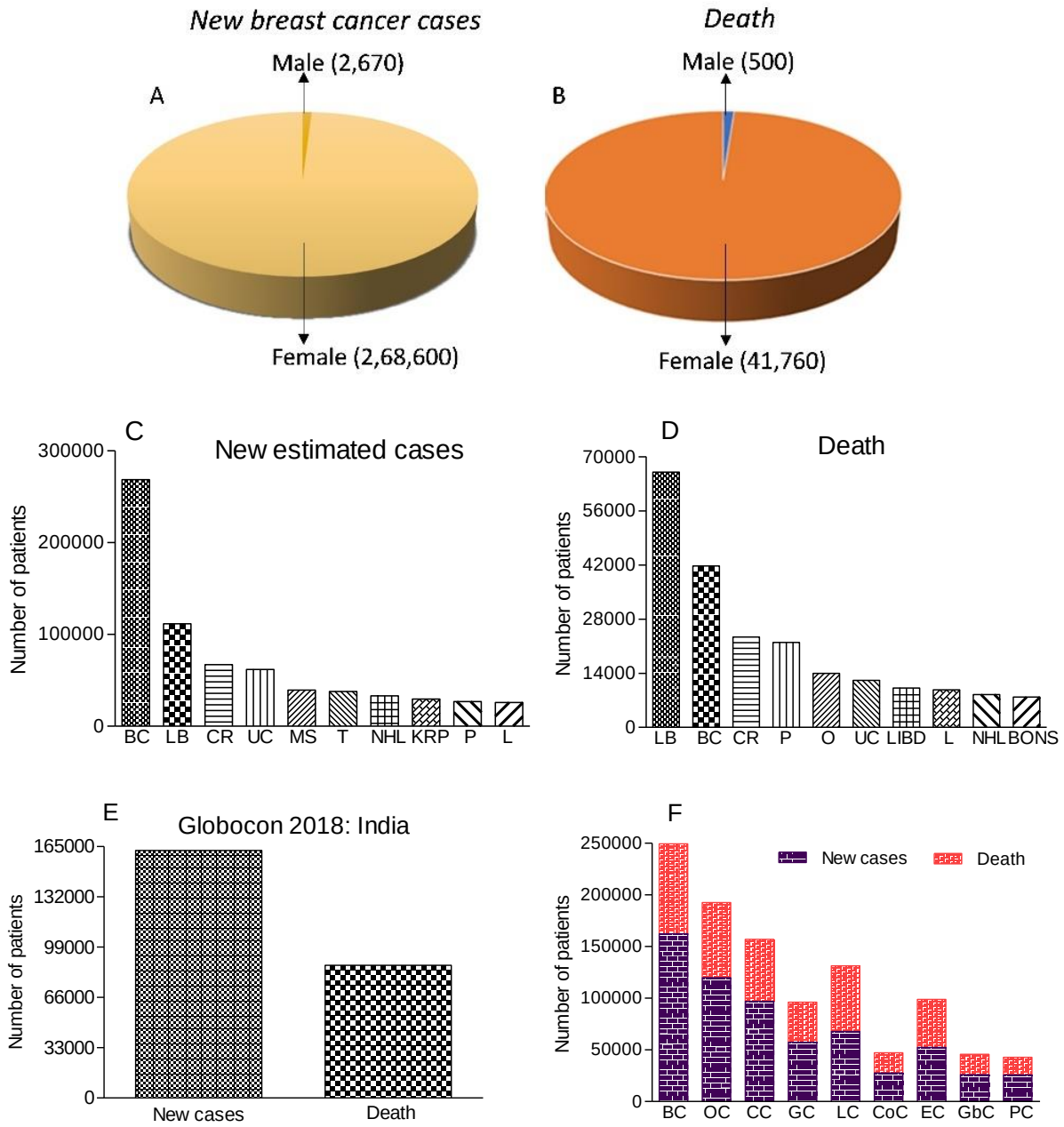


**Figure 2.1** Breast cancer statistics in India and worldwide. (A) and (B) showing the new breast cancer cases and deaths respectively in both males and females worldwide. (C) and (D) representing the new estimated cases and deaths respectively in terms of the number of breast cancer patients in comparison to patients with other types of cancer. (E) Graph representing the number of new breast cancer cases and deaths occurred due to breast cancer in India reported by Globocon 2018. (F) The number of patients of new breast cancer cases and deaths in breast and other cancer in India reported by Globocon 2018. BC-Breast cancer; LB-Lung and bronchus; CR-Colon and rectum; UC-Uterine and corpus; MS-Melanoma of the skin; T-Thyroid; NHL-Non-Hodgkin lymphoma; KRP-Kidney & renal pelvis; P-Pancreas; L- Leukemia; O-Ovary cancer; LIBD-Liver & intrahepatic bile duct; BONS-Brain & other nervous system; OC-Oral cancer; CC-Cervical cancer; GC-Gastric cancer; LC-Lung cancer; CoC-Colorectal cancer; EC-Esophageal cancer; GbC-Gallbladder cancer; PC-Prostate cancer

Deregulated or abnormal signaling turns these normal cells growth to cancer initiation and progression (Sever and Brugge, 2015). Genetic and epigenetic alteration helps in cancer initiation by altering various pathways that normally control survival, migration, and proliferation (Sever and Brugge, 2015). Alteration in cellular signaling pathways also regulates cell differentiation and fate, cell motility and cell death (Sever and Brugge, 2015). Cellular signaling pathways also get hyperactivated due to mutation in a proto-oncogene. Mutation in the tumor suppressor gene may also increase the chance of tumor initiation through alteration in these signaling pathways (Sever and Brugge, 2015).

## 2.1 Notch signaling

The notch signaling pathway performs a crucial role in cell development through communication between cell to cell contact. Notch signaling has been reported in breast cancer pathogenesis; thus, it may act as a potential therapeutic target. This signaling comprises single transmembrane proteins such as Delta-like ligand 1, 3, 4, and Jagged (JAG) 1, 2 (Radtke and Raj, 2003). Cell-cell contacts require notch receptors of one cell and notch ligand of other cells. The notch ligand-receptor complex is then cleaved by a membrane-bound protein called Ɣ-secretase. Gamma secretase is a high molecular weight protein of approximately 170 kDa, has an intramembrane aspartyl protease domain that cleaves its substrates with their transmembrane domains. It is composed of four essential subunits namely nicastrin, presenilin, presenilin enhancer and anterior pharynx defective 1. Gamma secretase releases the notch intracellular domain (NICD) within the cytosol which plays a central role in the canonical notch signal transduction pathway. NICD then translocates into the nucleus and regulates gene transcription via CSL (also known as CBF-1 or RBP-JK). Interaction between the CSL/NICD induces target gene expression including members of Hes and Hey families of transcription factors that ultimately promote cell proliferation (Radtke and Raj, 2003).

A number of studies explored that elevated Notch 1 or Jag 1 positively correlated with deprived outcomes (Reedijk et al. 2005; Dickson et al. 2007; Reedijk et al. 2008). Inhibition of Notch 4 or blocking Ɣ-secretase enzyme inhibited the mammosphere self-renewal property (Dontu et al. 2004; Farnie et al. 2007). Sansone et al. (2007) showed that Notch 3 and Jag 1 regulates hypoxia survival and cancer stem cell renewal in breast cancer cell line derived and primary breast tumor sphere (Sansone et al. 2007). Together, Notch signaling and HER2 signaling pathways are related to more aggressiveness in 20% of breast cancers.

## 2.2 Natural products as anticancer agents

In the 20$^{th}$ century, people throughout the world now are focusing on natural products to cure different diseases. Eventually, it was recognized that some natural products could in some instances be made more effective through the use of chemistry to produce semi-synthetic compounds (i.e. aspirin and later the penicillins) (Newman et al. 2000; Butler, 2004). In 2007, Newman and Cragg published the third in their series of analyses of the sources of drugs, covering the period from 01/1981 to the middle of 2006 and showing the sources of the listed 974 small molecule drugs. The analysis demonstrated the valuable contributions of Nature for potential chemotherapeutic agents and lead compounds that provided both foundation and motivation for total or semi-synthesis of effective novel drugs (Newman & Cragg, 2007). As synthetic techniques improved it became possible, in some cases, to create new medicinal compounds based on natural products that were more effective and/or cheaper than the original natural product template (Newman et al. 2000; Cragg & Newman, 2001; Koehn & Carter, 2005). Natural and synthetic compound derivatives containing a pharmacophore derived natural product comprises around 38% as a small molecule used in pharmaceuticals and 52% of whole anticancer drugs which is presently accessible in the market (Newman et al. 2003). This is of vital importance for the treatment of diseases that are capable of developing resistance to current drugs and for those to which no current treatment exists (Cragg et al. 1997). For these two classes of diseases, new chemical entities with new mechanisms of action are needed and

nature has proven to be the ultimate source of new compounds with unique modes of action (Koehn & Carter, 2005; Da Rocha et al. 2001). Several natural products are using for the treatment of various human diseases **(Figure 2.2).** Some natural product-based anticancer drugs and their mode of action are enlisted in **table 2.1.**

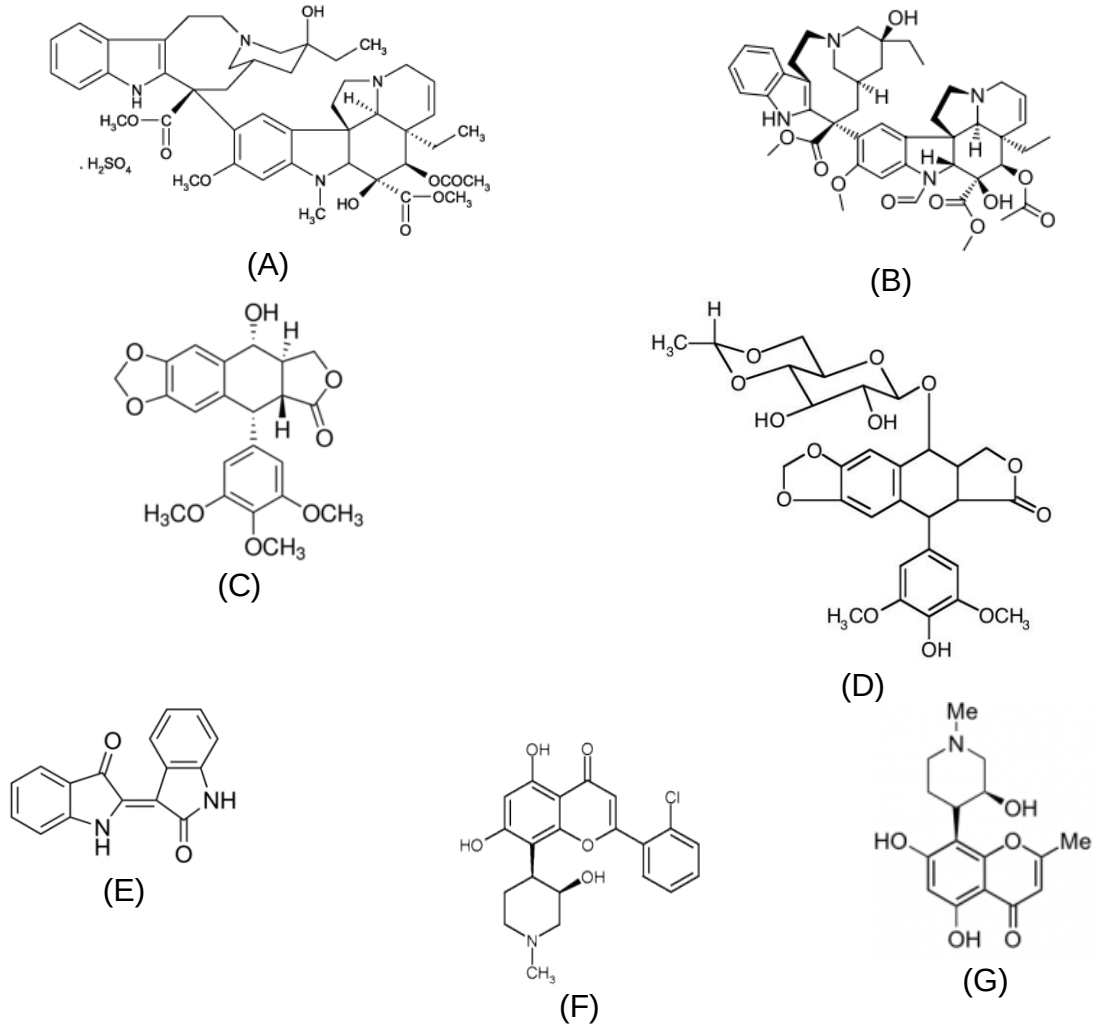


**Figure 2.2** Natural phytochemicals as active anticancer agents (A) Vinblastine (B) Vincristine (C) Podophyllotoxin (D) Etoposide (E) Indirubins (F) Flavopiridol (G) Rohitukine

## 2.2.1 Apigenin

Apigenin is a flavone prevailing mostly in parsley, celery, chamomile (Hoensch & Oertel, 2011) and an Egyptian plant *Moringa peregrina* (El-Alfy et al. 2011).

**Table 2.1** Important natural product-based anticancer drugs

| Name of the drug | Origin (source) | Therapeutic use |
|---|---|---|
| | **Preclinical** | |
| Dictyodendrin | *Dictyodendrilla verongiformis* | Telomerase |
| Gingerol | *Zingiber officinale* | Prevents cancer progression |
| Lamellarin D | *Lamellaria* species | Topoisomerase I/mitochondria |
| | **Phase I** | |
| Ascididemin | *Didemnum* species | Caspase-2/mitochondria |
| Discodermolide | *Discodermia dissolute* | Microtubule-stabilizing drug |
| Elsamitrucin | *Streptomyces distallicus* | Anticancer agent |
| NVP-LAQ824 | Hydroxamic acid derivative | HDAC/DNMT |
| NPI-2358 | Analog of halimide | Tubulin-depolymerizing agent |
| | **Phase II** | |
| Curcumin | *Curcuma longa* | Prevents cancer progression |
| Ecteinascidin-743 | *Ecteinascidia turbinate* | Antitumor agent |
| Epigallocatechin-3-gallate | *Camellia sinensis* | Chemotherapeutic activity |
| Genistein | Isoflavones | Breast and prostate cancers |
| Squalamine | *Squalus acanthias* | Phospholipid bilayers |
| Dolastatin | *Dolabella auricularia* | Inhibits tubulin polymerization |
| | **Phase III** | |
| Amrubicin | *Streptomyces peucetius var. caesius* | Antitumor activity |
| | **Approved** | |
| Camptothecin | *Camptoteca acuminate* | Inhibits DNA topoisomerases |
| Paclitaxel | *Taxus brevifolia* | Potent anticancer activity |
| Romidepsin | *Chromobacterium violaceum* | HDAC inhibitor |
| Crisantaspase | l-asparaginase from *Erwina chrysanthemi* | Inhibition of malign asparagine-dependent cells |
| Vincristine | Alkaloid from *Vincarosea (Apocynaceae)* | An antineoplastic agent used in therapies against SCLC, leukemia and malign lymphoma |

*Source:* Adopted and modified from Qurishi et al. (2011).

It shows cytotoxic properties against breast and colon cancer cells. It is also considered as an arbitrator for chemoprevention in the cancerous developmental processes and induces a process of autophagia but may prompt resistance against chemotherapy (Ferreira et al. 2006). Apigenin induces apoptosis and inhibits colon cancer cells proliferation (Chung et al. 2007; Turktekin et al. 2011), reduces azoxymethane (AOM) persuaded aberrant crypt foci (ACF) construction in male Sprague-Dawley rats and enhances apoptosis which may contribute to colon cancer inhibition (Leonardi et al. 2010). It affects the leptin/leptin receptor pathway and induces apoptosis in lung adenocarcinoma (Bruno et al. 2011). Apigenin also upsurges melanogenesis in B16 cells by triggering the p38 MAPK pathway and demonstrated that it or its derivatives may possibly be used for treating hypopigmentation syndromes (Ye et al. 2011).

### 2.2.2 Curcumin

Curcumin is the chief component of the Indian spice turmeric, *Curcuma longa* (Zingiberaceae). Its anticancer properties have been studied for breast, colon (Bachmeier et al. 2010), brain tumors, and lung metastases (Senft et al. 2010). Curcumin obstructs with NF-κB (Bachmeier et al. 2008), which associates with inflammatory diseases as well as cancer. It also has the potential to detach raptor from mTOR, prevent mTOR complex I and characterized as a new class of mTOR inhibitor (Beevers et al. 2009). Ravindran et al. (2009) demonstrated that curcumin controls growth of tumor via regulation of numerous cell signaling pathways such as cell proliferation (c-myc, cyclin D1), cell survival (XIAP, Bcl-x, Bcl-2, cFLIP, c-IAP1), caspase activation (caspase 3, 8, 9), tumor suppression (p21, p53), death receptor (DR4, DR5), mitochondrial and protein kinase pathway (JNK, AMPK, and Akt). Curcumin inhibits p65 and cell invasion by downregulation of MMP-2 and COX-2 expression by EGFR gene inhibition and inflection of Akt/mTOR signaling and cell growth (Chen & Johnson, 2006). Another study reported that curcumin defeats p38 mitogen-activated protein kinase stimulation, decreases IL-1 beta and matrix metalloproteinase-3, and increases IL-10 in the mucosa of children and adults with inflammatory bowel disease (Epstein et al. 2010). Curcumin prevents the Akta and

mTOR phosphorylation and their downstream substrate in prostate cancer. Curcumin dephosphorylates and inhibits Akt/mTOR signaling through the calyculin A-sensitive protein phosphatase (Yu et al. 2008).

### 2.2.3 Epigallocatechin gallate (EGCG)

It is the most plentiful catechin compound present in green tea. EGCG has advantageous effects in treating brain, prostate, cervical, and bladder cancer (Kumazoe & Tachibana, 2016). Among many studies, EGCG binds and inhibits Bcl-xl anti-apoptotic protein function. EGCG suppressed azoxymethane persuaded colonic premalignant lesions *in vivo*, obstructed with EGFR signaling and repressed hepatocyte growth factor-induced colon cancer cell proliferation (Larsen & Dashwood, 2010). It shows inhibition of cyclin-dependent kinases, mitogen-activated protein kinases, AP1 activation, growth factor-related cell signaling, and NF-κB, matrix metalloproteinases and topoisomerase I. Chen et al. (2003) reported that EGCG inhibits HT-29 cell growth and also showed nuclear condensation and fragmentation. They suggested that EGCG triggered mitochondrial damage and JNK mediated apoptotic cell death.

### 2.2.4 Fisetin

Fisetin (flavone) occurs in many plants like *Acacia berlandieri*, *Acacia greggii*, strawberries, cucumber, parrot tree, grape, persimmon, onion, and apple (Gabor & Eperjessy, 1966). It exerts anti-carcinogenesis effects in HCT-116 human colon cancer (Lim & Park, 2009). It is also a powerful antioxidant and regulates protein and lipid kinase pathways. Khan et al. (2012) found the inhibition of mTOR and PI3K/Akt signaling in NSCLC cells by fisetin. Fisetin also has the capability to inhibit Wnt signaling via the modulation of β-catenin expression, transcriptional activity, and Wnt target gene expression. Other studies reported that fisetin reduced cell viability with G1-phase arrest and interrupted Wnt/β- catenin signaling, showed an inhibitory conclusion on the capabilities of adhesion, migration, and invasion, and significantly diminished the nuclear levels of NF- κB and AP-1 (Liao et al. 2009).

### 2.2.5 Genistein

Genistein, an isoflavone found in the number of plants like lupine, fava beans, soybeans, and psoralea, *Flemingia vestita*, and coffee. It has been reported as an excellent antiangiogenic agent and also has the potential to block cancer-associated cell growth through the regulation of various cell survival and cell division related enzymes (Wang et al. 2012). Another study reported that genistein acts as a tyrosine kinase inhibitor (Markovits et al. 1989). *In vivo* and *in vitro* studies indicated that it also has the potency to treating leukemia (Raynal et al. 2007). It competes with 17-β-estradiol to bind to the estrogen receptor and shows an advanced affinity towards estrogen receptor β than towards estrogen receptor α. Genistein possibly involved in the JNK pathway regulation via modulating AP-1 activity (Gopalakrishnan et al. 2006).

### 2.2.6 Gingerol

It is the active constituent of ginger. Gingerol has anti-cancerous effects in colon, breast and ovarian, and pancreas tumors (Poltronieri et al. 2014). It has antioxidant, anti-inflammation, and antitumor promoting possessions reduced iNOS and TNFα expression through suppression of IκBα phosphorylation and NF-κB nuclear translocation. Gingerol treatment induces apoptosis in leukemia cells by the mitochondrial pathway (Zeng et al. 2010).

## 2.3 Drug development through *in silico* approaches

Computer simulations are a fast and comparatively cheap option for preliminary screening of both active targets and potential drugs. De novo pharmaceuticals in Cambridge, UK, have made a set of software for virtual screening, docking as well as for ligand-based design. If the structure of the active target is known, then their site explorer can predict the potential of drug binding sites and can estimate the interactions between these active sites and the drug. If the structure of the active target is unknown,

then its Quasi2 software will create a virtual protein known to be significant in binding (Wadood et al. 2013). The SkelGen suite of the packages can then use their own data to create a new chemical structure enhanced for interaction with a target's active site. The pharmaceuticals company is cooperating with GeneFormatics of San Diego, California, in an agenda dedicated to inhibitors of the M10 family of matrix metalloproteinases, enzymes that are involved in inflammatory and cancer ailments. GeneFormatics involves proteomics to identify the target enzymes and illustrate their active sites while De novo is a docking/virtual screen model of small molecules against the proteins. Ligand-receptor interaction can be studied using different software and is obtainable from different firms including Accelrys, Tripos and Metaphorics. Schrodinger provides different modules such as molecular modeling, chemical simulation, lead optimization, visualization, drug design and automation. The number of software is accessible free to researchers at non-profit organizations like GOLD and AutoDock 3. Molsoft in La Jolla, California, designs ICM molecular modeling software and releases an ICM browser for the Apple Macintosh (Wadood et al. 2013). Another suite for structural homology programs, Accelrys, identifies the potential function, fold family and 3D structure of target proteins by matching them with sequences and structural homologs of their known function. When the protein's structure is identified, then functional info can be collected using different modules within Accelrys's Insight II program which supports various processes including X-ray crystallography, NMR studies, and protein modeling. LION bioscience target engine in Heidelberg, Germany, supports target prediction by subscription the potential to examine the gene sequence and expression data, map potential functional features onto protein structure, find homologous structures, view related gene annotation and protein pathway info and use text mining to find functional interactions. Proteins themselves developed as active drugs in bio-therapeutics. Protein Design Automation (PDA) suite was designed to optimize protein function by Xencor. PDA computationally screens huge numbers of amino-acid changes in an acknowledged protein structure. It then initiates functional information from the 3D protein structure and designs novel features into the protein to enhance its function (Wadood et al. 2013).

## 2.4 Knowledge gap

Plenty of *in vitro* anticancer studies has been reported to assess the potential of natural compounds. Still, the appropriate mode of action of many potential natural compounds (based upon known primary screening test results) yet to be studied. A small sub-populations in tumor known as side population or cancer stem cells are the major problem in cancer drug resistance and recurrence of the disease in patients. This results in poor therapy outcomes and decreased life span of the patients. The notch signaling pathway is highly associated with the aggressiveness and cancer stem cell self-renewal process. Presently different clinical trials are going on to study the effect of notch signaling inhibitors in breast cancer patients world around but as per our knowledge there is no clinically approved notch signaling small molecule inhibitor is known for breast cancer treatment. Thus the present study is designed to explore the anticancer mode of action (notch signaling inhibition potential) of natural product/phytochemicals in breast cancer cells and breast cancer stem-like cells (mammosphere).

## 2.5 Hypothesis

Cancer cells escape cell cycle arrest, and apoptosis by modulating various molecular events and abrupt signaling pathways. Breast cancer stem cells are responsible for drug resistance, tumor aggressiveness and relapse in cancer patients. The notch signaling pathway is reported to be highly expressed in breast cancer and breast cancer stem cells. Thus, identification of novel natural notch signaling inhibitor could be utilized for breast cancer therapy either alone or in combination with other chemotherapeutic drugs.

## 2.6 Objectives

1. *In silico* identification of natural anticancer compounds.
    - Gamma-secretase protein (notch signaling pathway) will be selected as a target for the screening purpose

2. Effect of lead phytochemicals on breast cancer cell lines.

- Identified leads from objective 1 will be taken for their *in vitro* notch signaling pathway inhibition and anticancer potential in breast cancer cell lines.

3. Effect of potent anticancer compounds on cancer stem-like cells.

- Identified leads from objective 1 will be taken for their *in vitro* notch signaling pathway inhibition and anticancer potential in breast cancer stem-like cells (mammosphere).

# Chapter 3
# Material and Methods

# 3. Material and methods

## 3.1 Literature-based identification of lead anticancer natural products

Different kinds of literature were searched at different search engine platforms such as PubMed, Google Scholar, Web of Science, Science Direct, Scopus, Semantic Scholar, Medline, PubMed Central, etc. Medicinal plants databases such as Indian Medicinal Plants Database (IMPS) and Indian Medicinal Plants, Phytochemistry and Therapeutics (IMPPAT) were searched to know the known anticancer and other therapeutic potential.

### 3.1.1 Sample collection and extract preparation

The lead plant sample was obtained from “Farm Vredelus” located in Mariental, Namibia in 2018. The plant (voucher specimen number M2) was authenticated by Silke Rugheimer at the National Herbarium of Namibia. Bulb part of lead plant was collected, washed and wiped with ethanol properly. The sample was extracted in methanol (polar) and hexane (non-polar) separately for 48h. The semi-solid extract was further dried by using a rotary evaporator and stored until further use.

### 3.1.2 Identification of phytochemicals in lead plant extract

#### 3.1.2.1 Literature-based identification of phytochemicals present in lead plant extract

We searched the various databases such as PubMed, Google Scholar, Web of Science, PubMed Central, etc. for the enlisting of phytochemicals present in the lead plant extract.

#### 3.1.2.2 Gas Chromatography-Mass Spectroscopy (GC-MS) analysis

Secondary metabolites present in the test extracts were identified by using Gas-Chromatography coupled with Mass Spectroscopy (GC-MS) technique. Respective dried extracts were dissolved in 100% methanol and hexane for the analysis. The GC-MS analysis was performed using Shimadzu QP 2010 Ultra-Mass Spectrometer equipped with an integrated chromatograph with an RTXi-5MS column. The ion source temperature was 200℃ and the interface temperature was 260℃. The data was acquired using a mass detector from 5 minutes of the sample injection. Pressure mode at 66.7kPa controlled the flow of the sample. The total flow and column flow rate were 10.4 ml/min and 1.24 ml/min respectively. The maintenance of the split ratio was at 5:0. The column injector temperature was 250℃ and the column oven temperature was maintained for 10 minutes at 280℃. Dissolved samples had been delivered via injector running within the split mode with helium gas. The identity of phytoconstituents became completed with the aid of evaluation of retention time and fragmentation pattern with mass spectra inside the NIST11.0 spectral library. The chromatogram was processed by using GC-MS Real-Time Analysis Software version 1.10 beta.

## 3.2 *In silico* identification of natural gamma secretase inhibitor

### 3.2.1 Retrieval and preparation of ligands and protein

We retrieved the ligands from the MAPS Database established by Ashfaq et al. (2013). These ligands comprised a collection of terpenoids and flavonoids compounds. We downloaded a total of 349 compounds structures and subjected to their preparation. Phytochemicals present in the test extracts were downloaded from the PubChem database. LigPrep module of Maestro 11.2 was used to prepare the ligands and corrections such as 2D to 3D conversion, hydrogens addition, corrected bond angles and bond lengths, ring conformation, and low-energy structure were incorporated. Other parameters such as ionization and tautomers, were not generated. Optimized potential for liquid simulations (OPLS_2005) forcefield was used to optimize the atom

force field charges and atom types. One conformation for one ligand was selected for conformer generation.

The crystal structure of the Ɣ-secretase protein (PDB:4Y6K) was retrieved from the protein data bank. The protein preparation wizard module of Maestro 11.2 was used to perform the rectification in a raw PDB structure. Changes such as hydrogens addition, bond orders assign, zero-order bonds creation to metal, disulfide bond generation, charge fixation, and group orientation were incorporated. After the completion of ligands and protein preparation, a receptor grid file was generated.

### 3.2.2 Molecular docking

GLIDE module was used for receptor-based molecular docking. Enlisted ligands were docked in the receptor-binding site and the docked structure having the lowest binding energy was preferred for further validation.

### 3.2.3 Absorption, distribution, metabolism, excretion, and toxicity (ADME/T) properties and CYP-450 interaction analysis

QikProp module of Maestro 11.2 was used to predict the ADME/T (Absorption, distribution, metabolism, excretion, and toxicity) properties of best-docked compounds. QikProp module provides structural, physicochemical, biochemical, pharmacokinetics, and toxicity properties. It also predicts intrinsic properties (drug-like properties) of the ligands such as octanol/water partition, log BB, overall CNS activity, log $IC_{50}$ for HERG $K^+$ channel blockage, Caco-2, MDCK cell permeability and logKhsa for human serum albumin binding. XenoSite Cytochrome P450 prediction tool was used to analyze the Kurarinone-CYP450 interaction.

### 3.2.4 Simulation study

Based on the FlexX docking results, the ligand–DNA complexes with the lowest docking energy in two different binding clusters were selected to further assess the

stability of the complex structure. MD simulations were conducted in the YASARA v16.7.22 package (Sichuan University, China) by using the AMBER14 force field. MK-4827 was first introduced into the YASARA interface, and the partial atomic charges were computed using the AM1-BCC model. This step was followed by a general heating step in which the temperature was increased to 298 K, and the protonation state of ionizable residues was set considering a physiological pH (7.4). Periodic boundary conditions were applied to the system, and counter ions were added by randomly replacing water molecules with $Na^+$ or $Cl^-$ to provide a charge-neutral system. Particle-mesh Ewald summation was used to simulate the long-range Coulomb interactions with a cut-off of 8.0 Å. Multiple time steps were used in the simulation: 1.25 fs for intramolecular and 2.0 fs for intermolecular forces, and data were collected every 100 ps. MD trajectories were used to further analyze the root mean square deviations (RMSDs) of the complexes.

## 3.3 *In vitro* anticancer activities

### 3.3.1 Reagents

Dulbecco's modified eagle medium (DMEM), fetal bovine serum (FBS), trypsin, penicillin, streptomycin, JC-1 (5,5′,6,6′-tetrachloro-1,1′,3,3′-tetraethylbenzimidazolylcarbocyanine iodide), 2',7'-dichlorodihydrofluorescein diacetate (H2DCFDA), annexin V fluorescein Isothiocyanate (annexin V FITC), hoechst 33342, RNAase A, trizol, and lipofectamine 3000 were from Thermo Fisher Scientific, USA. MTT (3-(4,5-dimethylthiazol-2-yl)- 2,5- diphenyl tetrazolium bromide) was obtained from Sigma Aldrich, USA. The iScript™ cDNA synthesis kit and SYBR® green master mix were purchased from Biorad, USA. Propidium iodide (PI) and primers were purchased from Abcam, UK and GCC biotech, India respectively. Luciferase/Renilla vector and dual-luciferase reporter assay system were procured form Promega Corporation, USA. Primary antibody caspase 3 (Cat no. ab32351), Cyclin D1 (Cat no: MA514512), SOX2 (Cat no: PA1094), c-MYC (Cat no: 700648), CD44 (Cat no: PA5-21419), Hey1 (Cat no: PA5-68563), Hes1 (Cat no: PA5-28802), and E-cadherin (Cat no: PA5-85088) and

secondary antibody β-actin (Cat no: 4970S) were purchased from Abcam, UK, Thermo Fisher Scientific, USA, and Imperial Life Sciences, India.

### 3.3.2 Cell culture

Human breast cancer cells (MDA-MB-231 and T47D) and human embryonic kidney 293 (HEK293) cells were purchased from the National Centre for Cell Sciences, Pune. These cells were cultured in Dulbecco's Modified Eagle Medium (DMEM) supplemented with 10% (v/v) heat-inactivated FBS, 2 mM L-glutamine, 100 U/ml of penicillin, and 100 µg/ml of streptomycin. Cells were maintained at 37℃ under a humid environment in an incubator having 5% $CO_2$.

### 3.3.3 Cell viability assay

The effect of lead compounds on cell viability was measured by MTT assay following the method by Mosmann et al. (1983). Briefly, the cells ($1\times10^4$ cells/well) were seeded in a 96 well microtiter plate (100 µl/well) in triplicate. Treatments were done for different time intervals at different concentrations. After incubation, 10 µl of MTT solution (5 mg/ml) was added to each well and incubated for 4h at 37°C. Formazan crystals were solubilized with 100 µl dimethyl sulfoxide (DMSO) and the absorbance was measured at 590 nm using a microplate reader (BioTek Instruments, Inc. USA). The $IC_{50}$ value was calculated for cell viability. Regression analysis was done to calculate the $IC_{50}$, log $IC_{50}$, and $R^2$ values and graphs were designed using Graph pad Prism software. Sub $IC_{50}$ was also calculated to perform some of the experiments. Sub $IC_{50}$ ($IC_{25}$) stands for half of the value of $IC_{50}$ at which 25% of the cells of the given population get eradicated.

### 3.3.4 Cell cycle analysis

Breast cancer MDA-MB-231 and T47D cells ($1x10^5$) were seeded into a 6-well plate followed by treatment with test compounds/extract at different concentrations and time intervals. After incubation, cells were detached and fixed with 500 µl of 70% ethanol at

-20℃ for 2h. Subsequently, the cells were washed thrice with 1 ml of phosphate-buffered saline (PBS) (pH 7.4). Cells were finally re-suspended in 1 ml of PBS containing 0.1% triton X, 10 mM EDTA, 50 mg/ml RNase A and 2 mg/ml PI. The cells were analyzed by a flow cytometer (BD Accuri) (Darzynkiewicz & Juan, 1997).

### 3.3.5 Reactive oxygen species generation assay

The levels of ROS were determined quantitatively by using 2, 7-dichlorodihydrofluorescein diacetate (DCFH-DA) dye (Wu & Yotnda, 2011). Briefly, MDA-MB-231 and T47D cells ($3x10^3$ cells/well) were plated in 96-well plate with cell culture media contained 10% FBS and 1% penicillin/ streptomycin and incubated at 37℃ with 5% $CO_2$ overnight. The cells were treated for 48h at $IC_{50}$ concentration of test compounds/extract. The supernatant was removed, and attached cells were washed with PBS. The cells were further incubated for 4h after re-suspending in 100 µl H2DCFDA dye solution (20 µM). Subsequently, the fluorescence intensity was measured at an excitation/emission wavelength of 495/530 nm using a fluorescence microplate reader.

### 3.3.6 Mitochondrial membrane potential disruption assay

MDA-MB-231 and T47D breast cells ($3×10^3$ cells/well) were seeded in a 96 well microtiter plate (100 µl/well) in triplicates. Cells were treated for 48h at $IC_{50}$ concentration of test compounds/extract. After incubation, 100 µl of JC-1 dye solution (2 µM) was added to each well and incubated for 30 minutes at 37°C. The absorbance was measured at an excitation/emission wavelength of 529/590 nm using a microplate reader (White & Reynolds, 1996).

### 3.3.7 Annexin V/propidium iodide assay

Flow cytometric technique was used to quantify the drug-induced apoptotic cell death in breast cancer cells. Briefly, $1x10^5$ breast cancer cells (MDA-MB-231) were seeded

in 35mm treated culture dishes containing 1 ml of culture media. The cells were treated with test compounds/extracts for 12h at sub $IC_{50}$ and $IC_{50}$ concentrations. After incubation, cells were trypsinized and washed twice with cold PBS. The cells were resuspended in 100 µl annexin binding buffer containing annexin V FITC and PI (propidium iodide) and further incubated for 15 minutes at room temperature in the dark. Additionally, 400 µl annexin binding buffer was added and immediately analyzed through the flow cytometer (BD Accuri C6) (Wlodkowic et al. 2009).

### 3.3.8 Confocal microscopic analysis

#### 3.3.8.1 Mitochondrial membrane potential disruption

MDA-MB-231 and T47D cells were plated in 6-well plates and cultured overnight. Then, MDA-MB-231 and T47D cells were treated with different lead compounds/extracts at $IC_{50}$ concentrations for 16h. After that, MDA-MB-231 and T47D cells were stained with 5µM JC-1 dye for 20 minutes at 37℃ in the dark. Mitochondrial membrane potential depletion was observed under a confocal microscope (Olympus FluoView FV1000).

#### 3.3.8.2 Reactive oxygen species generation

For reactive oxygen species analysis, $0.2\times10^6$ cells were plated in 6 well plates in DMEM. After 24h, MDA-MB-231 and T47D cells were treated with different lead drugs at $IC_{50}$ concentration for the next 16h. After that, MDA-MB-231 and T47D cells were stained with 1µM H2-DCFDA for 20 minutes at 37℃ in the dark. Then ROS production levels were observed under a confocal microscope (Olympus FluoView FV1000).

#### 3.3.8.3 Nuclear morphology assessment

MDA-MB-231 and T47D cells at a density of $2x10^4$ cells/well were seeded in 24-well plates, and after incubation for 24h, fresh culture media containing lead compounds at $IC_{50}$ concentration were added and incubated in a humidified incubator at 37˚C for 16h.

After incubation, the cells were stained with Hoechst 33342 dye (5 µg/ml) in culture medium at room temperature in the dark for 20 minutes. Subsequently, the cells were washed twice with PBS and immediately evaluated by a confocal microscope (Olympus FluoView FV1000).

### 3.3.9 Notch promoter activity

Dual-luciferase assay technique was used to asses notch promoter activity. In this assay, we used pGL4[luc2P/RBP-JK-RE/Hygro] vector having NICD (Notch intracellular domain) binding site (notch promoter) fused with luciferase gene. p[Rluc-Neo/SV40] vector (renilla) was used as an internal control. HEK293 cells ($4x10^4$ cells/well) were seeded in a 96-well plate. The cells were transfected with pGL4[luc2P/RBP-JK-RE/Hygro] and p[Rluc-Neo/SV40] vectors using Lipofectamine 3000 transfection reagent (Thermo Fisher Scientific, Waltham, MA, USA) according to the manufacturer's guidelines. Transfected cells were treated with test compounds/extract at $IC_{50}$. DAPT (20µM) was used as a positive control. The plate was further incubated for 24h at 37℃. The Luciferase activity was measured by using the Dual-Luciferase Reporter Assay Kit (Promega Corporation, USA) on GloMax 20/20 Luminometer (Promega Corporation, USA).

### 3.3.10 Gene expression at mRNA levels

Gene involved in the notch signaling pathway, cell cycle, apoptosis, cancer cell self-renewal, etc. were studied at mRNA levels. One million cells/well were plated into the six-well plates in culture media supplemented with 10% FBS and 1% penicillin/streptomycin and incubated at 37℃. Cells were treated with different lead drugs at $IC_{50}$ concentration for 24, and 48h. Total RNA was extracted using Trizol (Thermo Scientific Fisher) solution according to the manufacturer's instruction. RNA was quantified at 260/280 nm using Thermo Scientific Nanodrop 2000 Spectrophotometer. The absorption ratio (A260 nm/A280 nm) between 1.90 and 2 was taken into consideration for cDNA preparation.

**Table 3.1** List of primers

| Gene | Forward sequence | Reverse sequence | Reference |
|---|---|---|---|
| *GAPDH* | 5'-AGCCTCAAG ATCATCAGCAATG-3' | 5'-ATGGACTGTGGTCATGAGT CCTT-3' | Scoumanne et al. 2010 |
| *Hes1* | 5'-TCAACACGACACCGGATAA AC-3' | 5'-GCCGCGAGCTATCTTTCTT CA-3' | Weng et al. 2015 |
| *HEY1* | 5'-GCTGGTACCCAGTGCTTTT GAG-3' | 5'-TGCAGGATCTCGGCTTTTT CT-3' | Belandia et al. 2005 |
| *Survivin* | 5'-TTCAAGGAGCTGGAAGGC TG-3' | 5'-AGCAATGAGGGTGGAAAG CA-3' | Jafari et al. 2016 |
| *Bcl-2* | 5'-CCTGTG GAT GAC TGA GTA CC-3' | 5'-GAGACA GCC AGG AGA AAT CA-3' | Mohamed et al. 2018 |
| *Caspase-3* | 5'-GCTGGATGCCGTCTAGAG TC-3' | 5'-ATGTGTGGATGATGCTGCC A-3' | Alotaibi et al. 2018 |
| *NF-κB-p65* | 5'-AGCACCATCAACTATGATG AGTTTC-3' | 5'GAGTTATAGCCTCAGGGT ACTCCAT-3' | Janbandhu et al. 2010 |
| *Cyclin D1* | 5'-ACAAACAGATCATCCGCAA ACAC-3' | 5'-TGTTGGGGCTCCTCAGGTT C-3' | Suzuki et al. 2001 |
| *CDK4* | 5'-CATCGTTCACCGAGATCTG A-3' | 5'-CCAACACTCCACATGTCCA C-3' | Samady et al. 2004 |
| *p21* | 5'-TGA GCC GCG ACTGTG ATG-3' | 5'-GTCTCGGTGACAAAGTCGA AGTT-3' | Scoumanne et al. 2010 |
| *NANOG* | 5′-TCCTCCTCTTCCTCTATACT AAC-3′ | 5′-CCC ACAATCACAGGCATAG-3′ | Ling et al. 2012 |
| *Oct4* | 5′-TGGAGAAGGAGAAGCTGG AGCAAAA-3′ | 5′-GGCAGAGGTCGTTTGGCT GAATAGACC-3′ | Ling et al. 2012 |
| *Sox2* | 5′-GGGAAATGGAGG GGTGCAAAAGAGG-3′ | 5′-TTGCGTGAGTGT GGATGG GATTGGTG-3′ | Ling et al. 2012 |
| *CD44* | 5′-TTCCCAAAAAGAGGCTGAG A-3′ | 5′-CAATGTTGCAAGGGTTTGT G-3′ | Cho et al. 2015 |
| *MYC* | 5′-AGCTGCTTAGACGCTGGAT TTT-3′ | 5′-TCGAGGTCATAGTTCCTGT TGG-3′ | Tseng et al. 2014 |
| *EpCAM* | 5′-CGCAGCTCAGGAAGAATG TG-3 | 5′-TGAAGTACACTGGCATTGA CG-3' | Osta et al. 2004 |

Approximately one microgram of total RNA was reverse transcribed into cDNA using a high capacity iScript™ cDNA Synthesis Kit (BIORAD). mRNA expression was quantified by RT-PCR by using Veriti® 96-well fast thermal cycler (Applied Biosystems). The following cycling parameters were optimized as follows: start at 95°C for 5 minutes, denaturing at 95°C for 30s, annealing at 55°C for 45s, elongation at 72°C for 45s, and a final 5 minutes extra extension at the end of the reaction to ensure that all amplicons were completely extended and repeated for 40 amplification cycles (Mechoulam & Pierce, 2005). GAPDH was used as a housekeeping gene to assure equal loading of the sample. List and sequence of primers are given in **table 3.1.**

### 3.3.11 Gene expression at protein levels

Western blot technique was used to detect the protein expression levels (cell cycle, apoptosis, notch responsive gene) in treated and non-treated breast cancer cells. The cells were seeded at the density of $2x10^5$ cells/well in a 6-well plate and incubated overnight for attachment followed by treatment with lead compounds/extract for different time intervals at $IC_{50}$ concentration. Subsequently, the treated cells were detached and harvested in RIPA buffer followed by 30 minutes incubation on ice and centrifuged at 10,000xg for 15 minutes. Bicinchoninic acid assay (BCA) protein quantitation reagent kit (Thermo Fisher Scientific) was used to estimate the protein content present in the lysate. The 2X SDS-PAGE loading buffer (200 mM DTT, 100 mM Tris-HCl (pH 6.8), 0.1 bromophenol blue, 4% SDS, and 20% glycerol) was used to load the sample on the gel. An equal amount of total protein and loading buffer was taken and boiled for 10 minutes before loading. The protein sample was electrophoresed in the tris-glycine electrophoresis buffer [250 mM glycine, 25 mM Tris-HCl (pH 8.3), and 0.1% SDS] at 100 V for 1.5h. The separated proteins were blotted on the PVDF membrane with transfer buffer (25 mM Tris, 20% methanol, 0.04% SDS and 192 mM glycine) for 2h. The 5% non-fat milk in TBST [150 mM NaCl, 20 mM Tris-HCl (pH 7.4) and 0.1% (v/v) Tween-20] was used to block the membrane for 2h at room temperature. The blotted membrane was incubated with primary antibody at 4℃ overnight followed by TBST wash thrice (10 minutes interval each). Horseradish

peroxidase-conjugated secondary antibody was diluted in blocking buffer for 2h at room temperature followed by three wash with TBST for 10 minutes. The blots were developed with the enhanced chemiluminescence (ECL) system (Thermo Fisher Scientific). The image was captured using image lab software 6.0.1 Bio-Rad.

### 3.3.12 Effects of lead compounds on self-renewal potential

One of the important phenotypic characteristics of cancer stem cells (CSCs) is the ability to form non-adherent spheres in the culture medium. The sphere of breast cancer cells in non-adherent media is known as the mammosphere. Sphere forming assay has been widely used to evaluate self-renewal and differentiation *in vitro*. The methodology for mammosphere formation in the presence and absence of test compounds is described below.

#### 3.3.12.1 Mammosphere formation assay

For sphere formation, cells were plated in non-treated, low adhesion, 96 wells plate at the concentration of 100 cells/100 µL/well in stem cell media (SCM) that consisted of Dulbecco's Modified Eagle's Medium (DMEM): F12: AA (Gibco), supplemented with 1×B27 (Gibco), 20 ng/mL epidermal growth factor (EGF), and 10 ng/mL fibroblast growth factor (FGF). The phase-contrast microscope was used to capture the images.

### 3.3.13 Notch signaling inhibition potential of lead compounds in mammosphere

The effect of lead compounds on notch signaling targeted genes (*Hes1* and *Hey1*) were studied at mRNA levels. The methodology is given in section 3.3.10. The primers sequence are given in table 3.1. Notch signaling downstream proteins (Hes1, Hey1 and E-cadherin) were studied in lead compound treated mammosphere as per methodology is given in section 3.3.11.

### 3.3.14 Self-renewal and stemness marker alteration by lead compounds in mammosphere

Effect of lead compounds on self-renewal and stemness marker (Nanog, SOX2, OCT4, EPCAM, MYC, and CD44) were studied at mRNA levels. The methodology is given in section 3.3.10. The primers sequence are given in table 3.1. Self-renewal and stemness marker proteins (SOX2, CD44 and c-Myc) were studied in lead compound treated mammosphere as per methodology is given in section 3.3.11.

### 3.3.15 Statistical Analysis

All data are presented as the mean ± standard deviation of at least three independent experiments. All statistical analyses were performed using GraphPad Prism 5.0 version software (GraphPad Software, San Diego, California). Statistical comparisons between the control and treatments were performed using one-way analysis of variance. $P<0.05$ was considered to indicate a statistically significant difference.

# Chapter 4
# Results

# 4. Results

## 4.1 Identification of lead anticancer natural products

### 4.1.1 Literature-based identification of plant products

The exhaustive literature study revealed that *Bulbine frutescens* (Asphodelaceae) has pharmacological potential but its effect on breast cancer cells and the underlying mechanism is yet to be established. Thus we decided to explore the anticancer effect and notch signaling inhibition potential of *B. frutescens* in cancer cells. The extraction procedure of phytochemicals from *B. frutescens* is given in the methodology section 3.1.1.

#### 4.1.1.1 Gas Chromatography-Mass Spectroscopy (GC-MS) analysis of *B. frutescens*

Methanolic and hexane extract of *B. frutescens* were used for the identification of compounds and anticancer potential against breast cancer cells. GC-MS analysis of *B. frutescens* methanolic and hexane extract showed the differential presence of various secondary metabolites **(Figure 4.1 A-B)**. Hexane extract showed comparatively greater number of phytochemicals (n=103) than methanolic extract (n=25). Name of identified compounds, their molecular formula, molecular weight, retention time and peak area are given in **table 4.1.** In hexane extract, tritetracontane; urs-12-ene; 1,1,6-trimethyl-3-methylene-2-(3,6,1013,14-pentamethyl-3-ethenyl-pentadec-4-enye)cyclohexane; docosane, 2,4-dimethy; phthalic acid, bis(7-methyloctyl) ester; bis(tridecyl) phthalate; terephthalic acid, dodecyl 2-ethylhexy ester; 1-nonene, 4,6,8-trimethyl; 9-octadecenamide; 2H-pyran-2-carboxylic acid, 3,6-dihydro-6-methoxy-, ethyl ester; 9,12,15-octadecatrienoic acid, 2-[(trimethylsilyl)oxy]-1-[[(trimethylsilyl)oxy]methyl]ethyl ester(Z,Z,Z); indan-1,3-diol monoacetate; nonane, 5-(1-methylpropyl); 6,10,14,18,22-tetracosapentaen-2-ol; bis(tridecyl) phthalate and 1,2-Benzenedicarboxylic acid, dinonyl ester compounds showed >1% peak area. In

methanolic extract, 2-propenoic acid, pentadecyl ester; tetradecanoic acid; n-hexadecanoic acid; 9-octadecenal; heptadecane; heptadecane, 2-methyl; tritetracontane; Z-11-pentadecenol; 2-methyloctacosane; 2,6,10,14,18-pentamethyl-2,6,10,14,18-eicosapentaene; and 1,2-octadecanediol showed >1% peak area **(Table 4.1).**

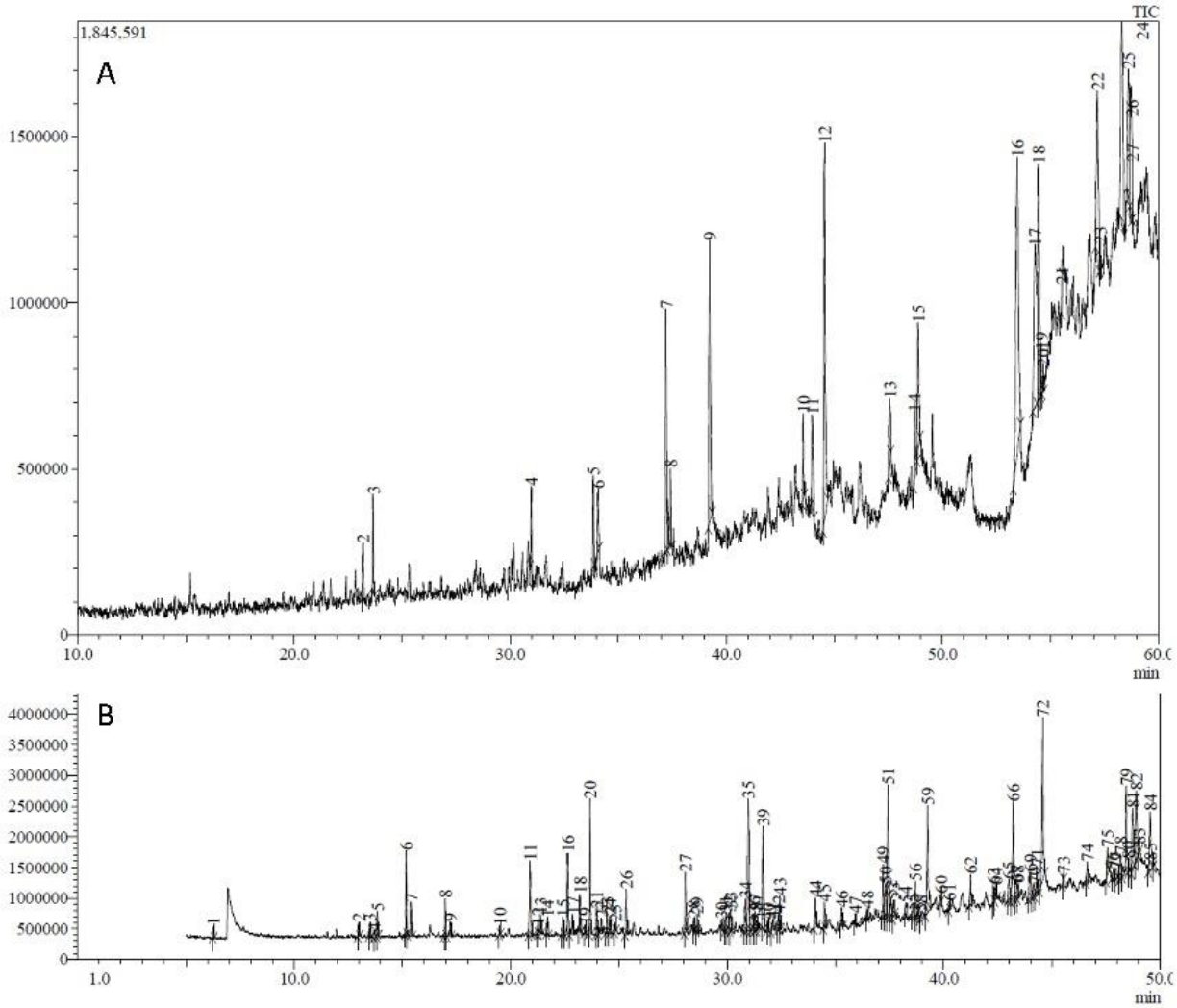


**Figure 4.1** Gas chromatography-mass spectroscopy chromatograph of *B. frutescens* (A) Methanolic and (B) Hexane extract

### 4.1.2 *In silico* identification of natural anticancer phytochemicals

The γ-secretase enzyme is one of the important targets in the notch signaling pathway inhibition mediated natural anticancer drug discovery. Keeping this in our mind, we tried

**Table 4.1** Phytoconstituents present in methanolic and hexane extract of *B. frutescens* identified in gas chromatography-mass spectroscopy analysis

| S. No. | RT | Compound name | Molecular formula | M.W. | Peak area (%) |
|---|---|---|---|---|---|
| **Hexane extract** | | | | | |
| 1 | 6.265 | Heptane, 2,4-dimethyl | $C_9H_{20}$ | 128 | 0.03 |
| 2 | 12.979 | Decane | $C_{10}H_{22}$ | 142 | 0.05 |
| 3 | 13.500 | Hexane, 2,2,3,3-tetramethyl | $C_{10}H_{22}$ | 142 | 0.04 |
| 4 | 13.700 | Nonane, 2,5-dimethyl | $C_{11}H_{24}$ | 156 | 0.02 |
| 5 | 13.856 | Decane, 4-methyl | $C_{11}H_{24}$ | 156 | 0.08 |
| 6 | 15.173 | Decane, 3,7-dimethyl | $C_{12}H_{26}$ | 170 | 0.30 |
| 7 | 17.205 | 2,6-Dimethyldecane | $C_{12}H_{26}$ | 170 | 0.07 |
| 8 | 19.501 | Undecane, 2-methyl | $C_{12}H_{26}$ | 170 | 0.03 |
| 9 | 20.887 | Dodecane | $C_{15}H_{32}$ | 212 | 0.35 |
| 10 | 21.243 | Undecane, 2,4-dimethyl | $C_{13}H_{28}$ | 184 | 0.02 |
| 11 | 21.372 | Undecane, 3,6-dimethyl | $C_{13}H_{28}$ | 184 | 0.08 |
| 12 | 21.694 | Undecane, 4,8-dimethyl | $C_{13}H_{28}$ | 184 | 0.06 |
| 13 | 22.404 | Undecane, 2,7-dimethyl | $C_{13}H_{28}$ | 184 | 0.07 |
| 14 | 22.638 | Benzene, 1,3-bis(1,1-dimethylethyl) | $C_{14}H_{22}$ | 190 | 0.34 |
| 15 | 22.851 | Dodecane, 2,6,11-trimethyl | $C_{15}H_{32}$ | 212 | 0.12 |
| 16 | 23.191 | 2,4-Dimethyldodecane | $C_{14}H_{30}$ | 198 | 0.13 |
| 17 | 23.425 | Tetradecane, 4-methyl | $C_{15}H_{32}$ | 212 | 0.02 |
| 18 | 23.663 | Dodecane, 2,6,11-trimethyl | $C_{15}H_{32}$ | 212 | 0.54 |
| 19 | 24.177 | Eicosane | $C_{21}H_{44}$ | 296 | 0.08 |
| 20 | 24.583 | 1-Nonene, 4,6,8-trimethyl | $C_{12}H_{24}$ | 168 | 0.07 |
| 21 | 24.820 | Undecane, 4-ethyl | $C_{13}H_{28}$ | 184 | 0.03 |
| 22 | 25.335 | Dodecane, 2,6,11-trimethyl | $C_{15}H_{32}$ | 212 | 0.18 |
| 23 | 28.069 | Tetradecane | $C_{15}H_{32}$ | 212 | 0.23 |
| 24 | 28.443 | Heptadecane | $C_{21}H_{44}$ | 296 | 0.04 |
| 25 | 28.602 | 2-methyloctacosane | $C_{29}H_{60}$ | 408 | 0.07 |
| 26 | 30.076 | Undecane, 4,8-dimethyl | $C_{13}H_{28}$ | 184 | 0.10 |
| 27 | 30.153 | Tetradecane, 5-methyl | $C_{15}H_{32}$ | 212 | 0.09 |
| 28 | 30.829 | 5,5-Diethyltridecane | $C_{17}H_{36}$ | 240 | 0.15 |
| 29 | 31.212 | Undecane, 3,7-dimethyl | $C_{13}H_{28}$ | 184 | 0.07 |
| 30 | 31.361 | Sulfurous acid, butyl undecyl ester | $C_{15}H_{32}O_3S$ | 292 | 0.03 |
| 31 | 31.651 | Phenol, 2,4-bis(1,1-dimethylethyl) | $C_{14}H_{22}O$ | 206 | 0.45 |
| 32 | 32.088 | 2-Bromotetradecane | $C_{14}H_{29}Br$ | 276 | 0.04 |
| 33 | 32.367 | 1-Undecene, 4-methyl | $C_{12}H_{24}$ | 168 | 0.06 |
| 34 | 34.063 | Diethyl Phthalate | $C_{12}H_{14}O_4$ | 222 | 0.15 |
| 35 | 34.485 | Heptadecane, 2,6,10,15-tetramethyl | $C_{21}H_{44}$ | 296 | 0.11 |
| 36 | 35.901 | Heptadecane, 2,6,10,14-tetramethyl | $C_{21}H_{44}$ | 296 | 0.03 |
| 37 | 36.451 | Pentadecane, 2,6,10-trimethyl | $C_{18}H_{38}$ | 254 | 0.02 |
| 38 | 37.191 | Methanone, (1-hydroxycyclohexyl)phen | $C_{13}H_{16}O_2$ | 204 | 0.24 |
| 39 | 38.228 | 1-Heptanol, 2-propyl | $C_{10}H_{22}O$ | 158 | 0.05 |
| 40 | 38.525 | Dodecane, 2,6,11-trimethyl | $C_{15}H_{32}$ | 212 | 0.08 |

| | | | | | |
|---|---|---|---|---|---|
| 41 | 38.673 | Tridecanol, 2-ethyl-2-methyl | $C_{16}H_{34}O$ | 242 | 0.15 |
| 42 | 38.842 | tert-Hexadecanethiol | $C_{16}H_{34}S$ | 258 | 0.04 |
| 43 | 38.925 | Hexadecane, 2,6,11,15-tetramethyl | $C_{20}H_{42}$ | 282 | 0.07 |
| 44 | 39.250 | Tetradecanoic acid | $C_{14}H_{28}O_2$ | 228 | 0.64 |
| 45 | 39.866 | 4-Oxononanal | $C_9H_{16}O_2$ | 156 | 0.03 |
| 46 | 40.249 | 10-Methylnonadecane | $C_{20}H_{42}$ | 282 | 0.02 |
| 47 | 41.232 | 2-methyltetracosane | $C_{25}H_{52}$ | 352 | 0.13 |
| 48 | 42.285 | 2-Bromotetradecane | $C_{14}H_{29}Br$ | 276 | 0.09 |
| 49 | 42.404 | Oxalic acid, hexyl tetradecyl ester | $C_{22}H_{42}O_4$ | 370 | 0.07 |
| 50 | 43.342 | Tetradecane, 5-methyl | $C_{15}H_{32}$ | 212 | 0.14 |
| 51 | 43.986 | trans-2-Hexadecenoic acid | $C_{16}H_{30}O_2$ | 254 | 0.20 |
| 52 | 44.150 | 5,5-Diethylheptadecane | $C_{21}H_{44}$ | 296 | 0.06 |
| 53 | 44.562 | n-Hexadecanoic acid | $C_{16}H_{32}O_2$ | 256 | 0.89 |
| 54 | 45.510 | Triacontane, 1-bromo- | $C_{30}H_{61}Br$ | 500 | 0.03 |
| 55 | 47.551 | 1-Decanol, 2-octyl | $C_{18}H_{38}O$ | 270 | 0.11 |
| 56 | 47.8 | Nonahexacontanoic acid | $C_{69}H_{138}O_2$ | 998 | 0.04 |
| 57 | 47.925 | Nonane, 5-butyl | $C_{13}H_{28}$ | 184 | 0.07 |
| 58 | 48.155 | 2-methyltetracosane | $C_{25}H_{52}$ | 352 | 0.16 |
| 59 | 48.517 | 1,5-Hexadiene-3,4-diol, 3,4-dimethyl | $C_8H_{14}O_2$ | 142 | 0.04 |
| 60 | 48.721 | Z,Z-8,10-Hexadecadien-1-ol | $C_{16}H_{30}O$ | 238 | 0.40 |
| 61 | 48.883 | 6-Octadecenoic acid, (Z) | $C_{18}H_{34}O_2$ | 282 | 0.45 |
| 62 | 49.008 | N-Ethylidenecyclohexaneamine, N-ox | $C_8H_{15}NO$ | 141 | 0.05 |
| 63 | 49.523 | Sulfurous acid, 2-propyl tridecyl ester | $C_{16}H_{34}O_3S$ | 306 | 0.42 |
| 64 | 49.667 | Heptyl heptadecafluorononanoate | $C_{16}H_{15}F_{17}O_2$ | 562 | 0.02 |
| 65 | 51.992 | 9-Oximino-3,6-dichloro-2,7-bis-(2-pipperidinoethoxy)fluorene | $C_{27}H_{33}Cl_2N_3O_3$ | 517 | 0.06 |
| 66 | 53.050 | Cyclododecanone, 2-(6-chloro-1-oxol | $C_{18}H_{31}ClO_2$ | 314 | 0.08 |
| 67 | 53.183 | Stearic acid, 3-(octadecyloxy)propyl ester | $C_{39}H_{78}O_3$ | 594 | 0.35 |
| 68 | 53.300 | Pentafluoropropionic acid, octyl ester | $C_{11}H_{17}F_5O_2$ | 276 | 0.14 |
| 69 | 53.431 | Tritetracontane | $C_{43}H_{88}$ | 604 | 1.00 |
| 70 | 53.550 | 2-Ethoxy-2-cyclohexen-1-one | $C_8H_{12}O_2$ | 140 | 0.19 |
| 71 | 53.717 | 2,2-Dimethyl-6-methylene-1-[3,5-dihydroxy-1-pentenyl]cyclohexan-1-perhydrol | $C_{14}H_{24}O_4$ | 256 | 0.79 |
| 72 | 53.774 | Decane, 2,3,5,8-tetramethyl | $C_{14}H_{30}$ | 198 | 0.68 |
| 73 | 53.842 | Dodecanoic acid, 3-hydroxy | $C_{12}H_{24}O_3$ | 216 | 0.54 |
| 74 | 53.918 | 2,3:5,6-Di-O-1-Cyclohexylieden-1,4-cyclohexandiallylether | $C_{24}H_{36}O_6$ | 420 | 0.30 |
| 75 | 53.959 | Acetic acid, 17-(1,5-dimethylhex-4-enyyl)-4,4,8,10,14-pentamethyl-2,3,4,5,6,7,8,9,10,11,12,14,15,16-tetradecahydro-1H-cyclopenta | $C_{32}H_{52}O_2$ | 468 | 0.42 |
| 76 | 54.025 | Cyclohexanone, 3-hydroxy-2,4,4-trimethyl-3-(3-methyl-1,3-butadienyl) | $C_{14}H_{22}O_2$ | 222 | 0.39 |
| 77 | 54.217 | Urs-12-ene | $C_{30}H_{50}$ | 410 | 1.71 |

| | | | | | |
|---|---|---|---|---|---|
| 78 | 54.350 | 1,1,6-trimethyl-3-methylene-2-(3,6,1013,14-pentamethyl-3-ethenyl-pentadec-4-enye)cyclohexane | $C_{32}H_{58}$ | 442 | 1.26 |
| 79 | 54.633 | Docosane, 2,4-dimethyl | $C_{24}H_{50}$ | 338 | 1.31 |
| 80 | 54.779 | Phthalic acid, bis(7-methyloctyl) ester | $C_{26}H_{42}O_4$ | 418 | 1.56 |
| 81 | 54.900 | Bis(tridecyl) phthalate | $C_{34}H_{58}O_4$ | 530 | 1.02 |
| 82 | 55.050 | Cyclooctane, (methoxymethoxy) | $C_{10}H_{20}O_2$ | 172 | 0.87 |
| 83 | 55.158 | Sulfurous acid, octadecyl 2-propyl ester | $C_{21}H_{44}O_3S$ | 376 | 0.87 |
| 84 | 55.300 | Terephthalic acid, dodecyl 2-ethylhexy ester | $C_{28}H_{46}O_4$ | 446 | 2.51 |
| 85 | 55.458 | 2,3-Nonadecanediol | $C_{19}H_{40}O_2$ | 300 | 0.32 |
| 86 | 55.492 | Tetrahydrofuran-2-one, 3-[1-fluoroethyl]-5-[[2-hydroxypropyl]benzeneethyl | $C_{17}H_{23}FO_3$ | 294 | 0.60 |
| 87 | 55.567 | Cyclopropane, 1-(1-hydroxy-1-heptyl)-2-methylene-3-pentyl | $C_{16}H_{30}O$ | 238 | 0.42 |
| 88 | 55.617 | 2-Allylpent-4-enoic acid, methyl ester | $C_9H_{14}O_2$ | 154 | 0.36 |
| 89 | 55.672 | 2,5-Furandione, dihydro-3-isooctadecyl | $C_{22}H_{40}O_3$ | 352 | 0.68 |
| 90 | 56.092 | Hexadecanoic acid, (2-phenyl-1,3-dioxolan-4-yl)methyl ester, cis | $C_{26}H_{42}O_4$ | 418 | 0.82 |
| 91 | 56.317 | Chloroacetic acid, 4-hexadecyl ester | $C_{18}H_{35}ClO_2$ | 318 | 0.77 |
| 92 | 56.358 | 2,6,10,14-Tetramethylpentadecan-7-on | $C_{19}H_{38}O$ | 282 | 0.90 |
| 93 | 56.492 | 1-Nonene, 4,6,8-trimethyl | $C_{12}H_{24}$ | 168 | 2.60 |
| 94 | 56.683 | Cholestan-3-ol, 4-methyl-, (3.alpha., 4.alpha.,5.alpha.) | $C_{28}H_{50}O$ | 402 | 0.31 |
| 95 | 56.879 | 9-Octadecenamide, (Z) | $C_{18}H_{35}NO$ | 281 | 5.12 |
| 96 | 57.150 | 2H-Pyran-2-carboxylic acid, 3,6-dihydro-6-methoxy-, ethyl ester | $C_9H_{14}O_4$ | 186 | 2.05 |
| 97 | 57.567 | 9,12,15-Octadecatrienoic acid, 2-[(trimethylsilyl)oxy]-1-[[(trimethylsilyl)oxy]methyl]ethyl ester(Z,Z,Z) | $C_{27}H_{52}O_4Si_2$ | 496 | 1.12 |
| 98 | 57.800 | Indan-1,3-diol monoacetate | $C_{11}H_{12}O_3$ | 192 | 2.84 |
| 99 | 58.358 | Nonane, 5-(1-methylpropyl) | $C_{13}H_{28}$ | 184 | 3.90 |
| 100 | 58.689 | 6,10,14,18,22-Tetracosapentaen-2-ol, | $C_{30}H_{51}BrO$ | 506 | 30.10 |
| 101 | 58.931 | Bis(tridecyl) phthalate | $C_{34}H_{58}O_4$ | 530 | 3.70 |
| 102 | 59.258 | Glutaric acid, isohexyl 2-(2-methoxyethyl)hexyl ester | $C_{20}H_{38}O_5$ | 358 | 0.07 |
| 103 | 59.698 | 1,2-Benzenedicarboxylic acid, dinonyl ester | $C_{26}H_{42}O_4$ | 418 | 1.34 |
| **Methanol extract** | | | | | |
| 1 | 23.196 | Tetradecane, 5-methyl | $C_{15}H_{32}$ | 212 | 0.39 |
| 2 | 23.669 | Dodecane, 2,6,11-trimethyl | $C_{15}H_{32}$ | 212 | 0.66 |
| 3 | 30.978 | Tridecanol, 2-ethyl-2-methyl | $C_{16}H_{34}O$ | 242 | 0.60 |
| 4 | 33.848 | Diethyl Phthalate | $C_{12}H_{14}O_4$ | 222 | 0.90 |
| 5 | 37.207 | 2-Propenoic acid, pentadecyl ester | $C_{18}H_{34}O_2$ | 282 | 2.06 |
| 6 | 37.429 | Eicosane | $C_{20}H_{42}$ | 282 | 0.99 |

| | | | | | |
|---|---|---|---|---|---|
| 7 | 39.234 | Tetradecanoic acid | $C_{14}H_{28}O_2$ | 228 | 2.77 |
| 8 | 43.561 | Hexadecanoic acid, methyl ester | $C_{17}H_{34}O_2$ | 270 | 0.64 |
| 9 | 43.978 | Cyclopentadecanone, 2-hydroxy | $C_{15}H_{28}O_2$ | 240 | 0.93 |
| 10 | 44.542 | n-Hexadecanoic acid | $C_{17}H_{34}O_2$ | 270 | 4.23 |
| 11 | 47.552 | n-Heptadecanol-1 | $C_{17}H_{36}O$ | 256 | 0.59 |
| 12 | 48.700 | 11,14-Eicosadienoic acid | $C_{21}H_{38}O_2$ | 322 | 0.85 |
| 13 | 48.869 | 9-Octadecenal | $C_{18}H_{34}O$ | 266 | 1.44 |
| 14 | 54.275 | Heptadecane | $C_{21}H_{44}$ | 296 | 6.32 |
| 15 | 54.275 | Heptadecane, 2- methyl | $C_{18}H_{38}$ | 254 | 3.40 |
| 16 | 54.431 | Tritetracontane | $C_{43}H_{88}$ | 604 | 3.56 |
| 17 | 54.567 | 1-Bromodocosane | $C_{22}H_{45}B$ | 388 | 0.30 |
| 18 | 54.658 | Dodecane, | $C_{18}H_{36}$ | 252 | 0.21 |
| 19 | 55.517 | 3-trsns-(1,1-dimethylethyl)-4-trans-methoxycyclohexanol | $C_{11}H_{22}O_2$ | 186 | 0.07 |
| 20 | 57.158 | Z-11-Pentadecenol | $C_{15}H_{30}O$ | 226 | 2.68 |
| 21 | 57.300 | Myristoyl chloride | $C_{14}H_{27}ClO$ | 246 | 0.23 |
| 22 | 58.299 | 2-methyloctacosane | $C_{29}H_{60}$ | 408 | 3.48 |
| 23 | 58.603 | :2,6,10,14,18-Pentamethyl-2,6,10,14,18-eicosapentaene | $C_{25}H_{42}$ | 342 | 1.72 |
| 24 | 58.750 | 1,2-Octadecanediol | $C_{18}H_{38}O_2$ | 286 | 1.70 |
| 25 | 58.783 | Cyclohexanol, 2-methyl-, cis | $C_7H_{14}O$ | 114 | 0.20 |

RT=Retention time; M.W.=Molecular weight

to identify the potential notch inhibitor present in *B. frutescens.* Moreover, various natural phytochemical database were also screened. Different phytochemicals present in *B. frutescens* were identified by published literature as per the methodology given in the methods section 3.1.2.1. Isofuranonaphthoquinone, Joziknipholone A, Joziknipholone B, Knipholone, Isoknipholone, 4'-Demethylknipholone 4'-β-D-glucopyranoside, Gaboroquinones A, Gaboroquinones B, and Bulbineloneside D phytochemicals were identified secondary metabolites present in *B. frutescens* plant (Bringmann et al., 2008; Tambama et al., 2014; Abegaz et al., 2002; Kuroda et al., 2003). Gamma secretase co-crystallized inhibitor 4B5 (N-{(2R,4S,5S)-2-benzyl-5-[(tert-butoxycarbonyl)amino]-4-hydroxy-6-phenylhexanoyl}-L-leucyl-L-phenylalaninamide) and DAPT (N-[(3,5-Difluorophenyl)acetyl]-L-alanyl-2-phenyl]glycine-1,1-dimethylethyl ester) the other known standard notch inhibitor were taken as positive control for *in silico* docking study. Co-crystalized and standard inhibitors showed approximately equal binding potential (-9.83 and -9.26 kcal/mol respectively) against γ-secretase enzyme binding pocket. Interestingly, bulbineloneside D from *B. frutescens* showed greater binding affinity (-11.22 kcal/mol)

for ϒ-secretase compared to standard inhibitors **(Figure 4.2 E)**. Further, *in silico* investigation showed the presence of hydrophobic interaction between bulbineloneside D and amino acid residue present on ϒ-secretase active site. Docking pose of standard and lead phytochemical is depicted in **figure 4.3 A-C**. The ϒ-secretase amino acid residues and type of interaction with standards/lead compounds are summarized in **table 4.3.** The actual position of amino acid residues and their type of interaction with standard (DAPT) and the lead compound is given in **figure 4.3 A-C**.

**Table 4.2** List of compounds selected for the study

| ***Medicinal Plant/ Phytochemical category*** | **PubChem CIDs of various compounds** | | | |
|---|---|---|---|---|
| *B. frutescens* (N=20) | PCID91932460; PCID25033784; PCID12178518; PCID11729754; PCID10072444; | PCID525546; PCID525545; PCID442753; PCID442731; PCID636652; | PCID5320386; PCID5315852; PCID189763; PCID68111; PCID10208; | PCID438991; PCID11190093; PCID10008440; PCID10093576; PCID102378267. |
| Flavonoids (N=286) | PCID5281801; PCID3519897; PCID5281296; PCID5281814; PCID6483649; PCID5281811; PCID5281810; PCID5281295; PCID5281805; PCID5386259; PCID1548994; PCID5319116; PCID5280862; PCID5281628; PCID6253344; PCID9972910; PCID5317750; PCID5281377; PCID5316900; PCID11708657; PCID10338075; PCID46883374; PCID44479223; PCID44479222; | PCID932; PCID9064; PCID1203; PCID1890; PCID6758; PCID8530; PCID2361; PCID1686; PCID17679; PCID10680; PCID97214; PCID72936; PCID91572; PCID73649; PCID96118; PCID79730; PCID68077; PCID68245; PCID68184; PCID68071; PCID97332; PCID11790; PCID64982; PCID10621; | PCID439533; PCID442811; PCID442456; PCID238782; PCID219100; PCID440832; PCID114627; PCID528044; PCID146093; PCID5322059; PCID5320471; PCID5281702; PCID5320686; PCID3666064; PCID5281613; PCID6443339; PCID5281665; PCID5319081; PCID5280805; PCID5320351; PCID5490139; PCID3085222; PCID5281707; | PCID5280666; PCID3065428; PCID5376979; PCID11635614; PCID10555277; PCID10063979; PCID46939886; PCID14033978; PCID11709595; PCID44559997; PCID11762505; PCID10424988; PCID25201019; PCID10980660; PCID22524423; PCID10801179; PCID10424295; PCID13846202; PCID11022960; PCID13983738; PCID44257423; PCID16376440; PCID10380681; PCID44254878; |

PCID26194552; PCID72344; PCID5459217; PCID44254877;
PCID24949855; PCID85705; PCID3084605; PCID10722001;
PCID24761044; PCID73447; PCID5458461; PCID42608061;
PCID11294177; PCID72281; PCID5280681; PCID42608060;
PCID11141878; PCID83489; PCID5280961; PCID10327269;
PCID11046839; PCID389484; PCID5317284; PCID10793085;
PCID10614892; PCID389483; PCID5086400; PCID42608059;
PCID10613719; PCID124211; PCID5487413; PCID44559998;
PCID10452362; PCID114909; PCID5352000; PCID44559999;
PCID10411554; PCID158280; PCID5281708; PCID10008443;
PCID10335921; PCID442361; PCID5491730; PCID10460896;
PCID44448192; PCID185609; PCID5281671; PCID10817087;
PCID44559966; PCID442670; PCID5281607; PCID42607959;
PCID44559965; PCID606171; PCID5281670; PCID11801874;
PCID21588173; PCID586491; PCID5318998; PCID10677118;
PCID10812923; PCID321346; PCID5352005; PCID10819468;
PCID10362969; PCID638288; PCID5280343; PCID53788628;
PCID15479637; PCID195652; PCID5281807; PCID10053761;
PCID10410005; PCID442824; PCID5317747; PCID10030972;
PCID44559964; PCID442431; PCID5282102; PCID10603133;
PCID44559963; PCID442428; PCID5481218; PCID10316935;
PCID44559956; PCID124052; PCID5280863; PCID10096171;
PCID10090306; PCID442459; PCID5281697; PCID46887866;
PCID42607512; PCID442458; PCID5377847; PCID12304093;
PCID11500744; PCID969516; PCID5315720; PCID16129642;
PCID44593449; PCID152430; PCID5281616; PCID11979368;
PCID13245586; PCID126540; PCID5271805; PCID11765182;
PCID12004532; PCID362562; PCID4986629 PCID11801102;
PCID10423880; PCID513197; 2; PCID65064; PCID44254876;
PCID15840592; PCID151670; PCID5281614; PCID21578577;
PCID46879996; PCID455251; PCID5280373; PCID10393772;
PCID21147013; PCID156707; PCID5471311; PCID10455035;
PCID45268827; PCID629965; PCID5280443; PCID10575105;
PCID11982641; PCID639665; PCID5281703; PCID10315196;
PCID10812923; PCID471688; PCID9988230; PCID10498462;
PCID44259518; PCID443652; PCID9985898; PCID42607927;
PCID13886678; PCID159287; PCID5281222; PCID10453852;
PCID10335676; PCID114829; PCID9829786; PCID10336729;
PCID14542255; PCID179651; PCID5281599; PCID10664858;
PCID44259641; PCID378567; PCID5280442; PCID11033908;
PCID10406203; PCID471694; PCID6482487; PCID10761665;
PCID15838767; PCID471695; PCID5322078; PCID46939793;
PCID10250777; PCID440735; PCID5321865; PCID42607849;
PCID14282776; PCID159029; PCID5281605; PCID10424762;
PCID10364206; PCID638278; PCID5281600; PCID44254875;
PCID42608135; PCID145659; PCID5319813; PCID46939887;
PCID10436583; PCID442826; PCID10348279;

| | | | | |
|---|---|---|---|---|
| | PCID44258230; | PCID390362. | PCID5318889; PCID5321864; | |
| Terpenoids (N=63) | PID10014355; PCID5281672; PCID10243131; PCID10327653; PCID10369667; PCID10445633; PCID10466743; PCID11120895; PCID11474040; PCID11954143; PCID12305935; PCID14165733; PCID14335960; PCID52947022; PCID52947048; PCID46912852; | PCID3503; PCID6654; PCID10114; PCID17100; PCID72421; PCID73170; PCID73296; PCID91458; PCID119034; PCID159573; PCID181183; PCID289984; PCID442360; PCID455262; PCID457901; PCID469744; | PCID472768; PCID500219; PCID470259; PCID588303; PCID636756; PCID3034821; PCID5281520; PCID5282108; PCID5318379; PCID5319791; PCID6444377; PCID6479753; PCID6506231; PCID9950773; PCID9974918; PCID9977821. | PCID15432541; PCID16401759; PCID21577087; PCID21597452; PCID42607999; PCID44555454; PCID44566526; PCID44566960; PCID44607275; PCID44607276; PCID44607277; PCID46186370; PCID46186371; PCID46186620; PCID46186621; |

**Table 4.3** Comparative interaction of standard ligands and predicted lead compound with ϒ-Secretase active site

| **Residues** | **4B5** | **DAPT** | **BD** | **Interaction of amino acids with ligands** |
|---|---|---|---|---|
| Leu275, Leu54, Leu158, Ala159, Phe57, Val215, Met218, Met216, Val138, Ile222, Met223, Ile134 | √ | √ | √ | Hydrophobic bond with 4B5, DAPT and BD |
| Tyr 161 | √ | √ | √ | Hydrogen bonds with 4B5<br>Hydrophobic bond with DAPT and BD |
| Ile226, Phe50, Phe142 | - | √ | √ | Hydrophobic bonding with DAPT and BD only |
| Ile51, Leu55, Phe79, Leu61, Ala75, Leu62, Phe72 | √ | - | - | Hydrophobic bonding with 4B5 only |
| Ala80, Leu81 | - | - | √ | Hydrophobic bonding with BD only |

4B5=N-{(2R,4S,5S)-2-benzyl-5-[(tert-butoxycarbonyl)amino]-4-hydroxy-6-phenylhexanoyl}-L-leucyl-L-phenylalaninamide; BD=Bulbineloneside D; DAPT= N-[N-(3,5-Difluorophenacetyl-L-alanyl)]-(S)-phenylglycine t-butyl ester; √=Presence.

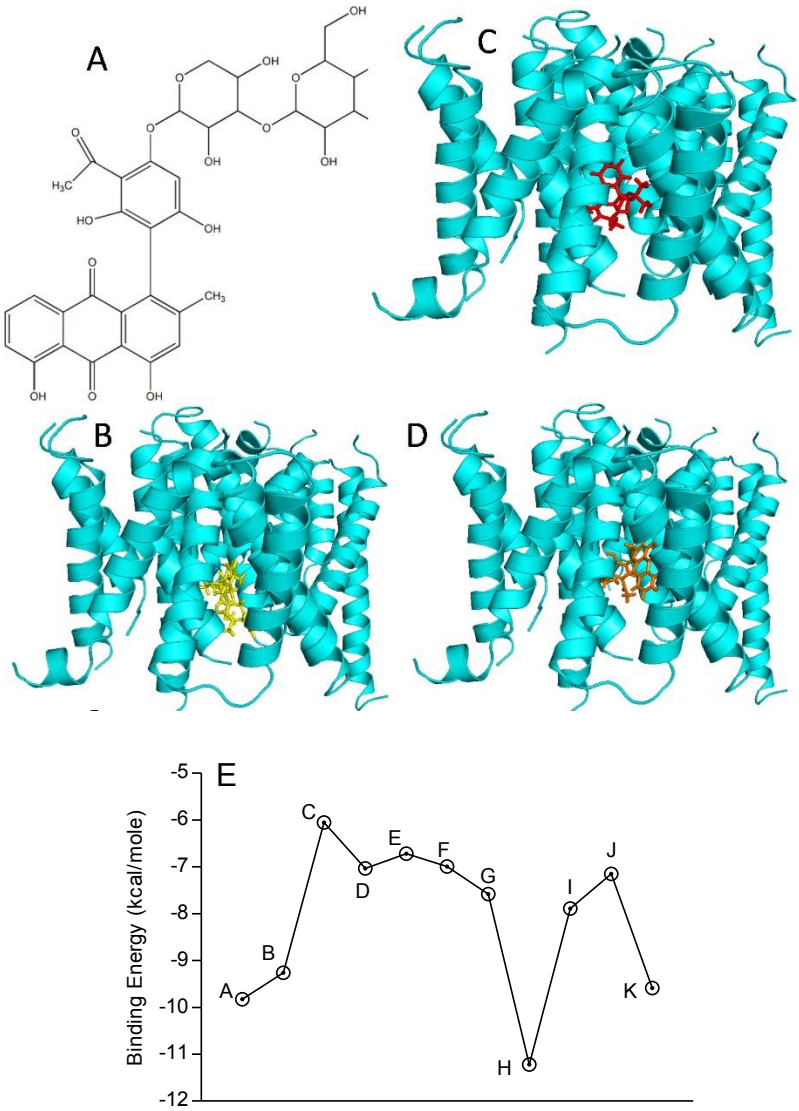


**Figure 4.2** Gamma-secretase inhibitory potential and binding energy of standard and lead identified molecule. Literature-based identified *B. frutescens* phytochemicals were used for *in silico* docking study against ϒ-Secretase protein. Detailed methodology and software used for the study are given the methodology section. (A) 2D **s**tructure of the lead compound bulbineloneside D (B) Interaction pattern of 4B5 ligand with ϒ-Secretase protein (C) Interaction pattern of DAPT with ϒ-Secretase protein (D) Interaction pattern of ϒ-Secretase with bulbineloneside D (PCID-10008440) (E) Binding energy score of different *B. frutescens* phytochemicals with ϒ-secretase protein. Alphabets A to K in the graph represents standard inhibitor and test ligands.

4B5- N-{(2R,4S,5S)-2-benzyl-5-[(tert-butoxycarbonyl)amino]-4-hydroxy-6-phenylhexanoyl}-L-leucyl-L-phenylalaninamide; A-N-{(2R,4S,5S)-2-benzyl-5-[(tert-butoxycarbonyl)amino]-4-hydroxy-6-phenylhexanoyl}-L-leucyl-L-phenylalaninamide; B-DAPT; C- Isofuranonapthoquinone; D-Joziknipholone A; E-Joziknipholone B; F- Knipholone; G- Gaboroquinone B; H- Bulbineloneside D; I-Gaboroquinone A; J- Isoknipholone; K- 4'-Demethylknipholone 2'-β-D-glucopyranoside

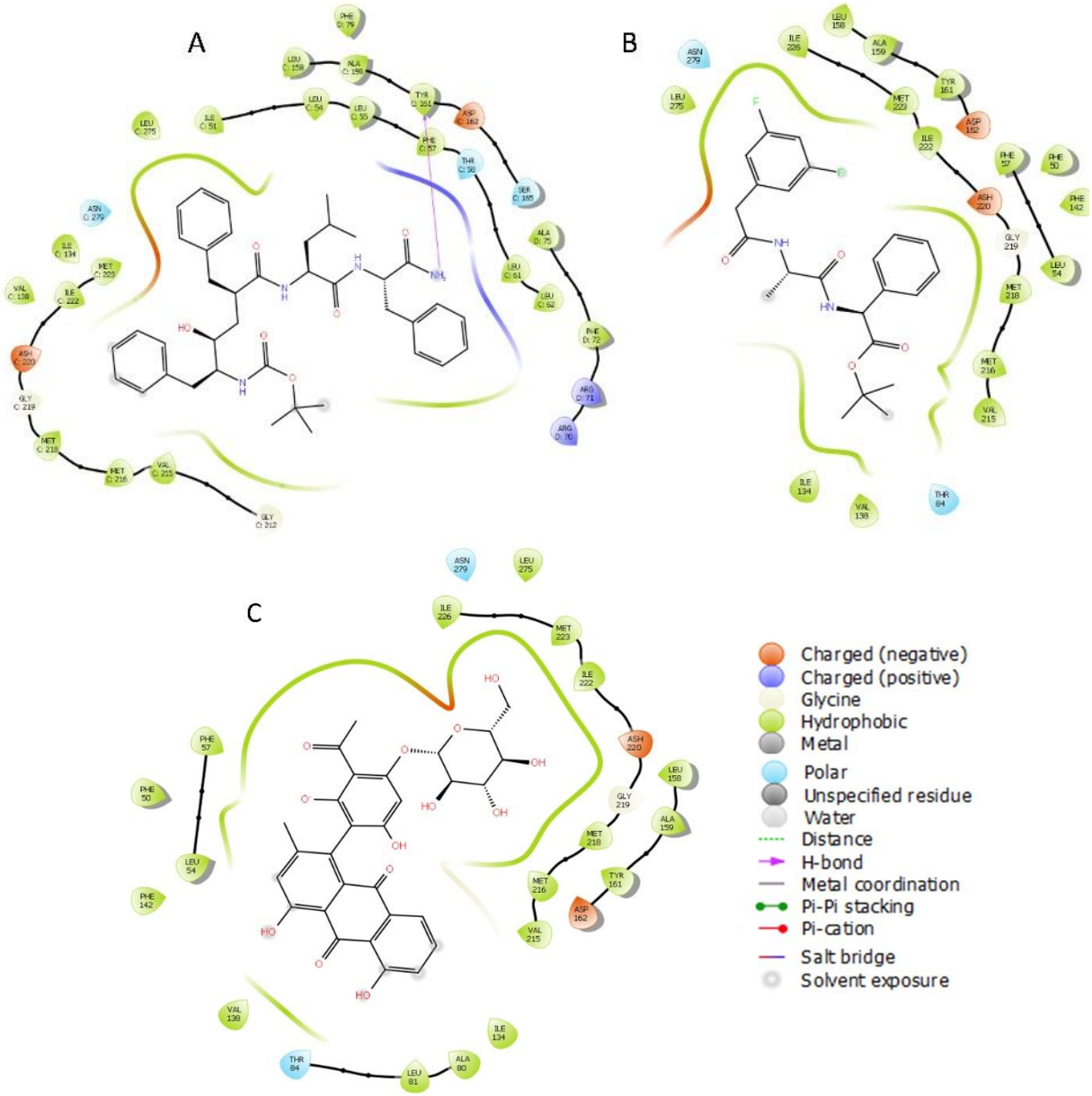


**Figure 4.3** Representation of interactive residues of ϒ-secretase with inhibitor (A) N-{(2R,4S,5S)-2-benzyl-5-[(tert-butoxycarbonyl)amino]-4-hydroxy-6-phenylhexanoyl}-L-leucyl-L-phenylalaninamide (B) DAPT (C) Bulbineloneside D

Various phytochemical libraries and databases were scanned to find novel natural ϒ-secretase inhibitors (GSIs). The study identified two potential inhibitors, Kurarinone and 3-O-(E)-p-Coumaroylbetulinic acid (CB) out of 349 phytochemical screened **(Table 4.2)**. The identified GSIs are natural occurring flavanone (Kurarinone) and triterpene (CB).

The lowest energy conformation, representing the best binding structure of inhibitors (KU and CB) to the receptor (Ɣ-secretase, PDB ID:4Y6K), was identified by the molecular docking procedure. Information about factors such as hydrogen bonds, salt bridges, metal interactions, lipophilic interactions, π-π, and π-cation interactions was generated in the protein-ligand interaction profiles.

The interaction pattern of Kurarinone and Ɣ-secretase protein is depicted in **figure 4.4.** In the present study, PCID11982640 (Kurarinone) showed similar Gscore (-8.3 kcal/mol) for Ɣ-secretase as compared to DAPT (-8.74 kcal/mol). Protein-ligand interaction revealed that Ala159, Ala75, Arg71, Asp220, Gly219, Leu158, Leu275, Met216, Met223, Phe57, Phe72, and Tyr161 amino acid residues of Ɣ-secretase involved in the hydrophobic interactions with the Kurarinone **(Figure 4.4 B)**. In addition, amino acid Thr58 involved in hydrogen bond at the active site of Ɣ-secretase. Moreover, protein-ligand interactions of Ɣ-secretase with the DAPT showed that Asp220, Ile222, Ile226, Leu158, Leu54, Met216, Met218, Met223, Phe142, Phe50, and Val138, involved in the hydrophobic interactions **(Figure 4.4 C).**

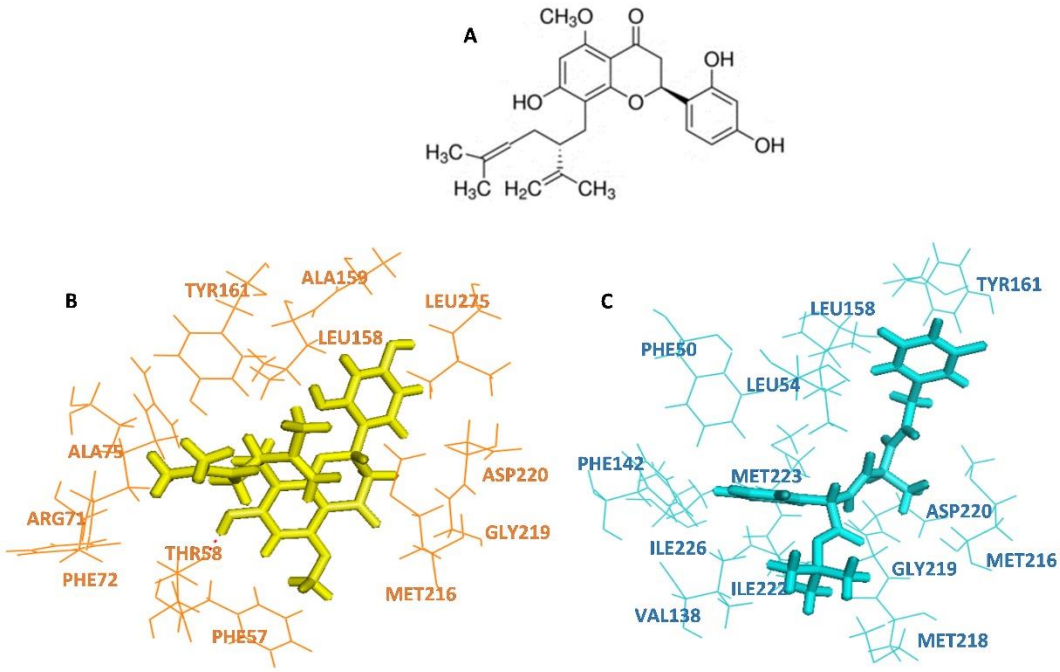


**Figure 4.4** Kurarinone structure and their interaction pattern with the gamma-secretase enzyme. Kurarinone was used for *in silico* docking study against Ɣ-Secretase protein. Detailed methodology and software used for the study are given the methodology section. (A) 2D **s**tructure of the Kurarinone (B) Interaction pattern of Kurarinone ligand with Ɣ-Secretase protein (C) Interaction pattern of DAPT with Ɣ-Secretase protein.

The interaction pattern of CB (3-O-(E)-p-Coumaroylbetulinic acid) and Ɣ-secretase protein are depicted in **figure 4.5.** In our study, 3-O-(E)-p-Coumaroylbetulinic acid (PCID6479753) showed similar Gscore (-8.59 kcal/mol) for Ɣ-secretase as compared to DAPT (-8.69 kcal/mol). Protein-ligand interactions revealed that Val138, Phe142, Ile226, Ile222, Phe50, Met218, Met223, Gly219, Leu54, Asp220, Leu158, Met216, and Tyr161 amino acid residues of Ɣ-secretase were involved in the hydrophobic interactions with the CB **(Figure 4.5 B)**. Protein-ligand interaction of Ɣ-secretase with the DAPT showed that Met53, Phe50, Leu54, Thr58, Ile226, Leu61, Met223, Gly219, Met216, and Val215 involved in the hydrophobic interactions **(Figure 4.5 C).**

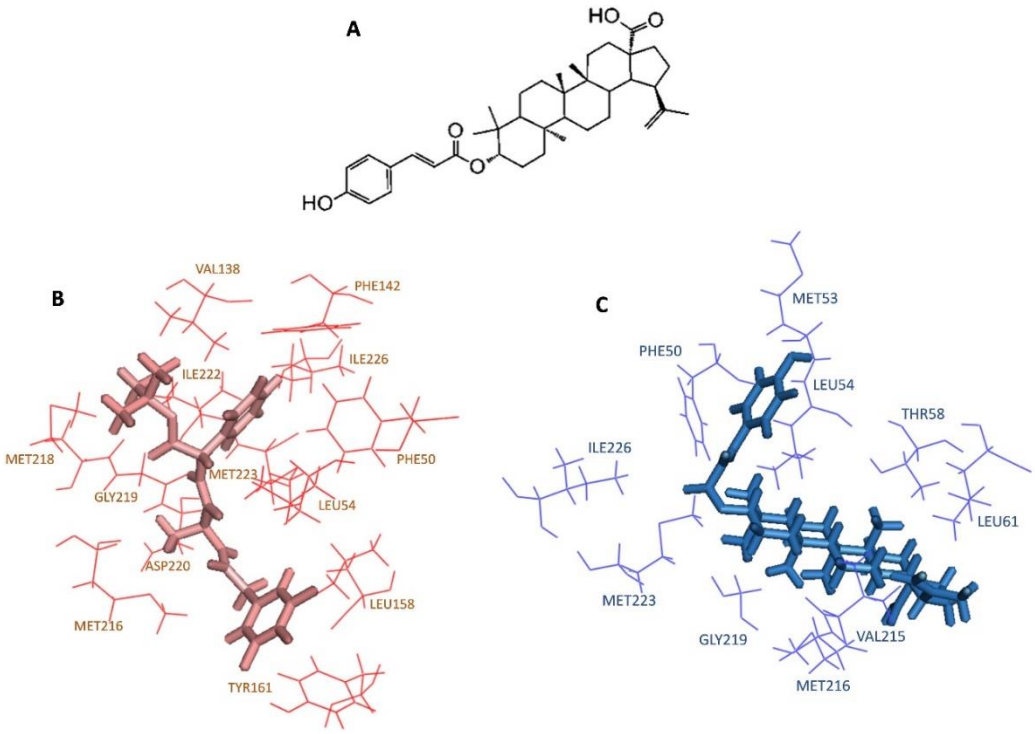


**Figure 4.5** The 3-O-(E)-p-Coumaroylbetulinic acid structure and their interaction pattern with the gamma-secretase enzyme. CB was used for *in silico* docking study against Ɣ-Secretase protein. Detailed methodology and software used for the study are given in the methodology section. **(A)** 2D **s**tructure of the 3-O-(E)-p-Coumaroylbetulinic acid **(B)** Interaction pattern of CB ligand with Ɣ-Secretase protein **(C)** Interaction pattern of DAPT with Ɣ-Secretase protein.

ADME/T (absorption, distribution, metabolism, elimination and toxicity,) properties of Kurarinone and CB (3-O-(E)-p-Coumaroylbetulinic acid) were assessed through the Qikprop application of Maestro 9.6. Both the inhibitors (KU and CB) were found to be encouraging based on their docking free energy score (Gscore) and ADME/T

properties. Kurarinone and CB showed satisfactory QPPCaco, QPPMDCK, percentage of human oral absorption, QPlogPo/w, QPlogHERG $K^+$ channels, QPlogBB, QPlogKP, QPlogKhsa values that fulfill the Lipinski's rule of five. Therefore, structural modifications and optimization in KU and CB are not required to improve their ADME/T properties.

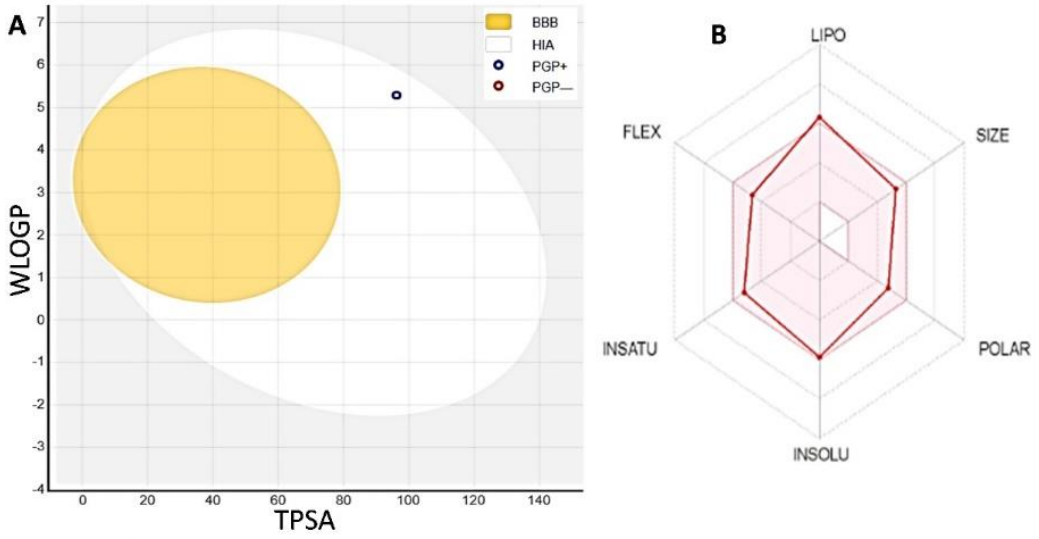


**Drug-like properties**

- QPlogPo/w 4.236
- QPlogS -5.182
- ClQPlogS -6.487
- QPlogHERG -4.743
- QPPCaco 372.956
- QPlogBB -1.365
- QPPMDCK 170.358
- QPlogKp -2.845
- QPlogKhsa 0.703

**Structural and physiochemical Properties**

- Mol MW 438.519
- Dipole 4.376
- SASA 697.537
- FOSA 383.265
- FISA 150.189
- PISA 164.083
- Volume 1357.258
- Donor HB 3
- Accept HB 5.75

**Figure 4.6** Drug likeness property of Kurarinone predicted by various online tools. (A) Egg model generated by SwissADME online tool showing potential to cross the blood-brain barrier (BBB), hydrogen acceptor (HA), p-glycoprotein inhibitor/non-inhibitor (+/-). (B) The Bioavailability Radar of Kurarinone predicted by SwissADME online server. Further drug like properties, structural and physiochemical properties of Kurarinone predicated by the online tool is given in the figure.

The color zone of the bioavailability radar dictates suitable physicochemical space for oral bioavailability where the following properties were taken into consideration as flexibility, lipophilicity, saturation, size, polarity, and solubility. **Figure 4.6** and **figure 4.7** showed the bioavailability radar of KU and CB respectively. The physicochemical

properties showed that KU and CB showed 5.75 and 4.75 hydrogen bond acceptors and 3 and 2 hydrogen bond donor respectively. The QPlog Po/w, QPlogS, CIQPlogS, CPlogHERG, QPlogBB, QPlogKp and QPlogKhsa of KU and CB are represented in **figure 4.6** and **figure 4.7** respectively. From the log P values overall it can be concluded that the compounds have good lipophilic character.

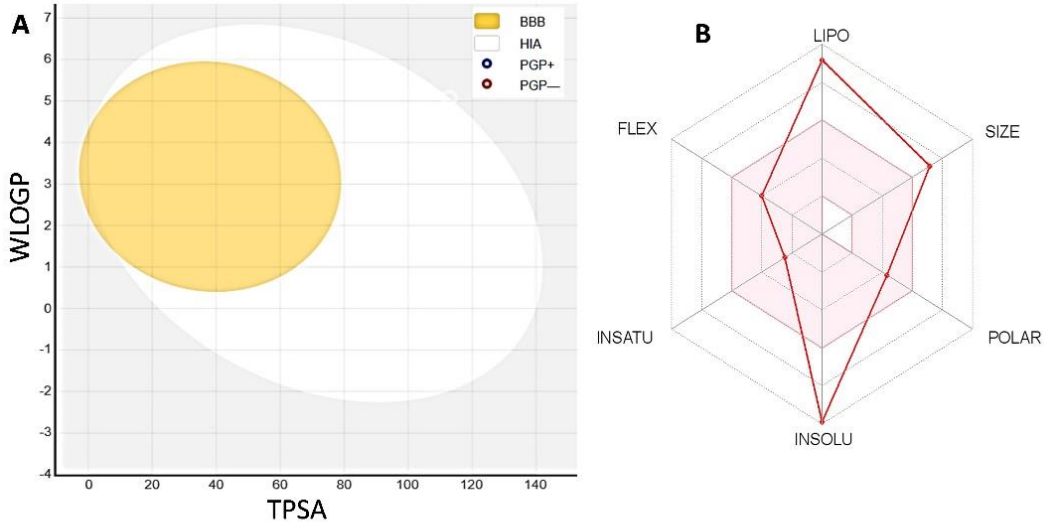


**Drug-like properties**

- QPlogPo/w 8.488
- QPlogS -10.025
- CIQPlogS -9.791
- QPlogHERG -4.112
- QPPCaco 96.345
- QPlogBB -1.459
- QPPMDCK 50.168
- QPlogKp -2.886
- QPlogKhsa 2.203

**Structural and physiochemical Properties**

- Mol MW 602.853
- Dipole 3.485
- SASA 924.043
- FOSA 572.438
- FISA 149.285
- PISA 202.32
- Volume 1849.154
- Donor HB 2
- Accept HB 4.75

**Figure 4.7** Drug likeness property of CB predicted by various online tools. (A) Egg model generated by SwissADME online tool showing potential to cross the blood-brain barrier (BBB), hydrogen acceptor (HA), p-glycoprotein inhibitor/non-inhibitor (+/-). (B) The Bioavailability Radar of CB predicted by SwissADME online server. Further drug-like properties, structural and physiochemical properties of CB predicated by the online tool is given in the figure.

The pharmacokinetic properties were studied using the boiled egg model. The model allows for intuitive evaluation of passive gastrointestinal absorption (HIA) and brain penetration (BBB) in the function of the position of the molecules in the WLOGP-versus-TPSA referential (**Figure 4.6** and **Figure 4.7**). The white region is for the high probability of passive absorption by the gastrointestinal tract, and the yellow region

(yolk) is for the high probability of brain penetration. Yolk and white areas are not mutually exclusive. Kurarinone molecule falling in the egg white region representing its highly absorptive potential in the intestine. CB molecule was unable to fall on the studied model.

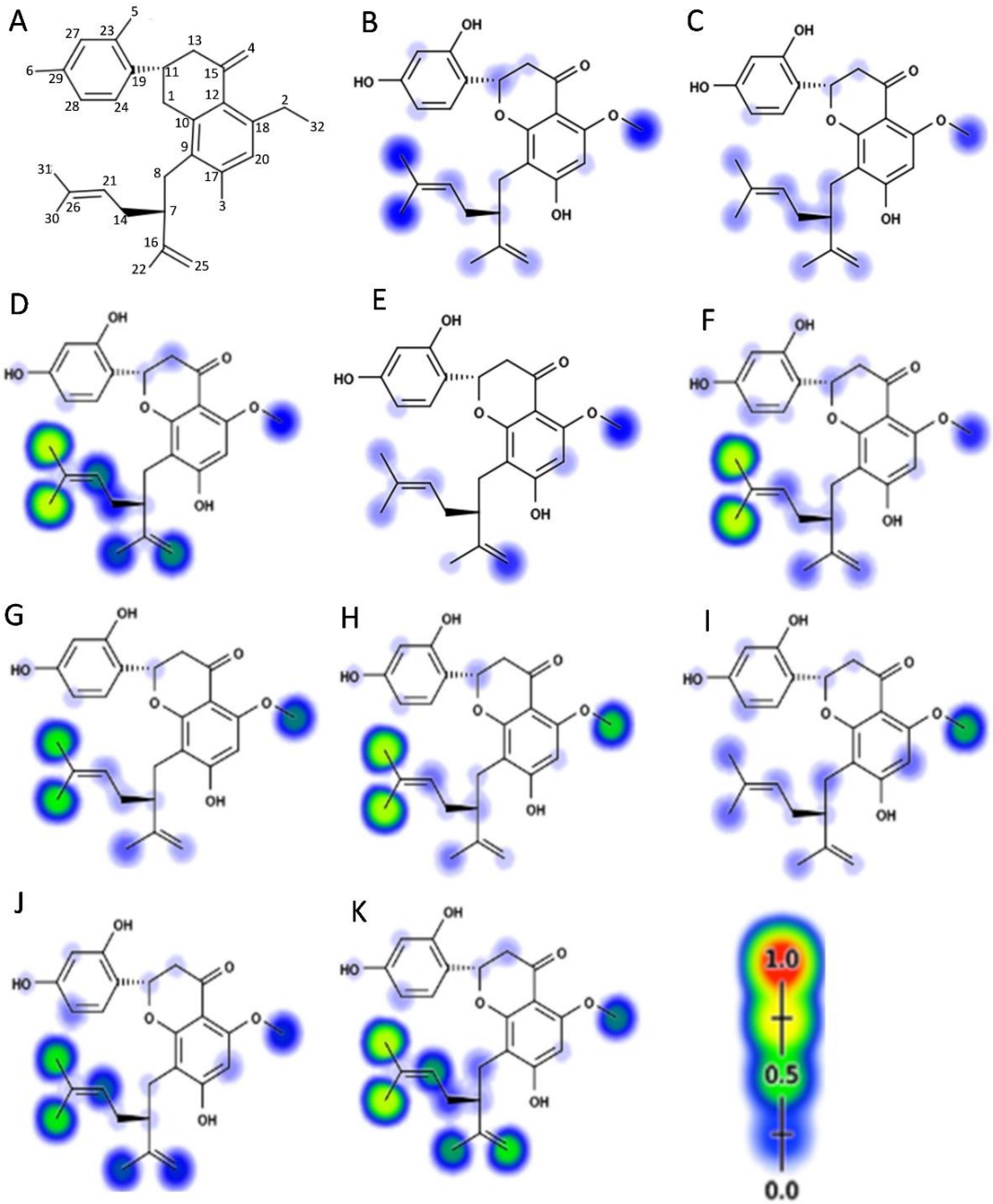


**Figure 4.8** Kurarinone xenosite prediction for the evaluation of metabolic toxicity. A=Kurarinone; B=CYP1A2; C= CYP2A6; D= CYP3A4; E= CYP2B6; F= CYP2C8; G= CYP2C9; H= CYP2C19; I= CYP2D6; J= CYP2E1; K= HLM (Human Liver Microsome)

CYP450 interactions analysis with KU and CB showed that the inhibitors are non- toxic in nature. Results showed less potential of toxicity attributed to active sites (**Figure 4.8** and **Figure 4.9**).

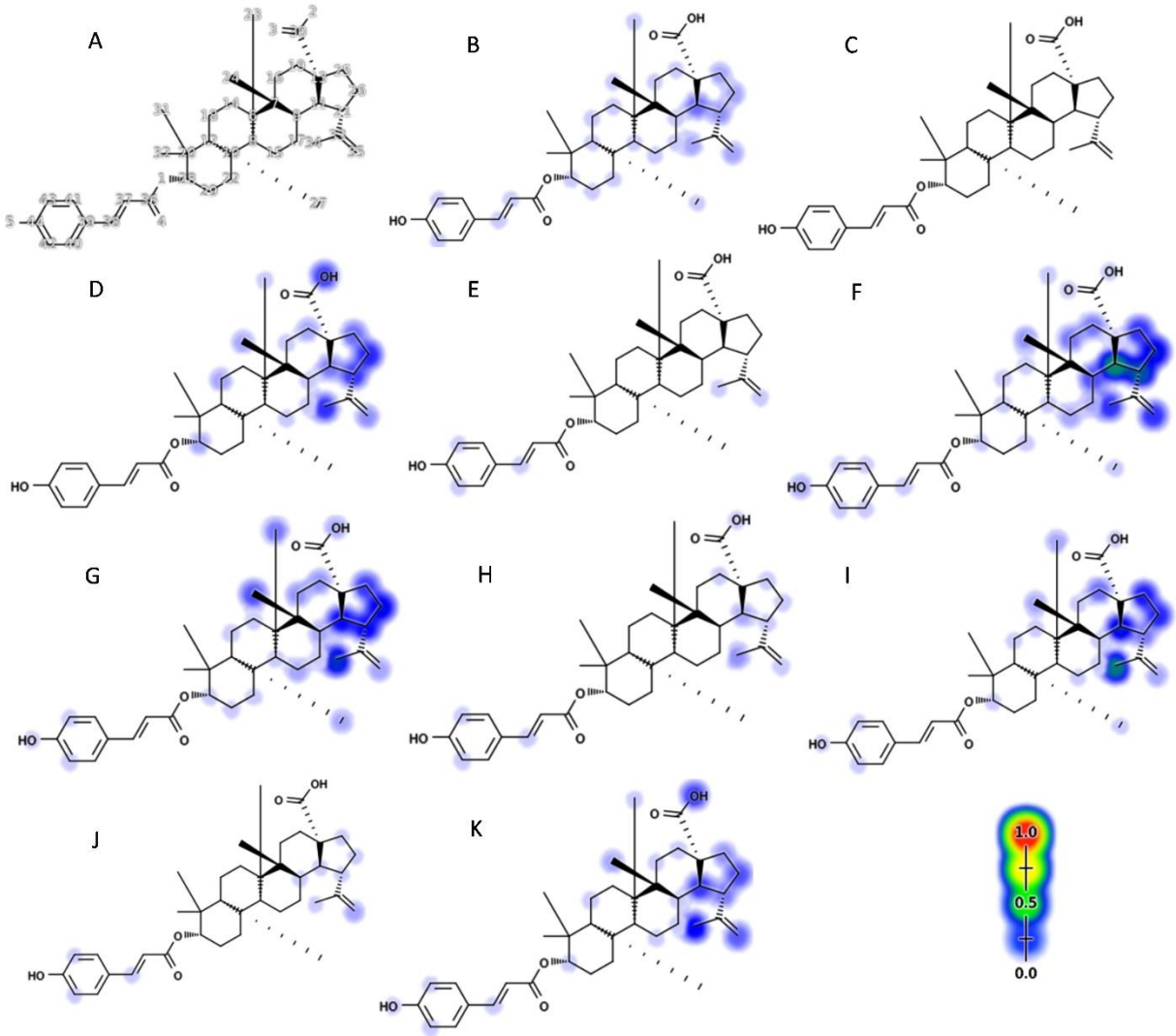


**Figure 4.9** 3-O-(E)-p-Coumaroylbetulinic acid xenosite prediction for the evaluation of metabolic toxicity. A=CB; B=CYP1A2; C= CYP2A6; D= CYP3A4; E= CYP2B6; F= CYP2C8; G= CYP2C9; H= CYP2C19; I= CYP2D6; J= CYP2E1; K= HLM (Human Liver Microsome)

## 4.2 *In silico* validation of lead compounds by molecular dynamics simulation

Interaction of Kurarinone with Ɣ-secretase protein was studied using molecular dynamics (MD) simulation method. RMSD analyses were carried out for the Ɣ-

secretase protein (PDB ID: 4Y6K) in the presence and absence of KU for 18 ns and 300K. Change in RMSD values with each nanosecond is depicted in **figure 4.10 A-B**.

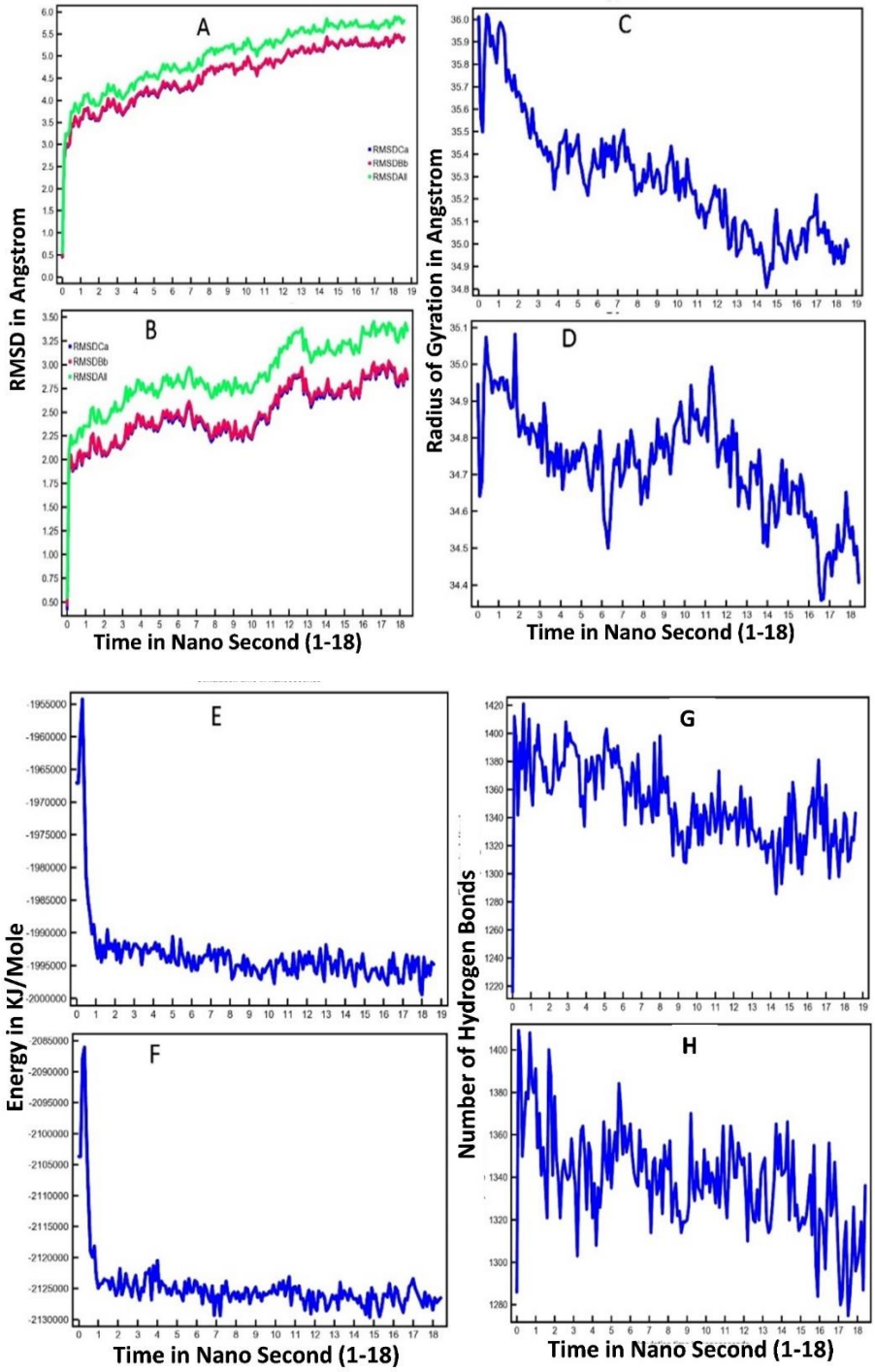


**Figure 4.10** Molecular simulation of Kurarinone and ϒ-secretase.
Root mean square deviations (RMSD) correspond to >18 ns MD simulation at 300 K. (A) Figure indicates ϒ-secretase protein without KU (B) Figure indicates ϒ-secretase protein with KU.
The radius of gyration corresponds to >18 ns MD simulation at 300 K. (C) Figure indicates ϒ-secretase protein without KU (D) Figure indicates ϒ-secretase protein with KU.

The potential energy of the system. (E) Potential energy and graph of Ɣ-secretase protein calculated during >18 ns MD simulations (F) Potential energy and graph of Ɣ-secretase-KU complex calculated during >18 ns MD simulations.
Hydrogen bond analysis. (G) Ɣ-secretase H-bonds for the entire duration of the simulation. (H) Number of intra-protein hydrogen bonds (presence of KU).

The Ɣ-secretase protein alone attained equilibrium at 0.55 nm (5.5 Å) at 18ns whereas the Ɣ-secretase-KU complex attained equilibrium at 0.325 nm (3.25 Å) at 18ns. Ɣ-secretase-KU complex showed a comparatively lower RMSD value than the protein without ligand (KU). To analyze the overall compactness of Ɣ-secretase protein in the presence or absence of KU, Radius of gyration (Rg) was calculated. As depicted in **figure 4.10 C-D**, Rg value of Ɣ-secretase protein fluctuated near 36Å and decreased to a minimum value of 34.5 Å, whereas the Ɣ-secretase-KU complex the fluctuation was near 36.1 Å, and decreased to a minimum value of 34.4 Å. Thus, Rg values for protein (Ɣ-secretase) alone and in protein-ligand (Ɣ-secretase-KU) complex were similar. Hydrogen bond interactions play a crucial role in the overall stability of the protein structure. In the present study, MD simulation was performed to assess the extent of intermolecular hydrogen bond formation potential of KU with Ɣ-secretase and the results are shown in **figure 4.10 G-H**.

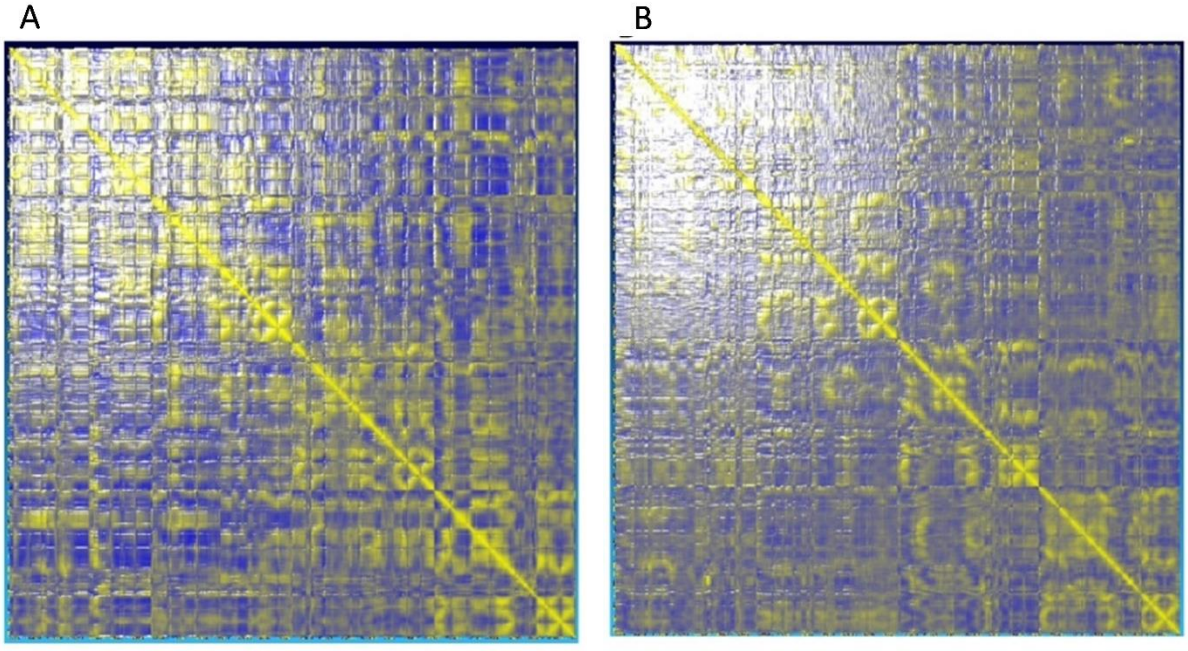


**Figure 4.11** Domain cross-correlation matrix (DCCM) analysis for the two systems. (A) Ɣ-secretase (B) Ɣ-secretase-KU complex

The analysis illustrated that Ɣ-secretase-KU complex formed many intermolecular hydrogen bonds throughout the simulation. Domain cross-correlation matrix (DCCM) analysis was performed to assess the changes in the secondary structure of the protein, prior to and after the binding of the ligand. As shown in **figure 4.11 A-B**, the results of DCCM analysis showed that the global dynamics of the two systems (protein alone and protein-ligand complex) were very similar to each other. The potential energy of the system was stable throughout the simulation indicating that no abnormal behavior occurred in the protein after the binding of KU **(Figure 4.10 E-F).**

## 4.3 Breast cancer cell proliferation inhibition potential of identified natural products

### 4.3.1 Cell viability assay

Cytotoxic potential of identified lead natural products/phytochemicals were studied using cell viability assay in breast cancer cells (MDA-MB-231 and T47D) at different concentration and time interval. GraphPad Prism software was used perform the regression analysis to study the effect of identified lead natural products/phytochemicals in breast cancer cells in 24h, 48h and 72h treatment.

Polar (methanol) and non-polar (hexane) extracts of *B. frutescens* were tested for their potential to inhibit breast cancer cell proliferation using MTT assay. The experiment was used to find a basis for the characterization of *B. frutescens* extracts induced a cellular response in two different breast cancer cell lines (MDA-MB-231 and T47D cell lines) models. Dose- and time-dependent antiproliferative property of BME and BHE extract was found in MDA-MB-231 and T47D cell lines **(Figure 4.12 A-D)**. BME extract showed ≈53% inhibition in MDA-MB-231 and T47D cell lines at 10 µg/ml concentration in 24h treatment. BHE extract showed about 75% and 63% inhibition in MDA-MB-231 and T47D cell lines respectively at 10 µg/ml concentration in 24h. BHE extract showed similar efficacy (about 33-37% viability) at higher concentration (70 and 100 µg/ml) in MDA-MB-231 cells in 48h and 72h.

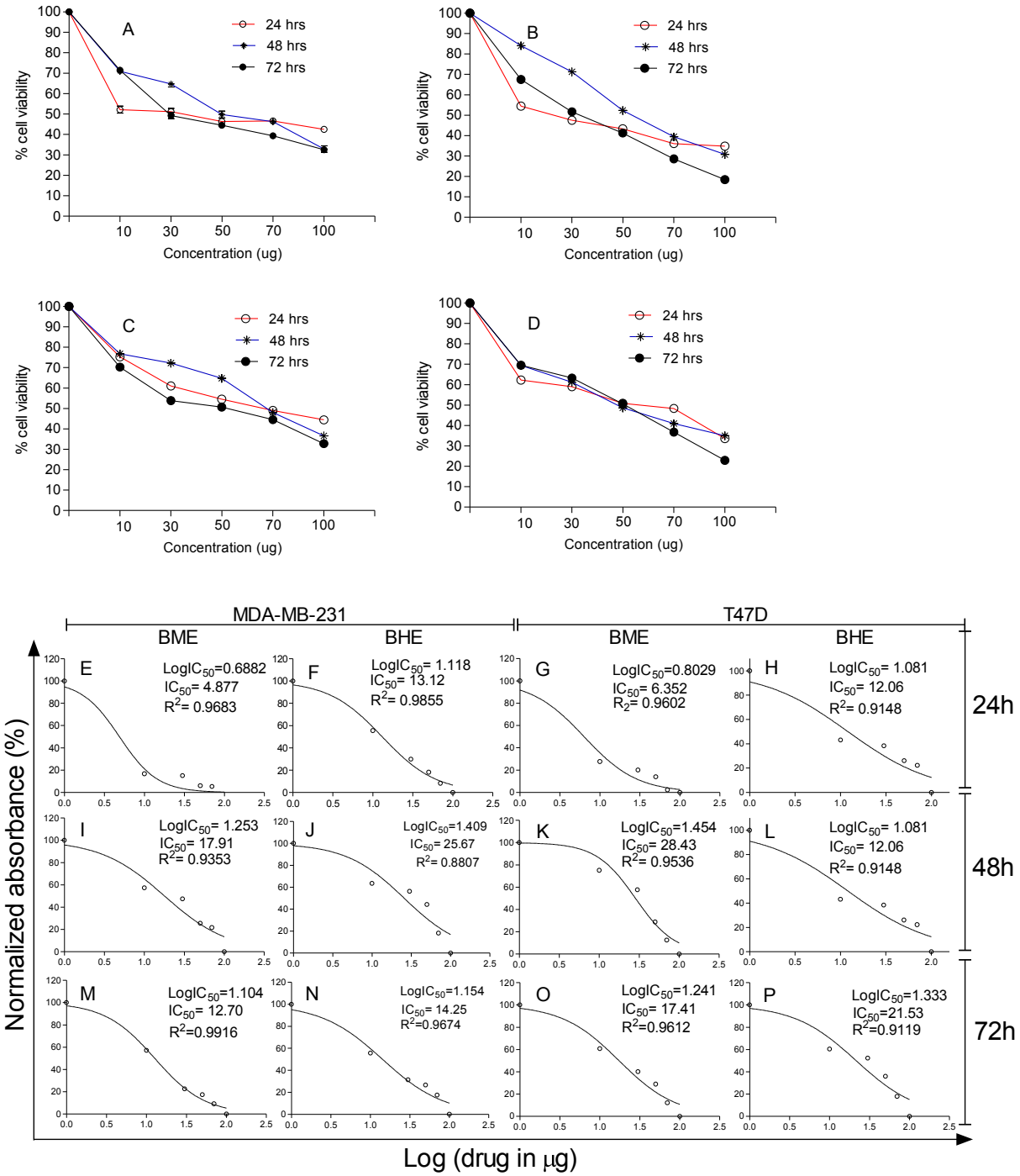


**Figure 4.12** Effect of *B. frutescens* extracts on human breast cancer cell proliferation and regression analysis using MTT assay. **(**A) *B. frutescens* methanolic extract efficacy on MDA-MB-231 breast cancer cell proliferation. B) *B. frutescens* methanolic extract efficacy on T47D breast cancer cell proliferation. C) *B. Frutescens* hexane extract efficacy on MDA-MB-231 breast cancer cell proliferation and D) *B. frutescens* hexane extract efficacy on T47D breast cancer cell proliferation. (E) – (P) Representation of $IC_{50,}$ Log $IC_{50}$ values and regression analysis of the effect of BME and BHE extract (10, 30, 50, 70 and 100 µg/ml) in MDA-MB-231 and T47D cells in different time interval (24, 48 and 72h) treatment. Results are expressed as mean±SD.

At 100 µg/ml concentration BHE extract showed comparatively lesser cell viability in T47D cells in 72h. Approximately similar patterns of cell viability were observed in the presence of the BME extract in MDA-MB-231 and T47D cell lines at 100 µg/ml in 72h. $IC_{50}$ value calculation and regression analysis were done using GraphPad Prism software to study the effect of BME and BHE extract treatment in MDA-MB-231 and T47D cells in 24h, 48h and 72h treatment **(Figure 4.12 E-P)**. The calculations were based on the MTT results obtained after the test extract treatment in MDA-MB-231 and T47D cells at different time intervals. BME and BHE extract showed 4.877 µg and 13.12 µg $IC_{50}$ value in MDA-MB-231 cells in the initial 24h treatment. Similarly, BME and BHE extract showed 6.35 µg and 12.08 µg $IC_{50}$ value in T47D cells in the initial 24h treatment **(Figure 4.12 G-H)**. Regression analysis of different experimental setup showed the $R^2$ values in the range of 0.9119-0.9916 **(Figure 4.12 E-P)**.

Anticancer properties of Kurarinone (KU) in breast cancer cells was tested in MDA-MB-231 and T47D cell lines using MTT assay. The experiment was used to characterize the KU induced cellular response in two different breast cancer cell line models. Dose- and time-dependent antiproliferative property of KU was found in MDA-MB-231 and T47D cell lines **(Figure 4.13 A-B)**. KU showed about 78% and 80% inhibition in MDA-MB-231 and T47D cell lines at the lowest test concentration (1 µM) in 24h treatment. KU showed similar efficacy (about 30-31% viability) at higher (25 µM) concentration in both MDA-MB-231 and T47D cells in 72h treatment. At 1 µM concentration, KU showed comparatively lesser cell viability in T47D cells in 72h.

$IC_{50}$ value calculation and regression analysis were done using GraphPad Prism software to study the effect of Kurarinone treatment in MDA-MB-231 and T47D cells in 24h, 48h and 72h treatment **(Figure 4.13 C-H)**. The calculations were based on the MTT results obtained after the KU treatment in MDA-MB-231 and T47D cells at different time intervals. KU showed 2.87 µM $IC_{50}$ value in MDA-MB-231 cells in the initial 24h treatment. In T47D cells, KU showed 3.423 µM $IC_{50}$ value in the initial 24h treatment. Regression analysis of different experimental setup showed the $R^2$ values in the range of 0.9070-0.9717 **(Figure 4.13 C-H)**.

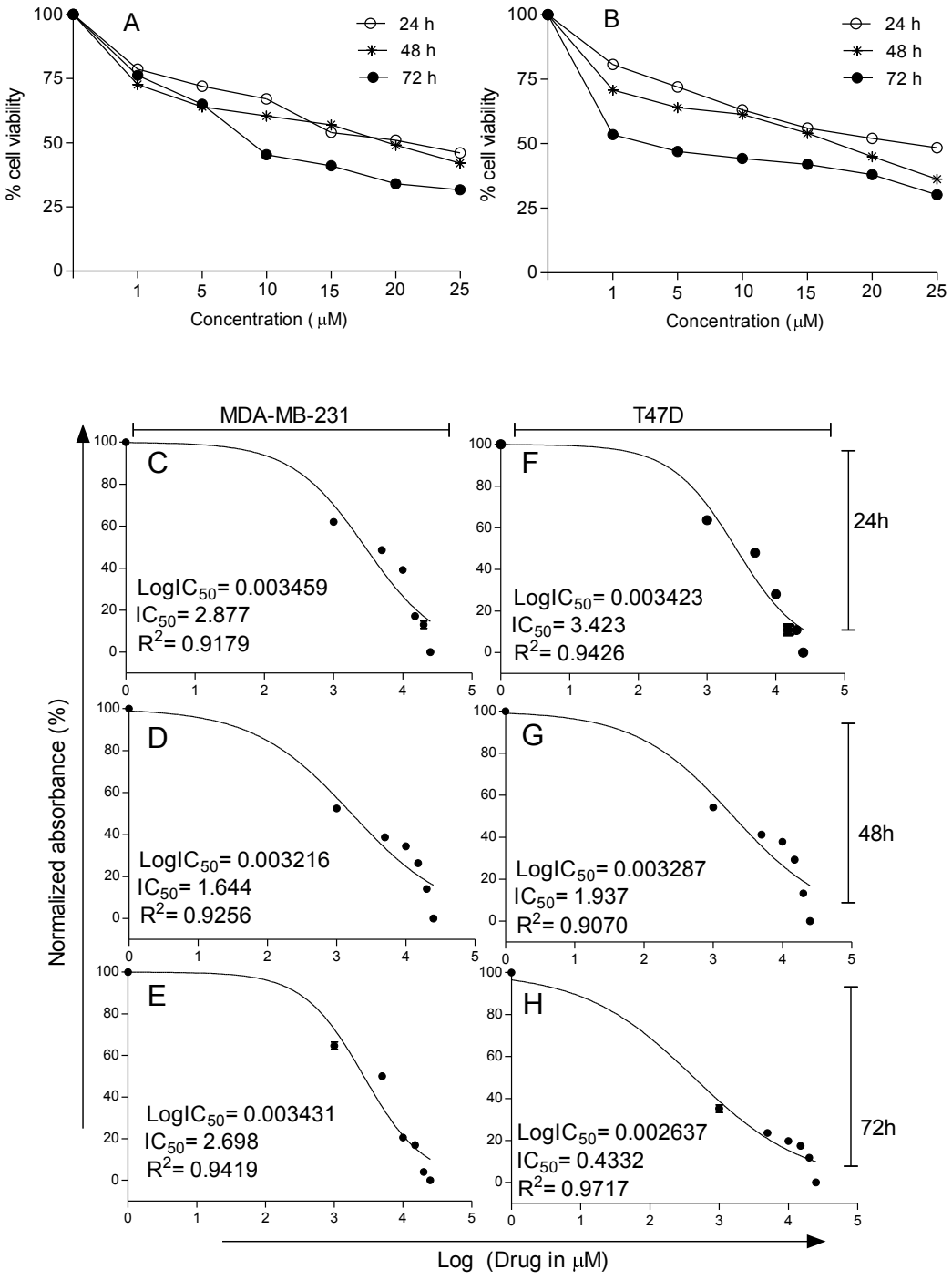


**Figure 4.13** Effect of Kurarinone on breast cancer cell proliferation and regression analysis using MTT assay. (A) and (B) Kurarinone efficacy on MDA-MB-231 and T47D breast cancer cell proliferation respectively at different time intervals. (C) – (H) Representation of $IC_{50}$, Log $IC_{50}$ values and regression analysis of the effect of Kurarinone (1, 5, 10, 15, 20 and 25 μM) in MDA-MB-231 and T47D cells in different time interval (24, 48 and 72h) treatment. Results are expressed as mean±SD of the three replicates.

Cytotoxic potential of CB against breast cancer cells (MDA-MB-231 and T47D) was also evaluated by MTT assay. The experiment was conducted to characterize the CB induced cytotoxicity in breast cancer cell line models. Dose-and time-dependent antiproliferative property of CB was observed in both cells **(Figure 4.14 A-B)**. CB showed ≈55% and ≈52% inhibition in MDA-MB-231 and T47D respectively at the higher test concentration (25 µM) in 24h treatment. CB showed similar efficacy (about 38-36% viability) at higher (25 µM) concentration in both MDA-MB-231 and T47D cells in 72h treatment. At 1 µM concentration, CB produced comparatively lesser cell viability in T47D cells in comparison to MDA-MB-231 cells in 72h treatment.

Determination of $IC_{50}$ and regression analysis was done by GraphPad Prism software to evaluate the effect of CB treatment against breast cancer cells (MDA-MB-231 and T47D) at 24h, 48h and 72h treatment **(Figure 4.14 C-H)**. The calculations were performed on the basis MTT results obtained after the CB treatment in MDA-MB-231 and T47D cells at different time intervals. CB showed 5.884 µM $IC_{50}$ against MDA-MB-231 cells in the initial 24h treatment. In T47D cells, CB showed 2.708 µM $IC_{50}$ value in the initial 24h treatment. Regression analysis showed the $R^2$ values in the range of 0.8981-0.9365 **(Figure 4.14 C-H)**.

### 4.3.2 Cell cycle analysis

Cell cycle inhibition potential of identified lead natural products/phytochemicals were studied by using several techniques. First of all, the effect of test samples on cell cycle phase distribution was studied by flow cytometry technique in breast cancer cells. Then, cell cycle regulators (cyclin D1, CDK4 and p21) were studied at mRNA levels at $IC_{50}$ concentration of test samples in time dependent manner. Further, cyclin D1, a master cell cycle regulator was studied at protein levels in test sample treated breast cancer cells in time dependent manner.

To understand the underlying mechanism of BME and BHE extract induced cell proliferation we studied the cell cycle distribution in the MDA-MB-231 ($ER^-/PR^-$ breast cancer cell model) and T47D breast cancer cells ($ER^+/PR^+$ breast cancer cell model).

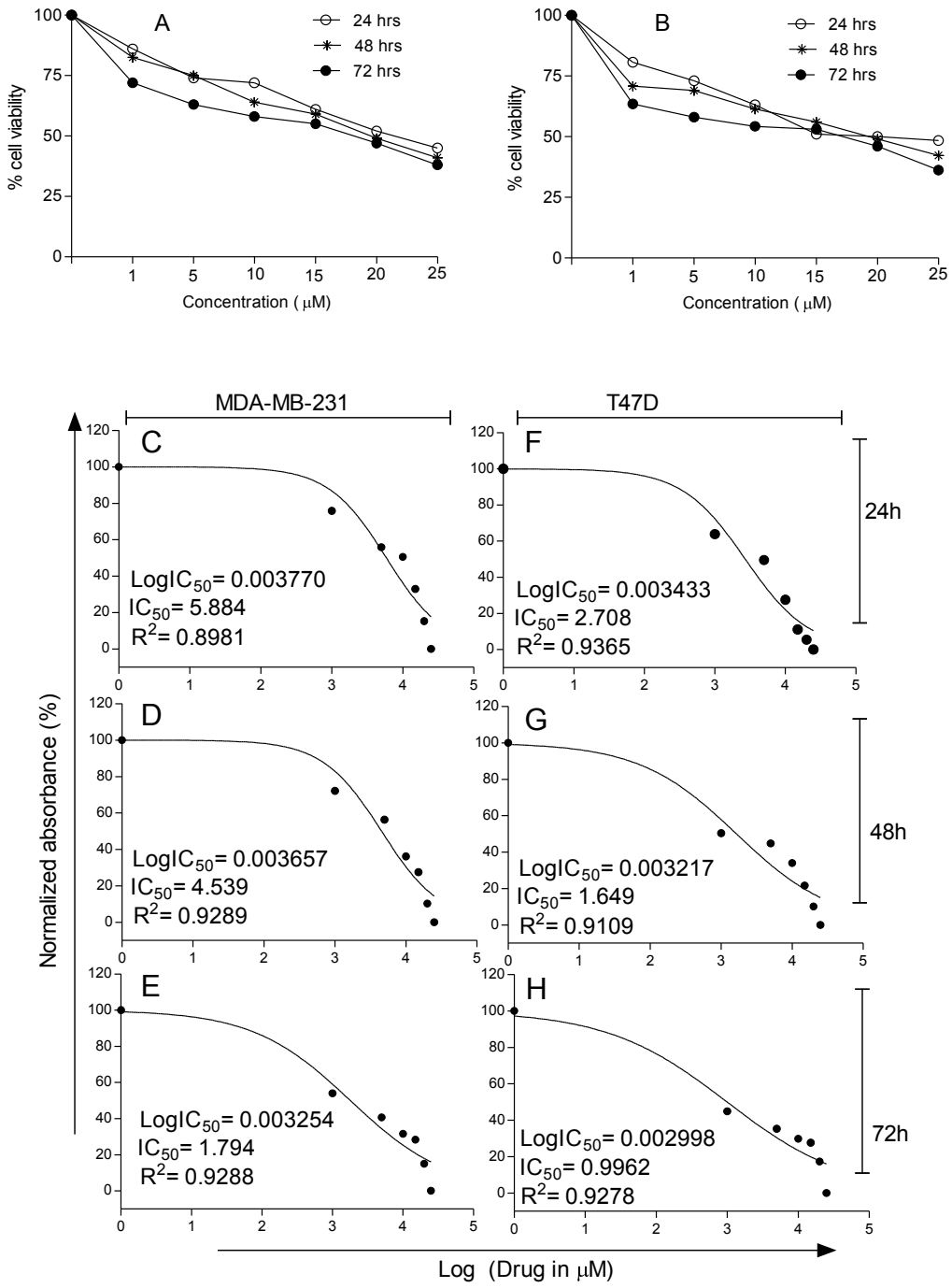


**Figure 4.14** Proliferation and regression analysis of the effect of 3-O-(E)-p-Coumaroylbetulinic acid (CB) on breast cancer cells using MTT assay. (A) and (B) effect of CB on MDA-MB-231 and T47D cell proliferation respectively at 24, 48 and 72h treatment. (C) – (H) Representation of $IC_{50}$, Log $IC_{50}$ values and regression analysis of the effect of CB (1, 5, 10, 15, 20 and 25 μM) in MDA-MB-231 and T47D cells in 24, 48 and 72h treatment. Results are given as mean±SD of the three replicates.

Untreated T47D cancer cells showed 42.33, 8.53 and 21.57% cell distribution in G1, S and G2/M phase of cell cycle respectively **(Figure 4.15 A' and F')**. BME treated T47D cells showed increased levels of G1 cell populations, both in 24h (54.7%) and 48h (51.3%) of the treatment **(Figure 4.15 B'-C')**. Treatment of T47D cells with the BHE extract also showed the similar efficacy of cell cycle arrest in the G1 phase in 24h (55%) and 48h (58%) of the treatment **(Figure 4.15 D'-E')**. It should be noted that BHE extract showed better cell cycle G1 phase arrest (58%) in the $ER^+/PR^+$ breast cancer cell line in 48h treatment **(Figure 4.15 G')**. BME treated MDA-MB-231 cells showed increased levels of G1 cell populations, both in 24h (47%) and 48h (42.33%) of the treatment **(Figure 4.15 B-C)**. Treatment of MDA-MB-231 cells with the BHE extract also showed cell cycle arrest potential in the G1 phase in 24h (46%) and 48h (39%) of the treatment. It should be noted that BHE extract showed better cell cycle G1 phase arrest (58%) in the $ER^-/PR^-$ breast cancer cell line in 24h treatment **(Figure 4.15 G)**.

Further, we examined the effect of BME and BHE extract on mRNA levels of cyclin D1 and CDK4 in breast cancer cells. Interaction of cyclin D1 with cyclin-dependent kinases (CDK4/6) induces the expression of genes involved in the G1-S phase transition and promotes cellular proliferation. BME treatment (24h) significantly reduced the cyclin D1 and CDK4 mRNA levels in MDA-MB-231 and T47D cells **(Figure 4.16 A-B)**. BME extract significantly reduced cyclin D1 mRNA levels in MDA-MB-231 and T47D cancer cells in 24h treatment **(Figure 4.16 A-B)**. In comparison to BME extract, BHE treatment showed less potential to decrease mRNA levels of cyclin D1 and CDK4 in MDA-MB-231 and T47D cells in 24h treatment **(Figure 4.16 C-D)**.

It should be noted that in 48h BME and BHE extracts exert similar potential to decrease cyclin D1 and CDK4 mRNA levels in MDA-MB-231 and T47D cells **(Figure 4.16 A-D)**. To explore the modulatory role of cyclin D1 and CDK4 in the presence of BME and BHE extracts in MDA-MB-231 and T47D breast cancer cells we examined the mRNA levels of p21.

p21 protein is a member of the cyclin kinase inhibitor family which downregulates the CDK4/6 signaling pathway. Hexane and methanolic extracts exert a similar fold increase of p21 mRNA levels (3.2-3.6 fold) in MDA-MB-231 cells in 24h treatment.

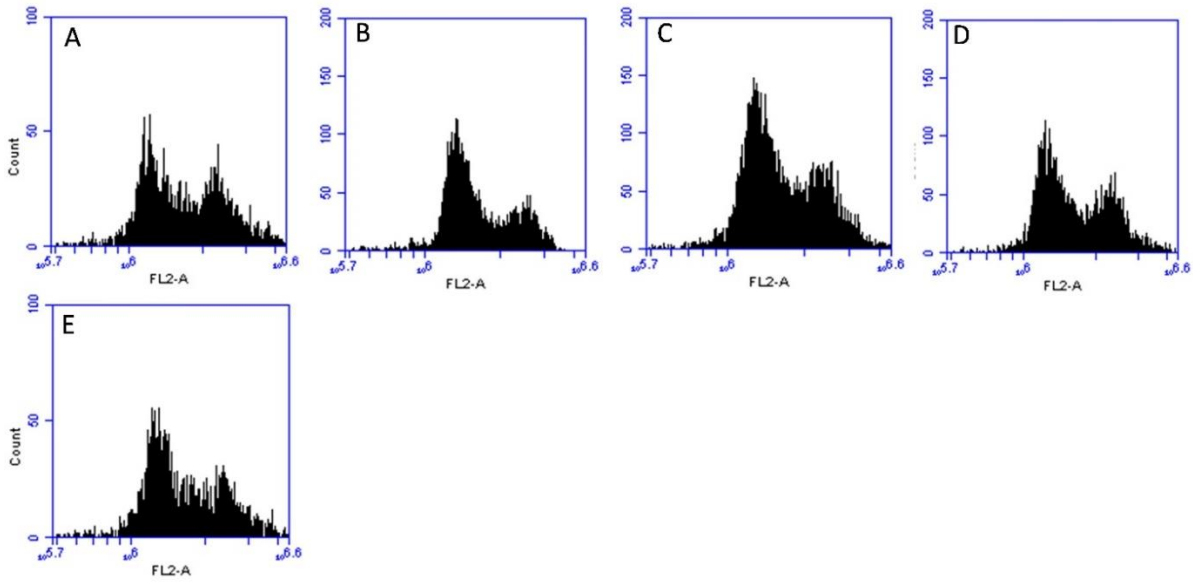
A
B
C
D
E
Count
FL2-A

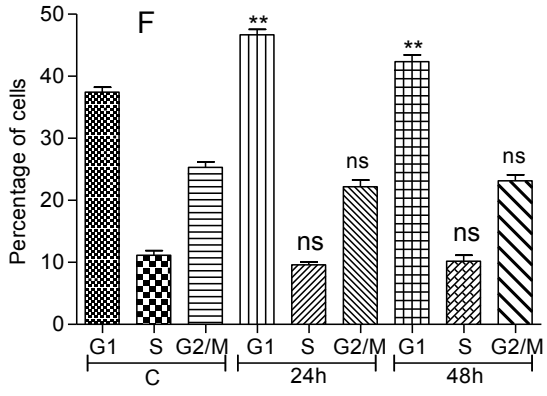
F
Percentage of cells
G1
S
G2/M
C
24h
48h
**
ns

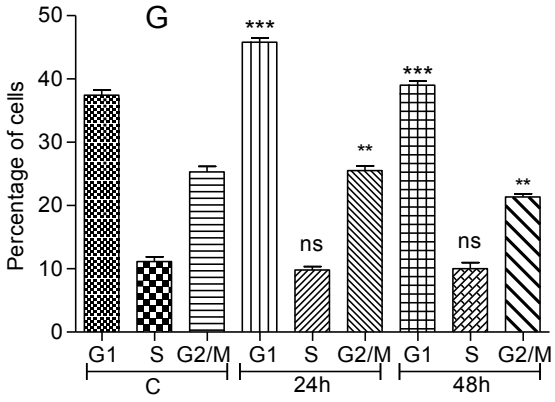
G
Percentage of cells
G1
S
G2/M
C
24h
48h
***
**
ns

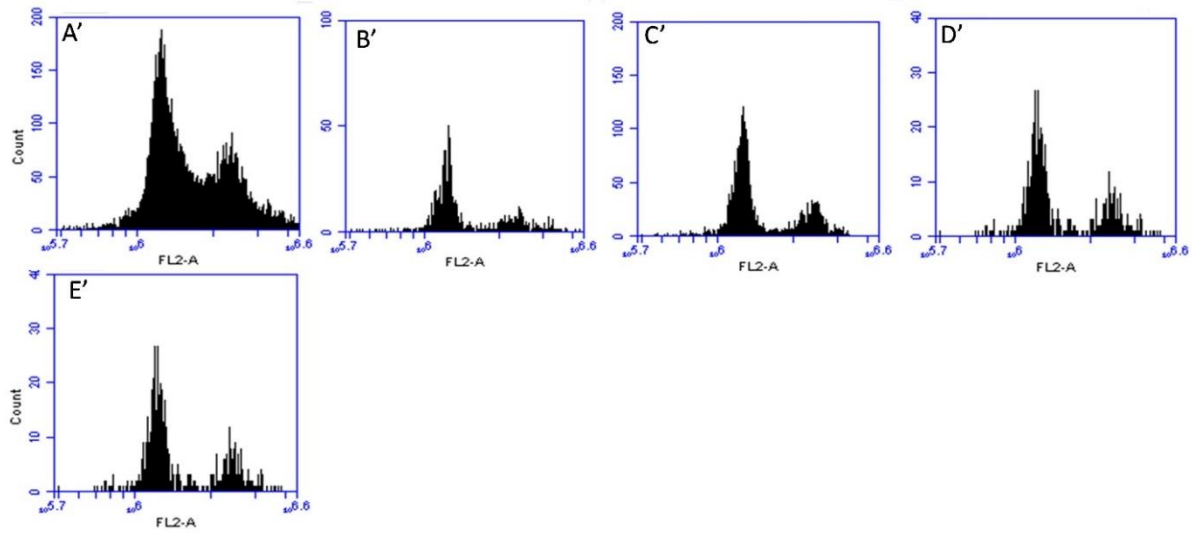
A'
B'
C'
D'
E'
Count
FL2-A

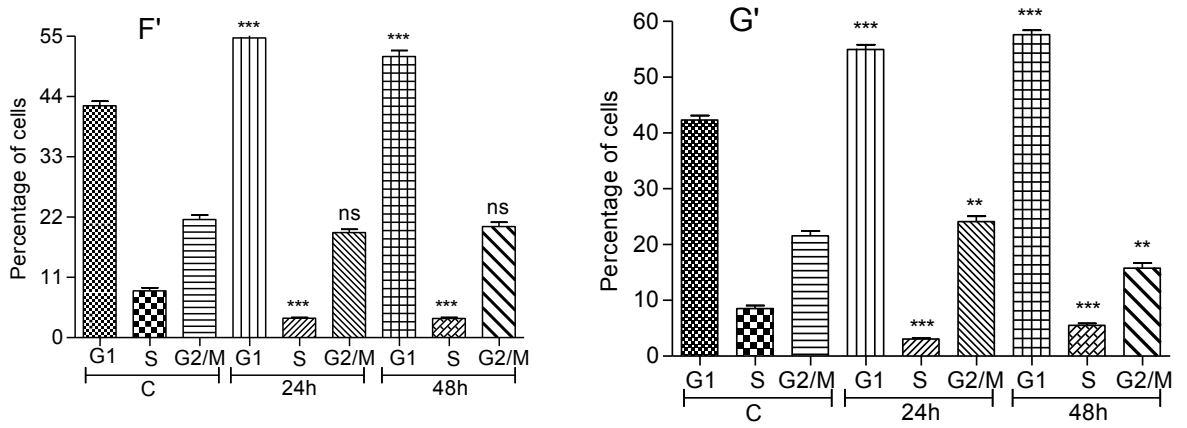


**Figure 4.15** Effect of *B. frutescens* extracts (BHE and BME) on cell cycle phase distribution in MDA-MB-231 and T47D breast cancer cell lines in 24h and 48h treatment at $IC_{50}$ (A) Cell cycle phase distribution in untreated MDA-MB-231 cells. (B) and (C) *B. frutescens* methanolic extract efficacy on MDA-MB-231 cell cycle phase distribution in 24h and 48h of treatment respectively. (D) and (E) *B. frutescens* hexane extract efficacy on MDA-MB-231 cell cycle phase distribution in 24h and 48h of treatment respectively. (F) Graphical representation of the cell cycle phase distribution in untreated (A) and BME extract-treated cells (B and C). (G) Graphical representation of the cell cycle phase distribution in untreated (A) and BHE extract-treated cells (D and E).
(A') Cell cycle phase distribution in untreated T47D cells. (B') and (C') *B. frutescens* methanolic extract efficacy on T47D cell cycle phase distribution in 24h and 48h of treatment respectively. (D') and (E') *B. frutescens* hexane extract efficacy on T47D cell cycle phase distribution in 24h and 48h of treatment respectively. (F') Graphical representation of the cell cycle phase distribution in untreated (A') and BME extract-treated T47D cells (B' and C'). (G') Graphical representation of the cell cycle phase distribution in untreated (A') and BHE extract-treated cells (E' and F'). Results are expressed as mean±SD. ***P<0.0005 vs. control; **P<0.005 vs. control; *P<0.05 vs. control.

On the contrary, BME exerts a potential increase (10 fold) in p21 mRNA levels in T47D cells in comparison to BHE extract treatment in T47D cells in 24h **(Figure 4.16 E).** Lesser effect of BME and BHE extracts on p21 mRNA levels was observed in test cell lines in 48h treatment.

To understand the underlying mechanism of Kurarinone induced cell proliferation we studied the cell cycle distribution in MDA-MB-231 and T47D breast cancer cells. Untreated T47D cancer cells showed 42.2, 8.6 and 21.6% cell distribution in G1, S and G2/M phase of cell cycle respectively **(Figure 4.17 H)**. KU treated T47D cells showed increased levels of G1 cell populations, both in 24h (46.3%) and 48h (55%) of the treatment **(Figure 4.17 H)**. It should be noted that KU showed better cell cycle G1 phase arrest (55%) in the T47D breast cancer cell line in 48h treatment **(Figure 4.17 H)**. KU treated MDA-MB-231 cells showed increased levels of G1 cell populations only

in 24h (58.4%) treatment **(Figure 4.17 G)**. In should be noted that KU also showed cell cycle G2/M phase arrest (37.7%) in the MDA-MB-231 breast cancer cell line in 48h treatment **(Figure 4.17 G)**. Further, we studied the effect of Kurarinone on mRNA levels of cyclin D1 and CDK4 in breast cancer cells. Kurarinone treatment (24h) significantly reduced the cyclin D1 and CDK4 mRNA levels in MDA-MB-231 and T47D cells **(Figure 4.17 I-J)**. It should be noted that in 48h Kurarinone treatment significantly decreased the cyclin D1 mRNA levels in MDA-MB-231 and T47D cells **(Figure 4.17 I-J)**. The cyclin D1 protein expression analysis showed that KU strongly reduced its expression in MDA-MB-231 cells in 48h treatment.

To evaluate the effect of Kurarinone on cyclin D1 and CDK4 in MDA-MB-231 and T47D breast cancer cells, we examined the mRNA levels of p21. Kurarinone exerts a 1.6 fold increase of p21 mRNA levels in MDA-MB-231 cells in 24h treatment. In T47D cells, Kurarinone exerts a potential increase (about 2 fold) in p21 mRNA levels in 48h treatment in comparison to 24h treatment **(Figure 4.17 K).** Lesser effect of Kurarinone treatment on p21 mRNA levels was observed in MDA-MB-231 cells in 48h treatment in comparison to 24h treatment.

Cell cycle distribution analysis was done to find out the CB induced cell proliferation inhibition in MDA-MB-231 and T47D cells. Untreated T47D cancer cells showed 41.06, 7.23 and 20.83% cell distribution in G1, S and G2/M phase of cell cycle respectively **(Figure 4.18 F)**. CB treated T47D cells showed a high number of G1 cell populations (62.63%) in 48h **(Figure 4.18 F)**. In should be noted that CB showed better G1 phase cell cycle arrest (62.63%) in the T47D breast cancer cell line in comparison to MDA-MB-231 cells in 48h treatment.

Further effect of CB treatment on mRNA levels of cyclin D1 and CDK4 in breast cancer cells was studied. CB treatment (24h) significantly reduced the expression level of cyclin D1 and CDK4 mRNA in MDA-MB-231 and T47D cells **(Figure 4.18 G-H)**. It should be mentioned that CB treatment (48h) significantly decreased the mRNA levels of cyclin D1 and CDK4 in both test cells **(Figure 4.18 G-H)**. The cyclin D1 protein expression analysis showed that CB strongly reduced its expression in MDA-MB-231 cells in 48h treatment **(Figure 4.18 J)**.

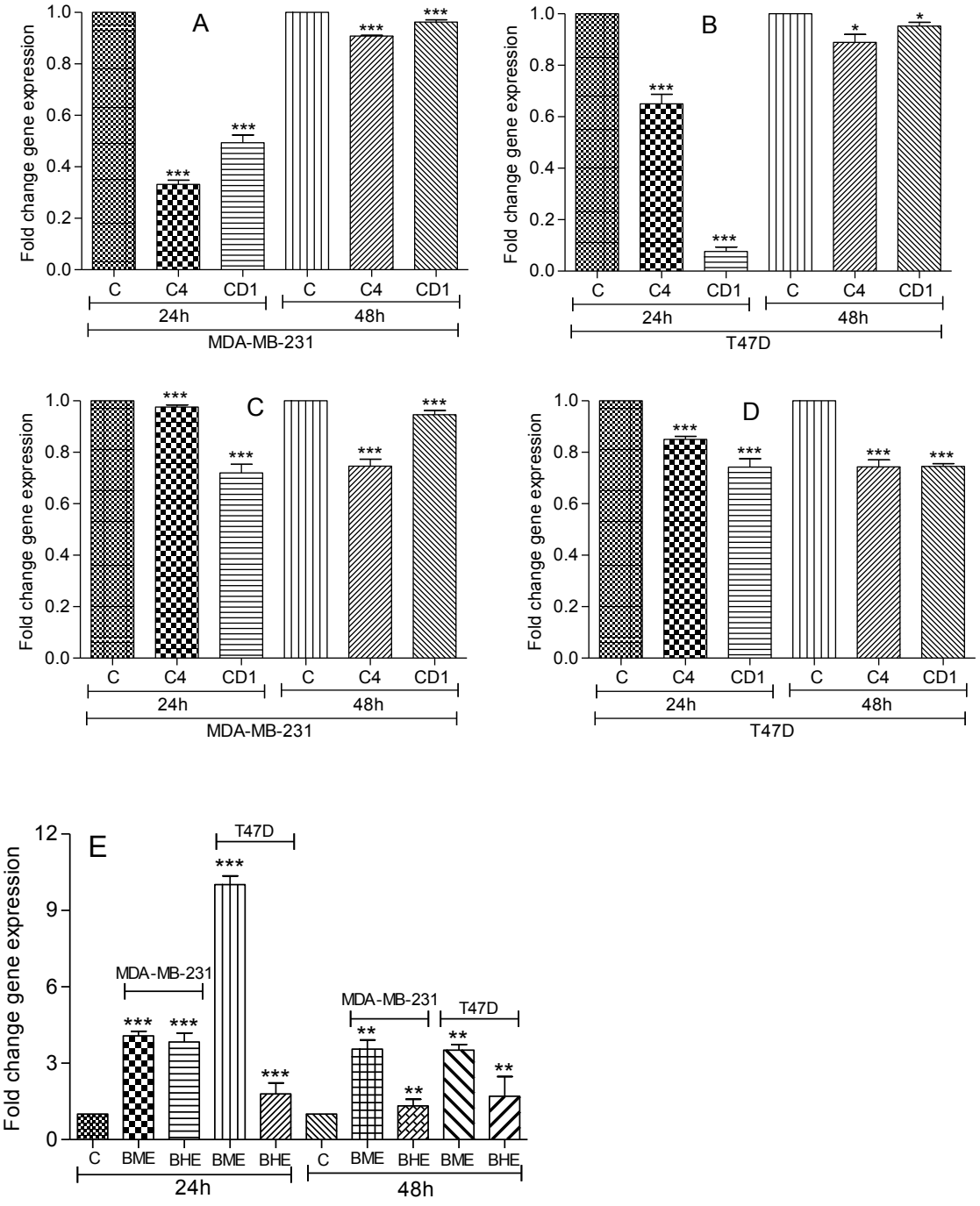


**Figure 4.16** Effect of *B. frutescens* extracts (BME and BHE) on mRNA levels of cell cycle markers (cyclin4, CD1, and p21) in human breast cancer cell proliferation at $IC_{50}$ concentration for 24, and 48h. (A) and (B) mRNA levels of CDK4 and cyclin D1 in *B. frutescens* methanolic extract treated MDA-MB-231 and T47D breast cancer cell respectively (C) and (D) mRNA levels of CDK4 and cyclin D1 in *B. frutescens* hexane extract-treated MDA-MB-231 and T47D breast cancer cell respectively (E) p21 mRNA levels in *B. frutescens* methanol and hexane extract-treated MDA-MB-231 and T47D breast cancer cell. Results are expressed as mean±SD of the three replicates. ***P<0.0005 vs. control; **P<0.005 vs. control; *P<0.05 vs. control. C=Control; C4=CDK4; CD1-Cyclin D1.

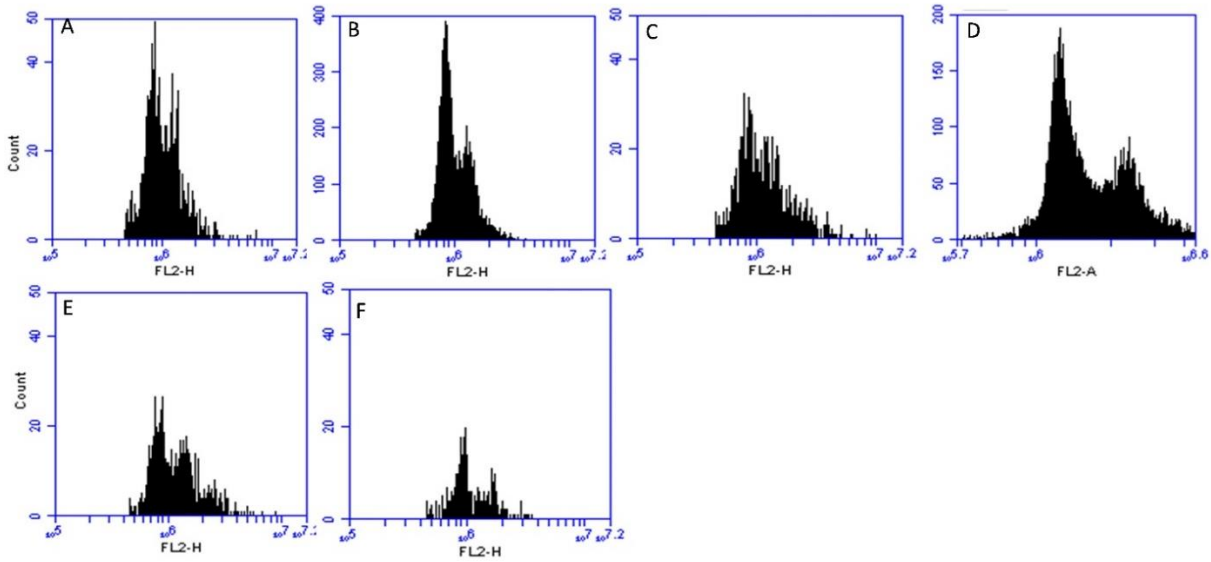
A
B
C
D
E
F
Count
FL2-H
FL2-A

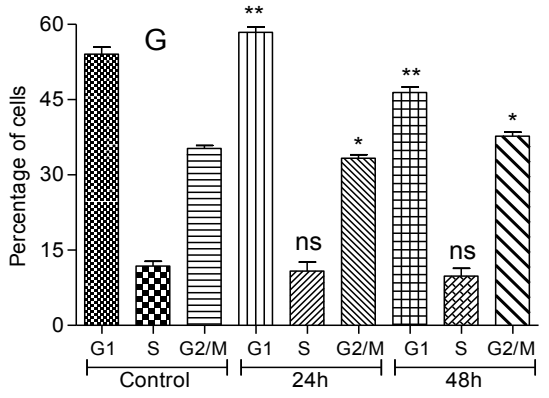
G
Percentage of cells
G1
S
G2/M
Control
24h
48h
ns

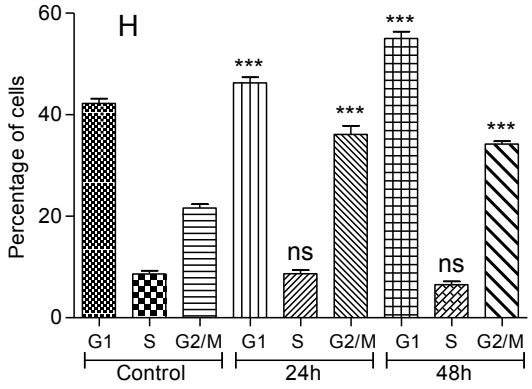
H
Percentage of cells
G1
S
G2/M
Control
24h
48h
ns

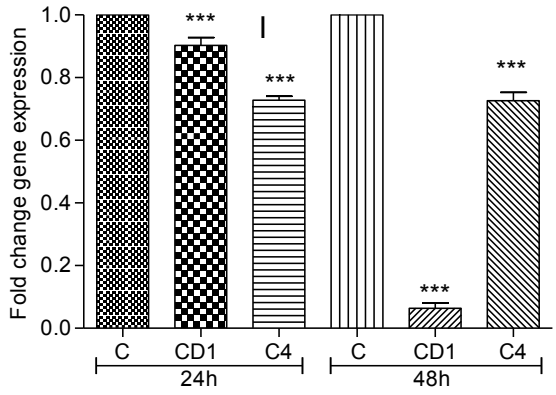
I
Fold change gene expression
C
CD1
C4
24h
48h

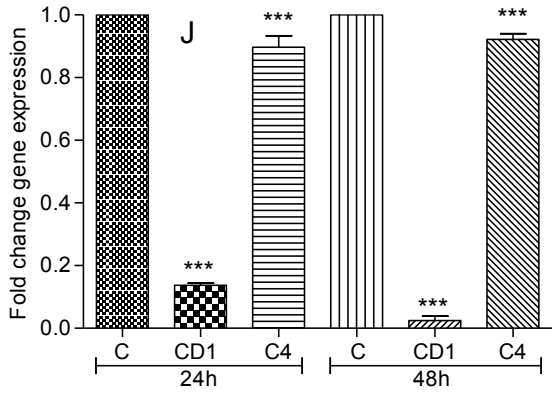
J
Fold change gene expression
C
CD1
C4
24h
48h

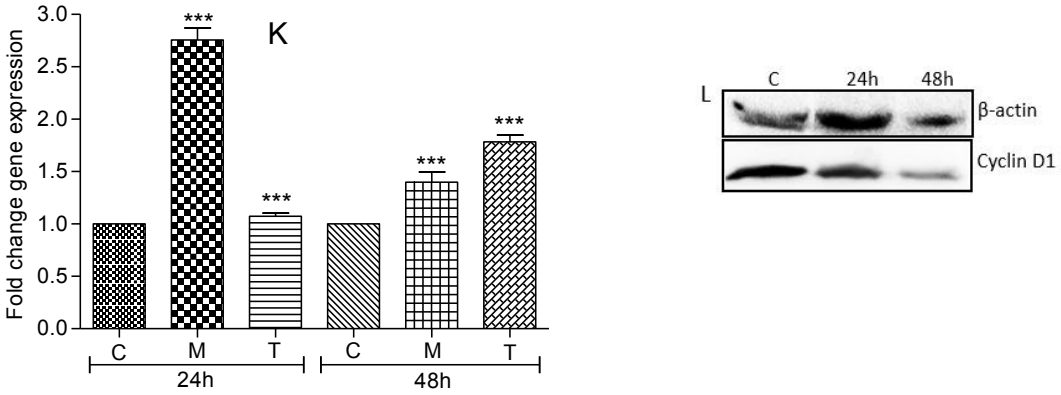


**Figure 4.17** Effect of Kurarinone on cell cycle phase distribution and mRNA levels of cell cycle markers (cyclin4, CD1, and p21) in MDA-MB-231 and T47D breast cancer cell lines in 24h and 48h treatment at $IC_{50}$ values. (A) Cell cycle phase distribution in untreated MDA-MB-231 cells. (B) and (C) Kurarinone efficacy on MDA-MB-231 cell cycle phase distribution in 24h and 48h of treatment respectively. (D) Cell cycle phase distribution in untreated T47D cells. (E) and (F) Kurarinone efficacy on T47D cell cycle phase distribution in 24h and 48h of treatment respectively. (G) Graphical representation of the cell cycle phase distribution in untreated (A) and Kurarinone treated cells (B and C). (H) Graphical representation of the cell cycle phase distribution in untreated (D) and Kurarinone treated cells (E and F).
RT-PCR technique was used to show the effect of Kurarinone on mRNA levels of cyclin4, CD1 and p21 markers in human breast cancer cells at $IC_{50}$ concentration in 24, and 48h treatment. (I) and (J) mRNA levels of CDK4 and cyclin D1 in Kurarinone treated MDA-MB-231 and T47D breast cancer cell respectively (K) p21 mRNA levels in Kurarinone treated MDA-MB-231 and T47D breast cancer cell.
Effect of Kurarinone on cyclin D1 protein expression was studied in MDA-MB-231 cells using western blot technique. The cell samples were collected after 24 and 48h Kurarinone treatment at $IC_{50}$ concentration. (L) cyclin D1 protein expression in Kurarinone treated MDA-MB-231 cells. β-actin was used as an internal control.
Results are expressed as mean±SD of the three replicates. ***P<0.0005 vs. control; **P<0.005 vs. control; *P<0.05 vs. control. C=Control; C4=CDK4; CD1-Cyclin D1; M-MDA-MB-231 breast cells; T-T47D breast cells.

CB treatment (48h) increased the levels of p21 mRNA ≈10 fold in MDA-MB-231 cells in comparison to non-treated cells. CB treated (48h) T47D cells increased >2 fold p21 mRNA levels in comparison to 24h treated T47D cells **(Figure 4.18 I).** Lesser effect of CB treatment on p21 mRNA levels was reported in both MDA-MB-231 and T47D cells in 24h treatment, in contrast to 48h treatment.

## 4.4 Effect of reactive oxygen species generation and mitochondrial membrane potential disruption ability of identified/lead natural products

### 4.4.1 Estimation of reactive oxygen species production by using fluorescence spectrophotometer and confocal microscopy

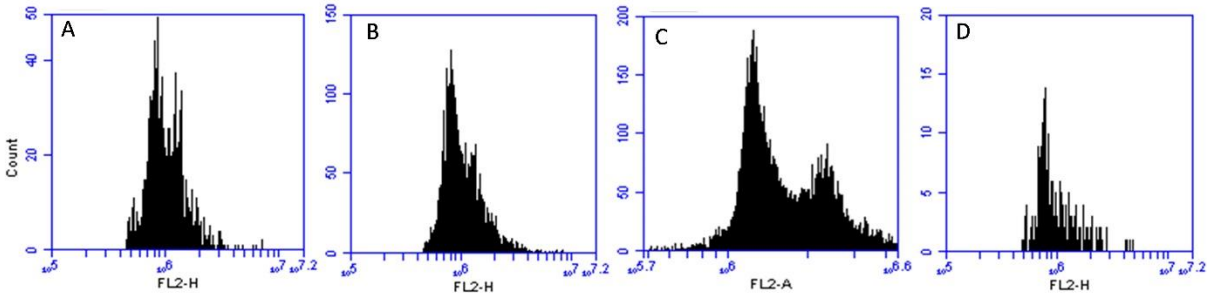
A
B
C
D
Count
FL2-H
FL2-H
FL2-A
FL2-H

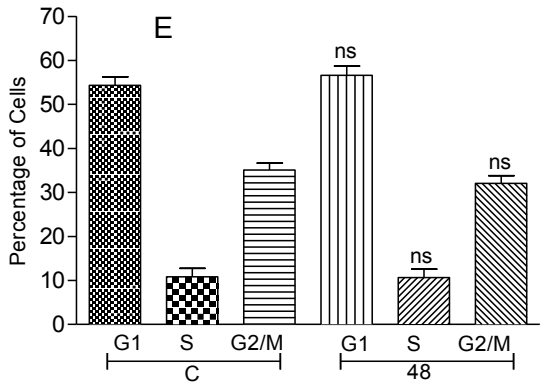
E
Percentage of Cells
ns
ns
ns
G1
S
G2/M
G1
S
G2/M
C
48

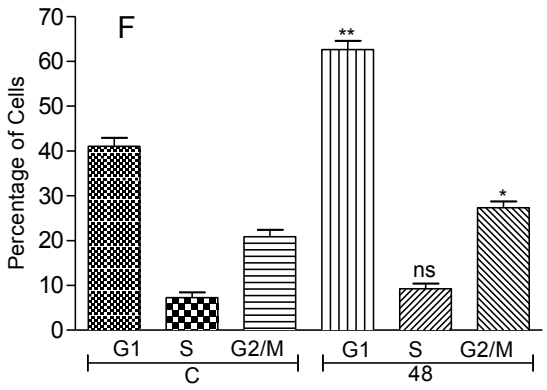
F
Percentage of Cells
**
ns
*
G1
S
G2/M
G1
S
G2/M
C
48

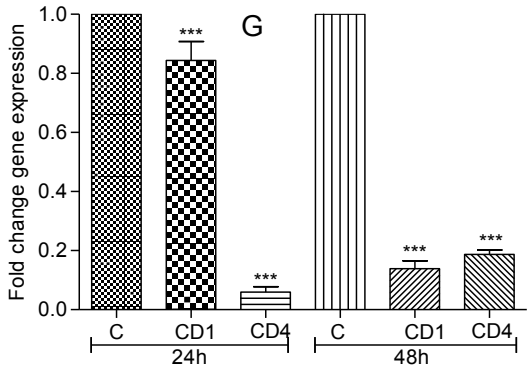
G
Fold change gene expression
***
***
***
***
C
CD1
CD4
C
CD1
CD4
24h
48h

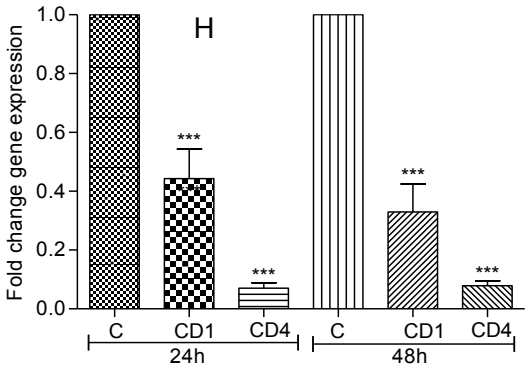
H
Fold change gene expression
***
***
***
***
C
CD1
CD4
C
CD1
CD4
24h
48h

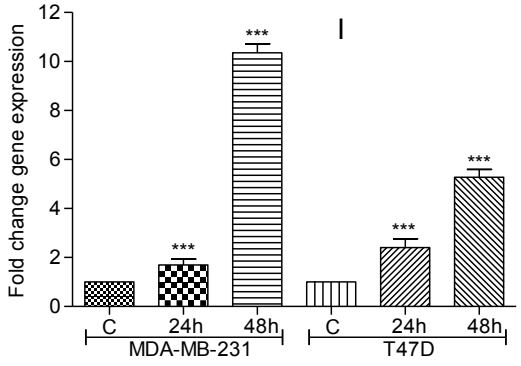
I
Fold change gene expression
***
***
***
***
C
24h
48h
C
24h
48h
MDA-MB-231
T47D

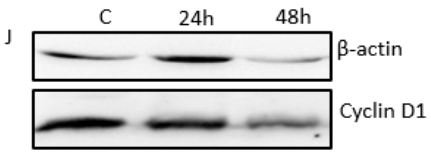
J
C
24h
48h
β-actin
Cyclin D1

**Figure 4.18** Effect of 3-O-(E)-p-Coumaroylbetulinic acid (CB) on cell cycle phase distribution and mRNA levels of cell cycle markers (cyclin4, CD1, and p21) in MDA-MB-231 and T47D breast cancer cell lines in different time intervals at $IC_{50}$ values. (A) Cell cycle phase distribution in untreated MDA-MB-231 cells. (B) CB efficacy on MDA-MB-231 cell cycle phase distribution in 48h of treatment. (C) Cell cycle phase distribution in untreated T47D cells. (D) CB efficacy on T47D cell cycle phase distribution in 48h of treatment. (E) Graphical representation of the cell cycle phase distribution in untreated (A) and CB treated cells (B). (F) Graphical representation of the cell cycle phase distribution in untreated (C) and CB treated cells (D).
RT-PCR technique was used to show the effect of CB on mRNA levels of cyclin4, CD1 and p21 markers in human breast cancer cells at $IC_{50}$ concentration in 24, and 48h treatment. (G) and (H) mRNA levels of CDK4 and cyclin D1 in CB treated MDA-MB-231 and T47D breast cancer cell respectively (I) p21 mRNA levels in CB treated MDA-MB-231 and T47D breast cancer cell.
Effect of CB on cyclin D1 protein expression was studied in MDA-MB-231 cells using the western blot technique. The cell samples were collected after 24 and 48h CB treatment at $IC_{50}$ concentration. (J) cyclin D1 protein expression in CB treated MDA-MB-231 cells. β-actin was used as an internal control.
Results are expressed as mean±SD of the three replicates. ***P<0.0005 vs. control; **P<0.005 vs. control; *P<0.05 vs. control. C=Control; C4=CDK4; CD1-Cyclin D1.

To explore the possibility of reactive oxygen species (ROS) generation mediated toxicity in MDA-MB-231 and T47D breast cancer cells in the presence of identified natural product/lead compounds, confocal microscopy and fluorescence spectrophotometric technique using H2-DCFDA dye was utilized.

Confocal microscopy with H2-DCFDA showed enhanced green fluorescence implying ROS generation at sub $IC_{50}$ concentrations of BME, BHE, Kurarinone and CB in MDA-MB-231 and T47D cells in 16h treatment **(Figure 4.19 A, 4.19 B, 4.20, and 4.21).** It should be noted that in confocal microscopy, the increasing order of ROS generation capacity in MDA-MB-231 and T47D cells was CB<KU<BHE<BME and CB<KU<BHE<BME respectively.

Further, the ROS generation in test cells was quantified using a spectrophotometer applying the H2-DCFDA dye. For the quantitative assessment of ROS generation in test cells, $IC_{50}$ concentration of identified natural products/lead compounds were utilized. In the microscopic technique, sub $IC_{50}$ concentration was utilized to acquire a sufficient number of cells for the analysis. Treatment at $IC_{50}$ concentration in 48h showed an appreciable increase in ROS generation as depicted by the increased fluorescence count of test product/compounds **(Figure 4.19 C)** in MDA-MB-231 and T47D cells. BME and BHE extracts showed approximately similar efficacy to increase ROS generation independently in MDA-MB-231 and T47D cell lines. Comparatively, the BME extract depicted better ROS generation potential in both test cell lines **(Figure 4.19)**.

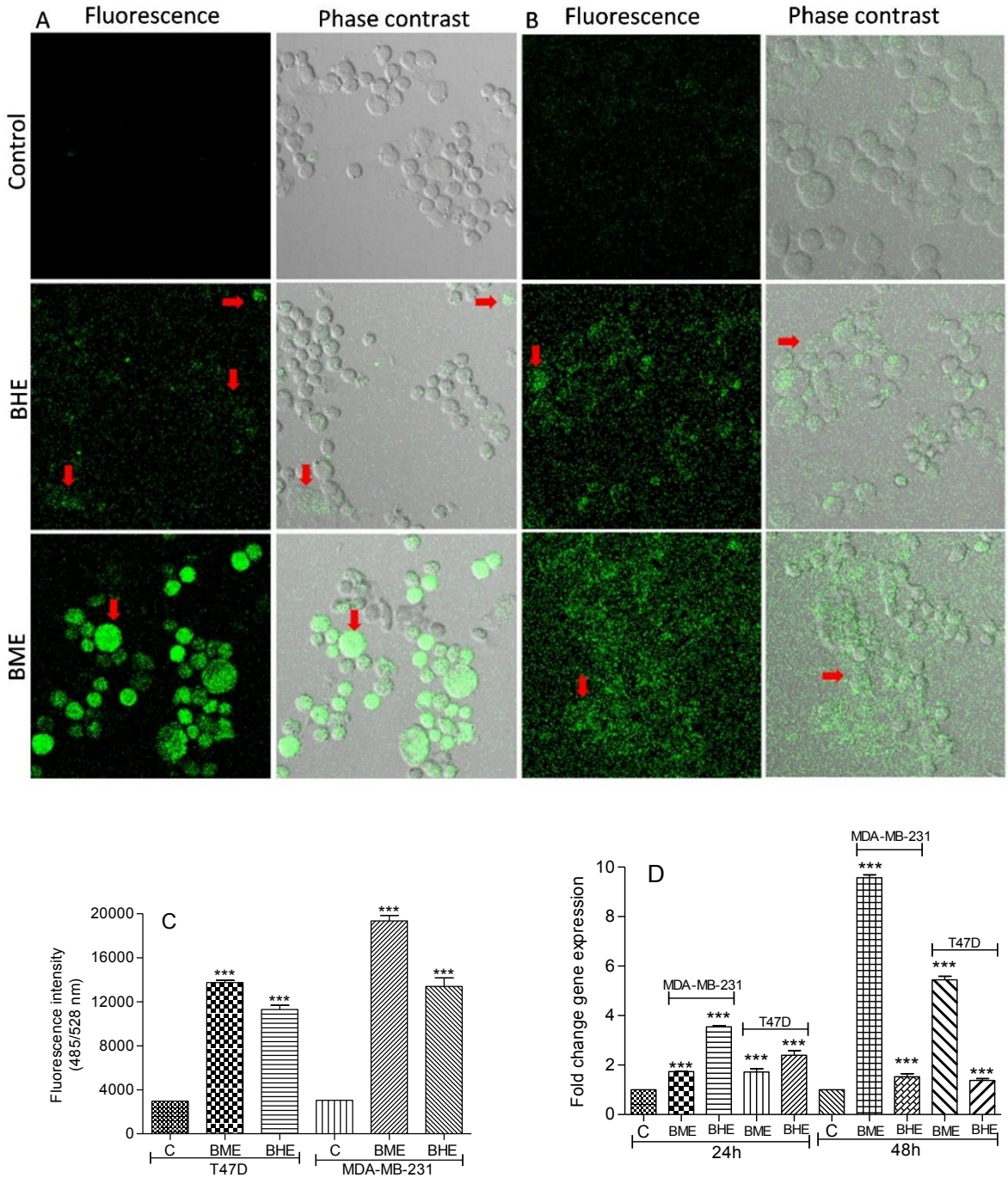


**Figure 4.19** Effect of BME and BHE extracts on ROS production and NF-κB mRNA levels in MDA-MB-231 and T47D cells. (A) and (B) Confocal microscopy showing the effect of *B. frutescens* extracts on ROS production in MDA-MB-231 and T47D breast cells respectively using H2-DCFDA dye at sub $IC_{50}$ concentration. Confocal images of MDA-MB-231 and T47D cells showed enhanced fluorescence of CH-H2DCFDA which is directly proportional to cellular ROS. (C) Effect of *B. frutescens* extracts on ROS production in human breast cancer cells at $IC_{50}$ concentration for 48h. (D) Effect of *B. frutescens* extracts on mRNA levels of NF-κB marker in human breast cancer cells at $IC_{50}$ concentration for 24 and 48h in RT-PCR analysis. Results are expressed as mean±SD of the three replicates. ***P<0.0005 vs. control; **P<0.005 vs. control; *P<0.05 vs. control.

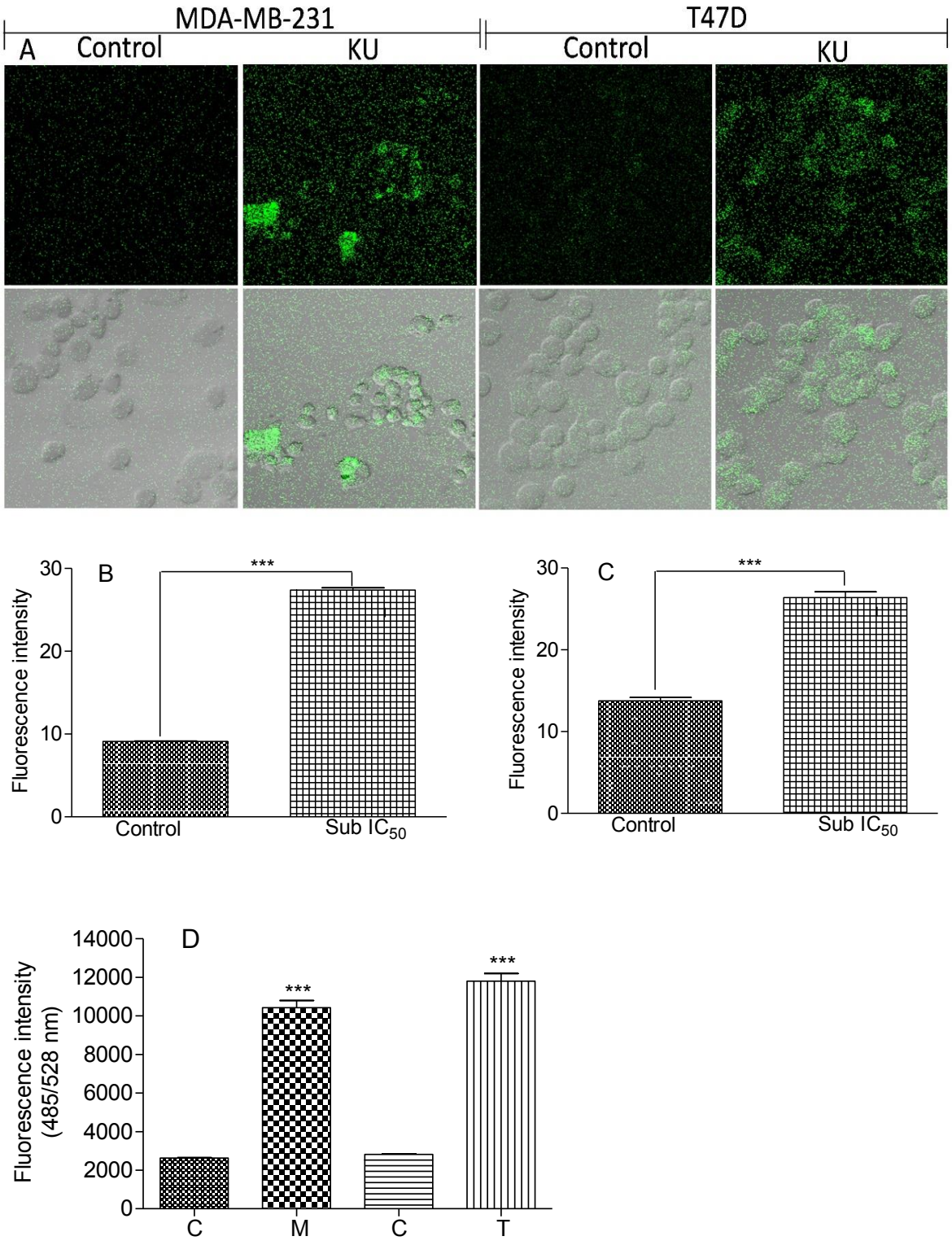


**Figure 4.20** Confocal microscopy and fluorescent spectroscopy showing the effect of KU on ROS generation in breast cells at sub $IC_{50}$ and $IC_{50}$ concentration. (A) Confocal microscopy showing the effect of KU on ROS production in MDA-MB-231 and T47D breast cells respectively using H2-DCFDA dye at sub $IC_{50}$ concentration. Confocal images of MDA-MB-231 and T47D cells showed enhanced fluorescence of CH-H2DCFDA which is directly proportional to cellular ROS. (B) Graph showing the

fluorescence intensity of KU treated and control MDA-MB-231 cells. (C) Graph showing the fluorescence intensity of KU treated and control T47D cells. (D) Effect of KU on ROS production in human breast cancer cells at $IC_{50}$ concentration for 48h. Results are expressed as mean±SD of the three replicates. ***P<0.0005 vs. control; **P<0.005 vs. control; *P<0.05 vs. control. KU=Kurarinone.

It should be noted that MDA-MB-231 breast cells produced more ROS in the presence of BME and BHE extracts in comparison to T47D cells **(Figure 4.19)**. KU treatment at $IC_{50}$ concentration in 48h showed an appreciable increase in ROS generation as depicted by the increased fluorescence count **(Figure 4.20 D)** in MDA-MB-231 and T47D cells. KU showed approximately similar efficacy to increase ROS generation independently in MDA-MB-231 and T47D cell lines **(Figure 4.20).** CB treated (16h) breast cancer cells showed little enhancement in green fluorescence suggesting low ROS production at sub $IC_{50}$ concentration as revealed by confocal microscopy. CB treatment (48h) at $IC_{50}$ concentration showed a considerable rise in ROS generation as represented by the enhanced fluorescence count in MDA-MB-231 and T47D cells **(Figure 4.21 D)**. CB exhibited better potential to increase ROS production in T47D cells in comparison to MDA-MB-231 cells **(Figure 4.21).**

ROS generation potential assay of lead samples showed that BME and BHE extract significantly increased ROS levels in breast cancer cells in comparison to KU and CB **(Figure 4.19, 4.20, and 4.21)**. Thus, to explore the oxidative stress inductive role of BME and BHE extracts in MDA-MB-231 and T47D breast cancer cells we examined the mRNA levels of NF-κB. BME treatment in 24h and 48h shows a significant fold increase (1.9-9.3 fold) in NF-κB mRNA levels in MDA-MB-231 and T47D cells **(Figure 4.19 D)**. Methanolic extract exerts time-dependent profound increase (5.1-9.3 fold increase) in NF-κB mRNA levels in MDA-MB-231 and T47D cells in 48h. Hexane extract also depicted a significant increase in NF-κB mRNA levels in MDA-MB-231 cells in 48h treatment in comparison to non-treated cells. It should be noted that in 48h treatment with BHE extracts exceptionally showed decreased levels of NF-κB in both the MDA-MB-231 and T47D cells in 48h than that of 24h treatment **(Figure 4.19 D)**.

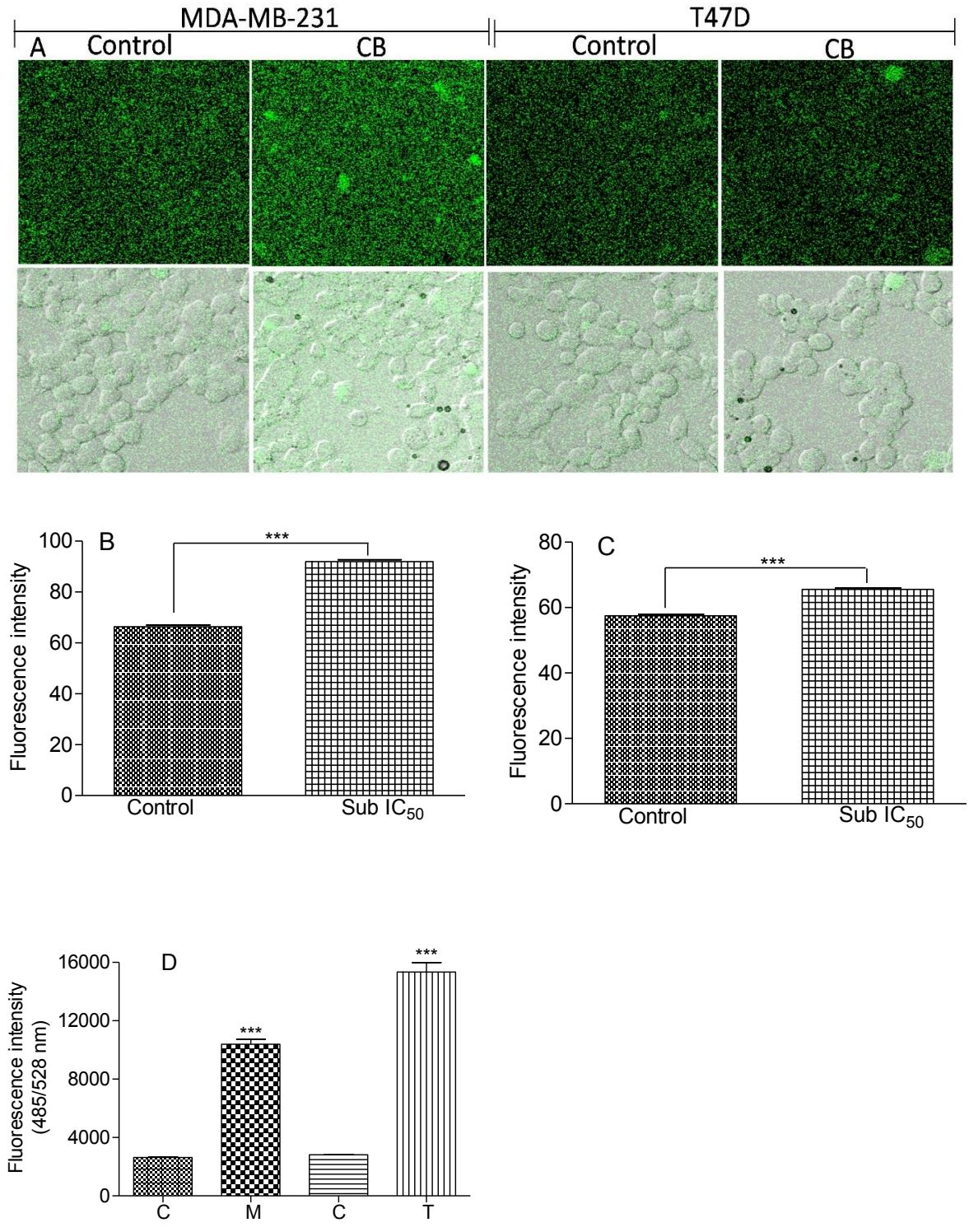


**Figure 4.21** Confocal microscopy and fluorescent spectroscopy showing the effect of 3-O-(E)-p-Coumaroylbetulinic acid (CB) on ROS production at sub $IC_{50}$ and $IC_{50}$ concentration in BCa cells. (A) Confocal microscopy demonstrating the potency of CB on ROS generation in MDA-MB-231 and T47D breast cells respectively using H2-DCFDA dye at sub $IC_{50}$ concentration. Confocal images of MDA-MB-

231 and T47D cells showed higher fluorescence of CH-H2DCFDA which is directly proportional to cellular ROS. (B) Graph showing the fluorescence intensity of CB treated MDA-MB-231 cells and control. (C) Graph showing the fluorescence intensity of CB treated T47D cells and control. (D) ROS production after CB treatment (48h) in human BCa cells at $IC_{50}$ concentration.
Results are presented as mean±SD of the three replicates. ***P<0.0005 vs. control; **P<0.005 vs. control. CB=3-O-(E)-p-Coumaroylbetulinic acid.

### 4.4.2 Estimation of mitochondrial membrane potential disruption by using fluorescence spectrophotometer and confocal microscopy

To explore the lead compound/extract mediated mitochondrial death in MDA-MB-231 and T47D breast cancer cells. Mitochondrial membrane potential disruption assay was performed using confocal microscopy and spectrophotometry techniques. Confocal microscopy with JC-1 dye showed reduced red to green ratio inferring disrupted mitochondrial membrane potential at sub $IC_{50}$ concentrations of BME, BHE, Kurarinone and CB in MDA-MB-231 and T47D cells in 16h treatment **(Figure 4.22, 4.23, and 4.24)**. It should be noted that in confocal microscopy, the decreasing order of mitochondrial membrane potential disruption in MDA-MB-231 and T47D cells was CB<BHE<BME<KU and KU<BHE<BME<CB respectively. Further, the mitochondrial membrane potential disruption in test cells was quantified using a spectrophotometer applying the JC-1 dye.

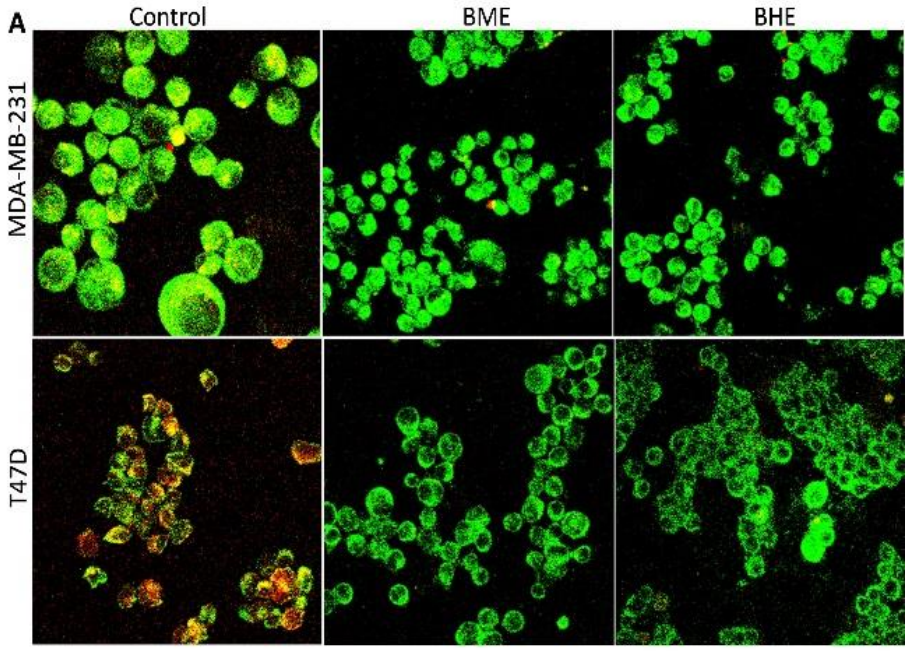

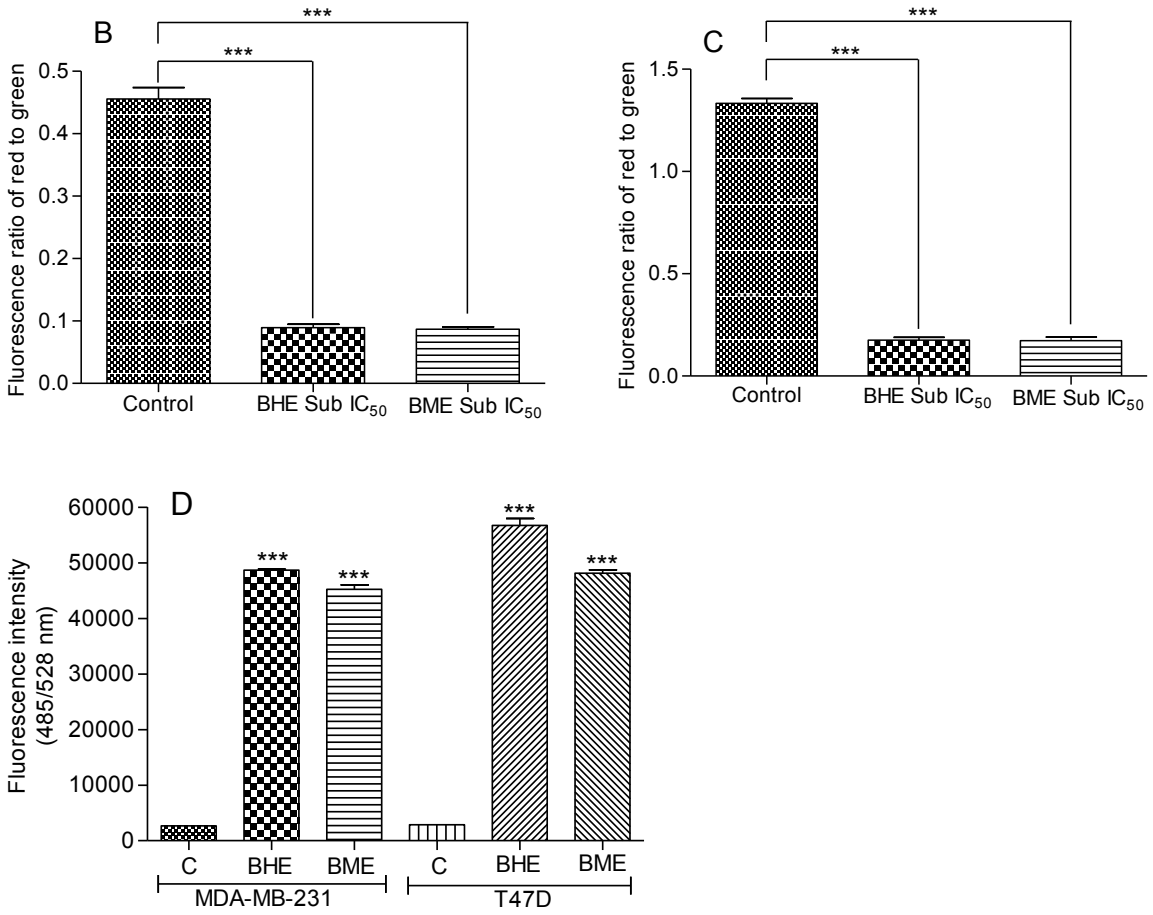


**Figure 4.22** Confocal microscopy and fluorescent spectroscopy showing the effect of *B. frutescens* extracts on mitochondrial membrane potential in breast cells at sub $IC_{50}$ and $IC_{50}$ concentration. (A) Effect of *B. frutescens* extracts on MDA-MB-231 and T47D cells. JC-1 fluorescent dye gathered in the matrix of mitochondria and produced red fluorescence in the control sample. Due to the decrease in mitochondrial membrane potential, JC-1 monomer produced green fluorescence in BME and BHE treated samples. (B) Graph showing the ratio of red and green fluorescence intensity in MDA-MB-231 cells. (C) Graph showing the ratio of red and green fluorescence intensity in T47D cells. (D) Effect of BME and BHE on MMP in human breast cancer cells at $IC_{50}$ concentration in 48h. BME= *B. frutescens* methanolic extract, BHE= *B. frutescens* hexane extract. Results are expressed as mean±SD of the three replicates. ***P<0.0005 vs. control; **P<0.005 vs. control; *P<0.05 vs. control.

For quantitative assessment of mitochondrial membrane potential disruption in test cells, $IC_{50}$ concentrations of test samples was utilized. In the confocal microscopic technique, sub $IC_{50}$ concentration was utilized to acquire a sufficient number of cells for the analysis. Treatment at $IC_{50}$ concentration in 48h showed an appreciable increase in mitochondrial membrane potential disruption as depicted by the decreased red to

green ratio fluorescence count of test product/compounds **(Figure 4.22 D)** in MDA-MB-231 and T47D cells.

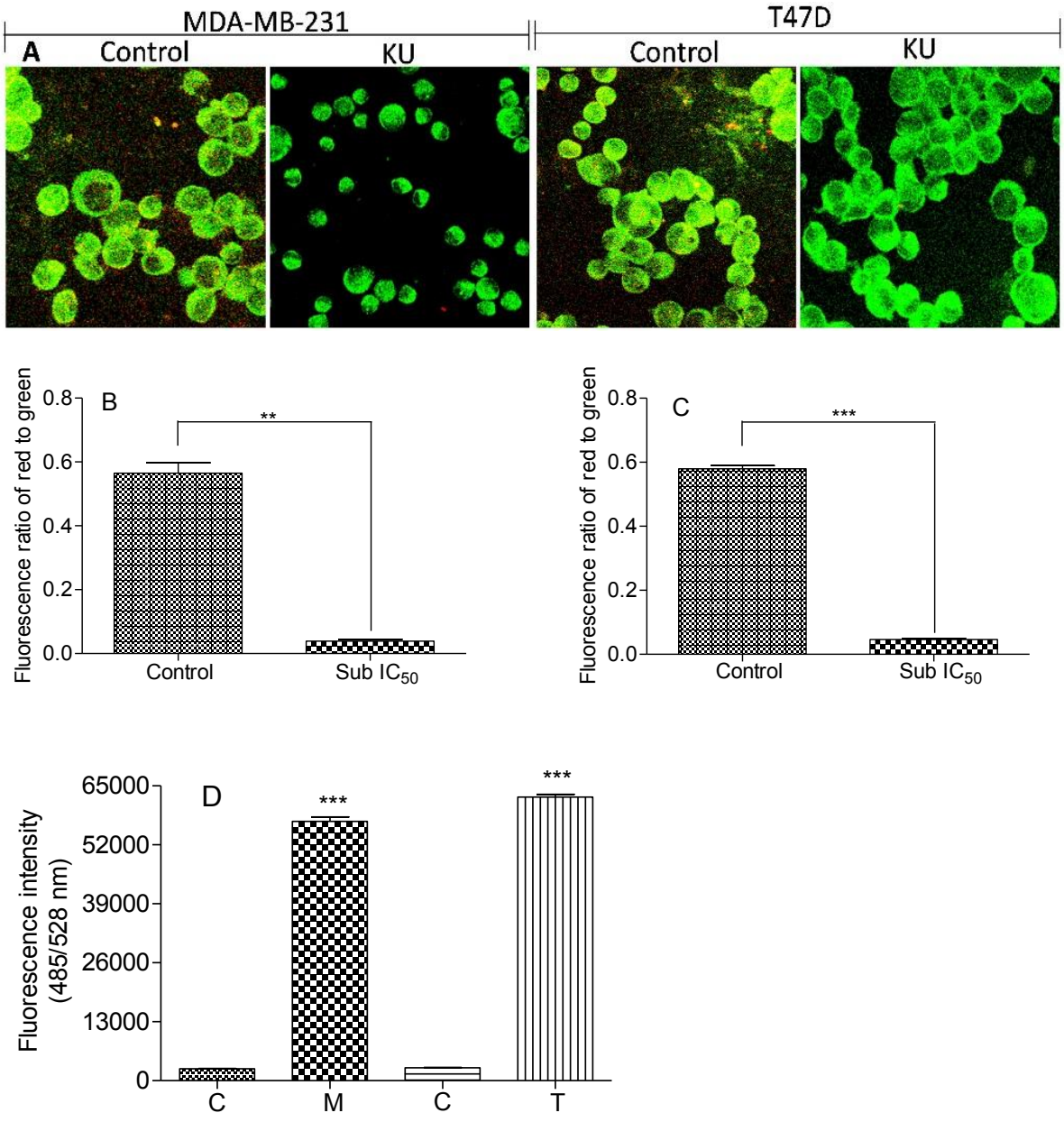


**Figure 4.23** Confocal microscopy and fluorescent spectroscopy showing the effect of KU on mitochondrial membrane potential in breast cells at sub $IC_{50}$ and $IC_{50}$ concentration.
(A) Effect of KU on MDA-MB-231 and T47D cells. JC-1 fluorescent dye gathered in the matrix of mitochondria and produced red fluorescence in the control sample. Due to the decrease in mitochondrial membrane potential, JC-1 monomer produced green fluorescence in KU treated samples. (B) Graph showing the ratio of red and green fluorescence intensity in MDA-MB-231 cells. (C) Graph showing the ratio of red and green fluorescence intensity in T47D cells. (D) Effect of KU on MMP in human breast cancer cells at $IC_{50}$ concentration in 48h. Results are expressed as mean±SD of the three replicates. ***P<0.0005 vs. control; **P<0.005 vs. control; KU=Kurarinone.

JC-1 fluorescent color changed from red to green in the BME and BHE treated MDA-MB-231 and T47D cell lines at sub $IC_{50}$ concentration in 16h, suggesting a decline in mitochondrial membrane potential **(Figure 4.22)**.

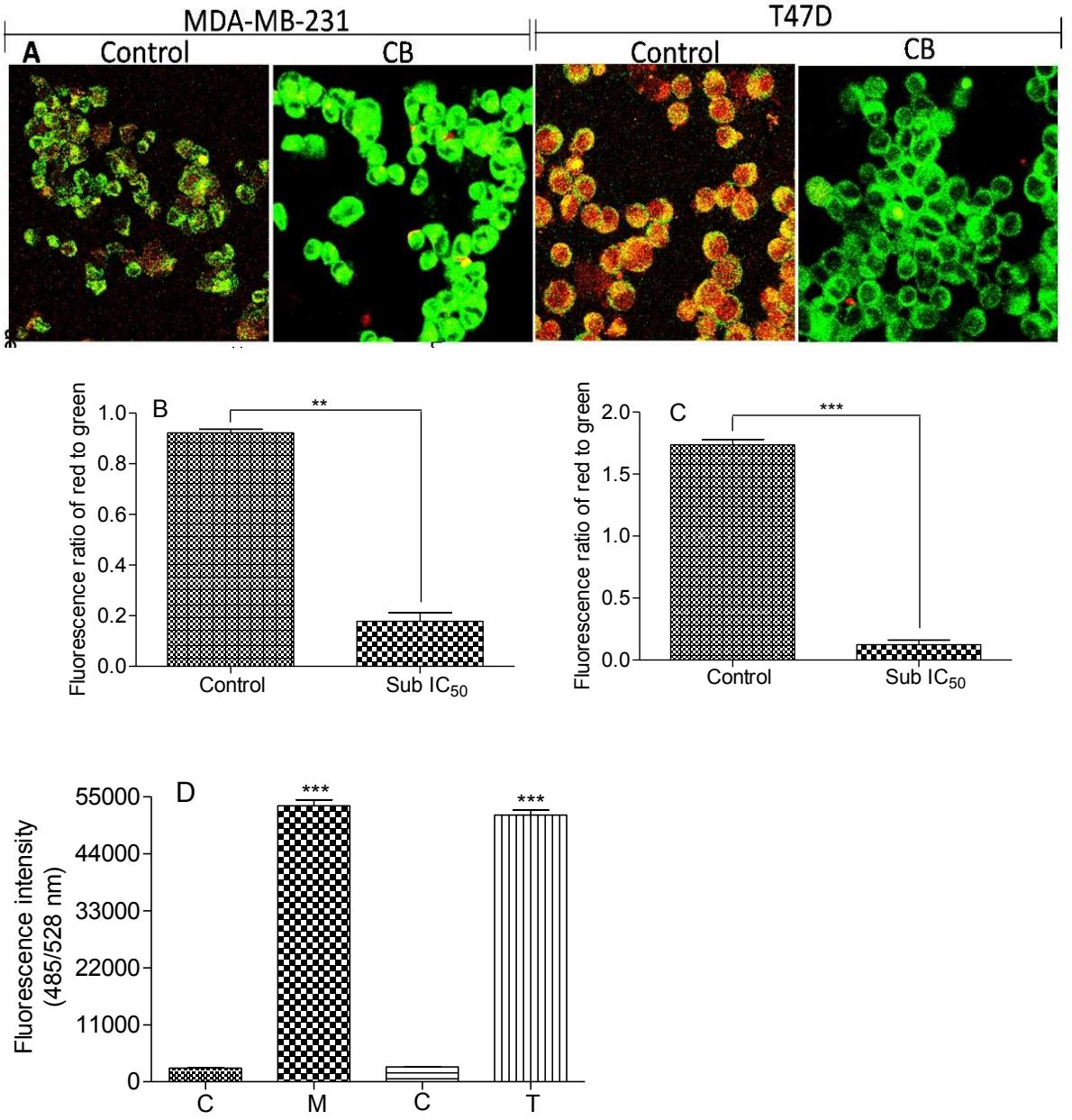


**Figure 4.24** Confocal microscopy and fluorescent spectroscopy showing the effect of 3-O-(E)-p-Coumaroylbetulinic acid (CB) on MMP at sub $IC_{50}$ and $IC_{50}$ concentration in BCa cells.
(A) Effect of CB on MDA-MB-231 and T47D cells. JC-1 fluorescent dye aggregates in the mitochondrial matrix and shows red fluorescence in the untreated samples. Due to the decline in MMP, JC-1 in the monomeric form produced green fluorescence in CB treated cells. (B) Graph showing the red: green fluorescence intensity ratio in MDA-MB-231 cells. (C) Graph depicting the red: green fluorescence intensity ratio in T47D cells. (D) Effect of CB treatment (48h) on MMP in human BCa cells at $IC_{50}$

concentration. Results are presented as mean±SD of the three replicates. ***P<0.0005 vs. control; **P<0.005 vs. control. CB=3-O-(E)-p-Coumaroylbetulinic acid.

BME and BHE extract treatment at $IC_{50}$ concentration in 48h showed an appreciable mitochondrial membrane potential disruption as revealed by decreased red to green ratio fluorescence count **(Figure 4.22 D)** in MDA-MB-231 and T47D cells. Both the extracts showed approximately similar potential to decrease the membrane potential in both the test cell lines. Comparatively, the BHE extract depicted better membrane potential lowering effect in MDA-MB-231 and T47D cell than BME extract **(Figure 4.22 B-C)**. JC-1 fluorescent color changed from red to green in the KU treated MDA-MB-231 and T47D cell lines at sub $IC_{50}$ concentration in 16h, suggesting a decline in mitochondrial membrane potential **(Figure 4.23)**. KU treatment at $IC_{50}$ concentration in 48h showed appreciable mitochondrial membrane potential disruption as revealed by decreased red to green fluorescence count **(Figure 4.23 D)** in MDA-MB-231 and T47D cells. KU showed approximately similar potential to decrease the membrane potential in both the test cell lines **(Figure 4.23)**. Color changed from red to green of JC-1 fluorescent dye in CB treated (16h) BCa cells at sub $IC_{50}$ concentration, suggesting a decline in MMP levels **(Figure 4.24)**. CB treatment (48h) at $IC_{50}$ concentration showed a substantial reduction in MMP as demonstrated by decreased red to green fluorescence count in BCa cells **(Figure 4.24 D)**. CB showed nearly similar potential to reduce the membrane potential in both test breast cancer cell lines **(Figure 4.24)**.

## 4.5 Apoptosis induction potential of identified/lead natural products by using real-time polymerase chain reaction (RT-PCR), western blot, flow cytometry, and confocal microscopy

Apoptosis induction potential of identified lead natural products/phytochemicals were studied by using several techniques. First of all, the gene expression of apoptotic and anti-apoptotic proteins was studied at mRNA levels in lead natural products/phytochemicals treated MDA-MB-231 and T47D breast cancer cells. The apoptotic potential of lead natural products/phytochemicals in breast cancer cells were studied on protein levels as well. To examine the early apoptosis, late apoptosis and

necrosis cell populations in lead natural products/phytochemicals treated breast cancer cells, flow cytometric technique was utilized. Lastly, the nuclear morphological changes in lead natural products/phytochemicals treated cells were studied using confocal microscopy technique with the help of Hoechst 33342 fluorescence dye.

Survivin and Bcl2 anti-apoptotic proteins are associated with breast cancer progression and poor prognosis. To explore the suppressive role of BME and BHE extract on anti-apoptotic proteins in MDA-MB-231 and T47D breast cancer cells, we examined the mRNA levels of *SURVIVIN* and *BCL2* gene. BME treatment (24h) significantly reduced the mRNA levels of survivin and Bcl2 in MDA-MB-231 and T47D cells at $IC_{50}$ concentration **(Figure 4.25 A-B)**. In comparison to Bcl2, mRNA levels of survivin in BME treated MDA-MB-231 and T47D cells were highly reduced in 24h treatment. 48h BME treatment reduced the survivin and Bcl2 levels in MDA-MB-231 and T47D cells in comparison to control cells (non-treated) **(Figure 4.25 A-B)**. BHE treatment showed an impressive reduction in survivin mRNA levels in MDA-MB-231 (in 24h) and T47D (in 48h) cells at $IC_{50}$ concentration **(Figure 4.25 C-D)**.

To explore the inductive role of lead natural products/phytochemicals on mitochondria-mediated apoptosis in MDA-MB-231 and T47D breast cancer cells we examined the mRNA levels of caspase 3. *B. frutescens* treatment showed a significant fold increase (4.7-26 fold) of caspase 3 mRNA levels in MDA-MB-231 and T47D breast cells at $IC_{50}$ concentration **(Figure 4.26 A)**. Methanolic extract exerts time-dependent profound increase (23.22 fold) in caspase 3 mRNA levels in T47D cells after 48h treatment **(Figure 4.26 A)**. Hexane extract also depicted a significant increase (26 fold) in caspase 3 mRNA levels in MDA-MB-231 cells in 48h treatment at $IC_{50}$ concentration. In 48h treatment with BME and BHE extracts in MDA-MB-231 and T47D cancer cells significant increase (20-26 fold) in caspase 3 level was observed at $IC_{50}$ concentration **(Figure 4.26 A)**. Comparatively better efficacy of extracts against MDA-MB-231 cells motivated us to study the procaspase expression at the protein level. Western blot analysis showed higher procaspase 3 protein levels in extract-treated cells in comparison to non-treated MDA-MB-231 breast cancer cells **(Figure 4.26 B)**.

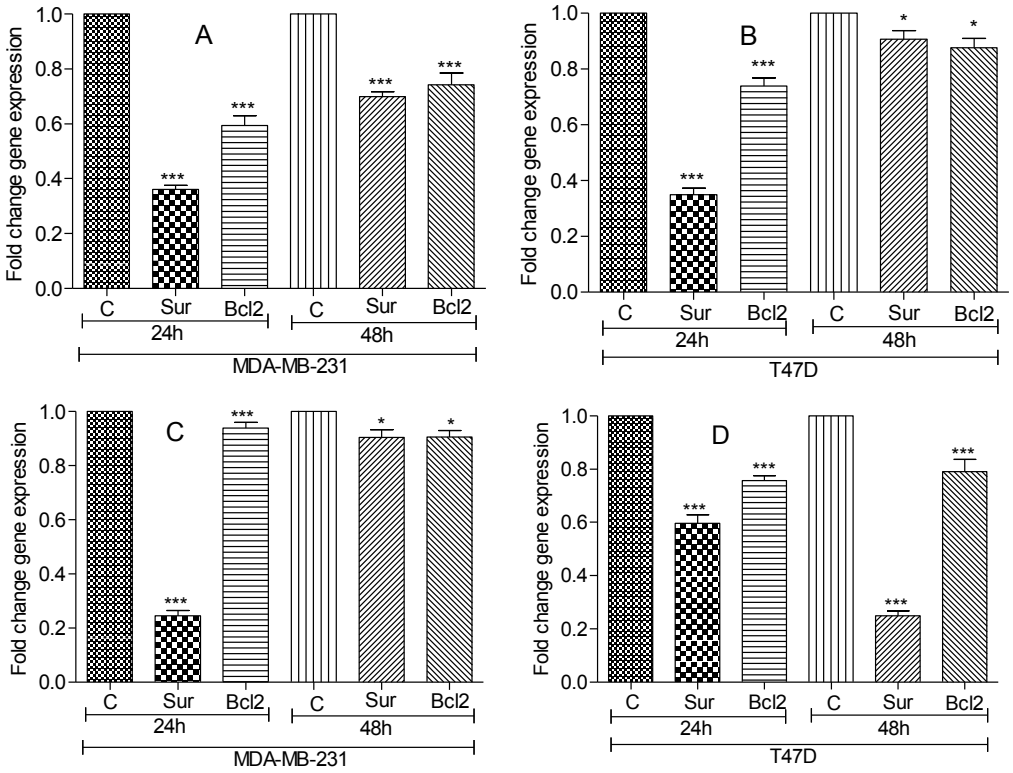


**Figure 4.25** Effect of *B. frutescens* extracts on survivin and Bcl2 markers in human breast cancer cells at $IC_{50}$ concentration in 24, and 48h treatment. (A) and (B) mRNA levels of survivin and Bcl-2 in *B. frutescens* methanolic extract treated MDA-MB-231 and T47D cells respectively (C) and (D) mRNA levels of survivin and Bcl-2 in *B. frutescens* hexane extract-treated MDA-MB-231 and T47D cells respectively. Results are expressed as mean±SD of the three replicates. ***P<0.0005 vs. control; *P<0.05 vs. control; C=Control.

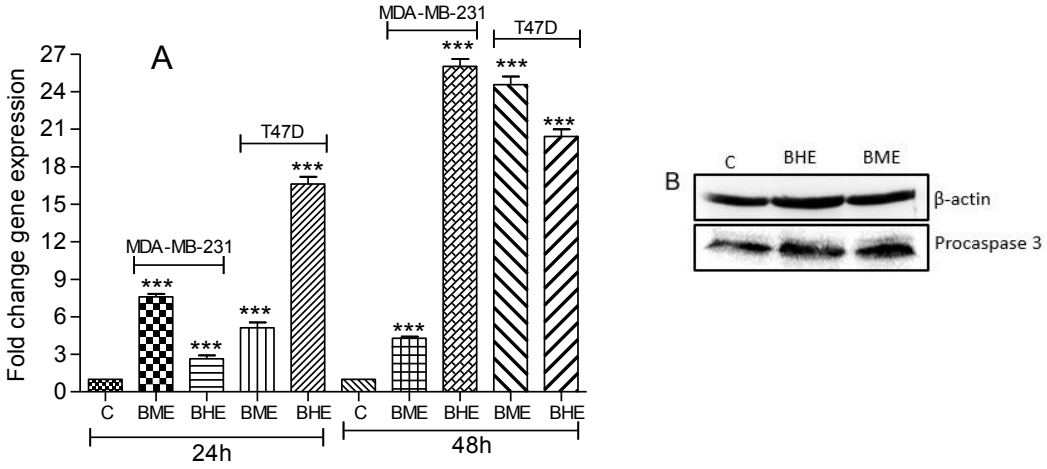


**Figure 4.26** Effect of *B. frutescens* extracts (BME and BHE) on caspase 3 markers in human breast cancer cells at $IC_{50}$ concentration in 24, and 48h treatment. (A) mRNA levels of caspase 3 in *B. frutescens* methanolic and hexane extract-treated MDA-MB-231 and T47D breast cancer cells.

Effect of *B. frutescens* extracts on procaspase 3 protein expression was studied in MDA-MB-231 cells using western blot technique. The cell samples were collected after 12 h BME and BHE treatment at $IC_{50}$ concentration. (B) Procaspase 3 protein expression in BHE and BME treated MDA-MB-231 cells. β-actin was used as an internal control.
Results are expressed as mean±SD of the three replicates. ***P<0.0005 vs. control. BHE= *B. frutescens* hexane extract; BME= *B. frutescens* methanol extract; C=Control.

*B. frutescens* extract showed better apoptotic inducing capacity (26 fold increase in caspase 3 mRNA level) in MDA-MB-231 cells **(Figure 4.26).** Thus we quantified apoptosis induction ability of BHE and BME extract in 12 h treatment MDA-MB-231 breast cells using Annexin-V/PI double staining assay. The result showed that BHE and BME have little impact on late apoptosis (2-4%) at both sub $IC_{50}$ and $IC_{50}$ concentration. BHE treatment increased the early apoptotic MDA-MB-231 cell population from ≈4% to ≈15% at sub $IC_{50}$ and $IC_{50}$ concentration respectively. BME treatment showed a 10% to 15% increase in early apoptotic cells at sub $IC_{50}$ and $IC_{50}$ concentration respectively in comparison to non-treated cells **(Figure 4.27 A-B).** It should be noted that BHE and BME treatment at $IC_{50}$ in 12h showed a 6% breast cancer cell necrotic population.

To verify the presence of apoptotic cells, we examined the change in nuclear morphology by using Hoechst 33342 staining dye in lead natural products/phytochemical treated MDA-MB-231 and T47D breast cancer cells and respective controls (non-treated cells). A significant number of apoptotic cells were observed in BHE and BME treated MDA-MB-231 cells at the sub $IC_{50}$ concentration in 16h treatment **(Figure 4.28 A).** The apoptotic cells nuclei were condensed and fragmented as revealed by the Hoechst 33342 nuclear-staining dye at 20X resolution in test cells **(Figure 4.28).** The deformed shape of the nucleus has appeared in the extracts treated cells compared to control cells at a higher resolution (100X). Similarly, BHE and BME treated T47D cells at sub $IC_{50}$ concentration showed a significant number of apoptotic cells in 16h treatment **(Figure 4.28 B)**.

Kurarinone (a lavandulyl flavanone) treatment (24h) significantly reduced the mRNA levels of survivin and Bcl2 in MDA-MB-231 and T47D cells **(Figure 4.29 A-B)**. KU treated T47D cells at $IC_{50}$ concentration showed a highly reduced expression of Bcl-2 mRNA in comparison to MDA-MB-231 cells in 24h treatment.

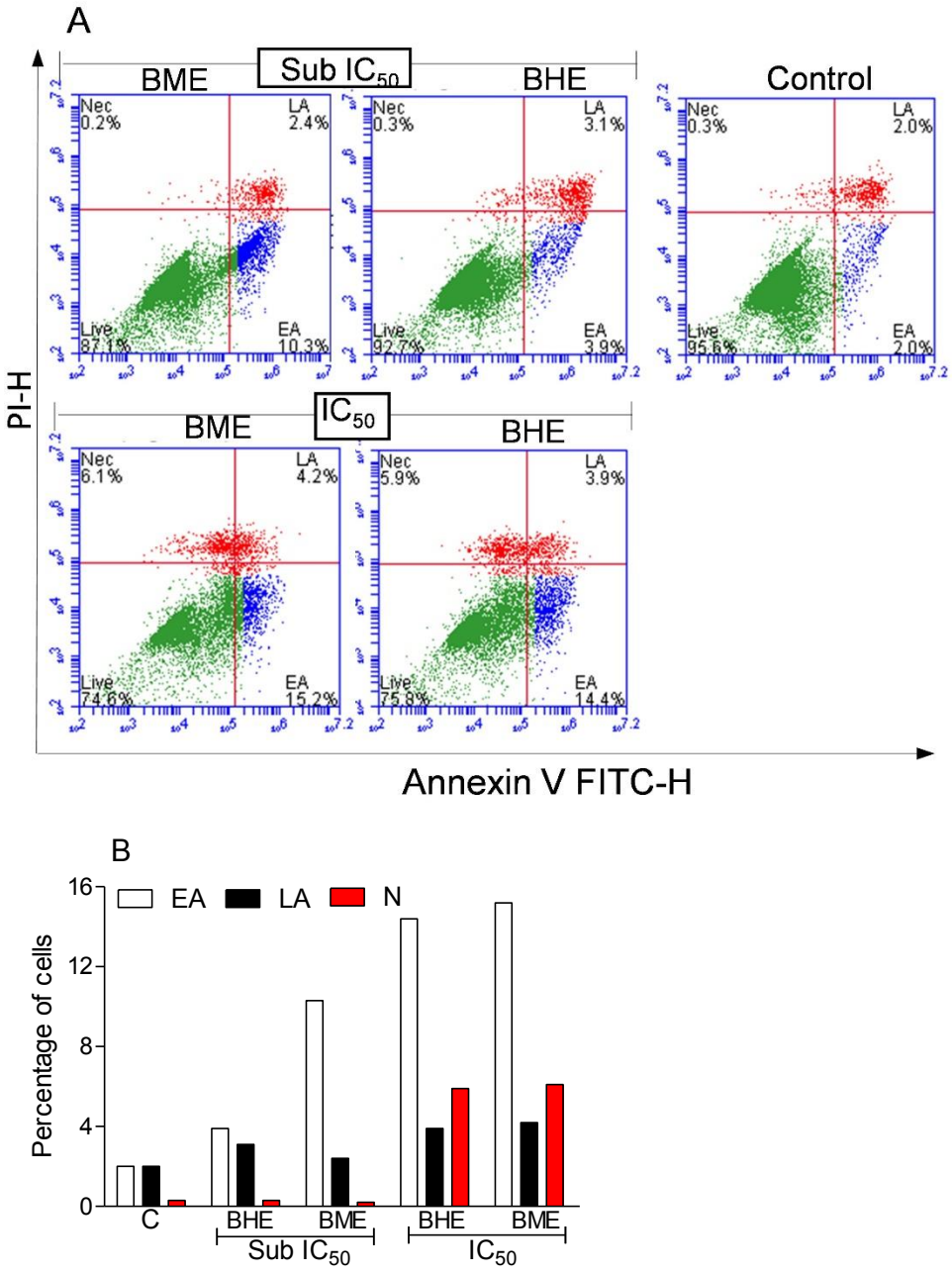


**Figure 4.27** Effect of *B. frutescens* extracts on apoptosis of breast cancer cells.
Flow cytometry technique was used to quantify the *B. frutescens* extracts apoptosis induction potential in breast cancer cells. (A) BME and BHE induced apoptotic cell death in MDA-MB-231 breast cancer cells at sub $IC_{50}$ and $IC_{50}$ concentration in 12h treatment. (B) Percentage representation of early apoptotic, late apoptotic and necrotic cell population in BME and BHE treated MDA-MB-231 cells in comparison to non-treated cells. BHE= *B. frutescens* hexane extract; BME= *B. frutescens* methanol extract; PI-H=Propidium iodide-height; EA=Early apoptosis; LA=late apoptosis; N=Necrosis; C=Control.

In 48h KU treatment (at $IC_{50}$ concentration), both survivin and Bcl-2 showed a significant decrease in mRNA expression in MDA-MB-231 cells. **(Figure 4.29 A-B)**. It

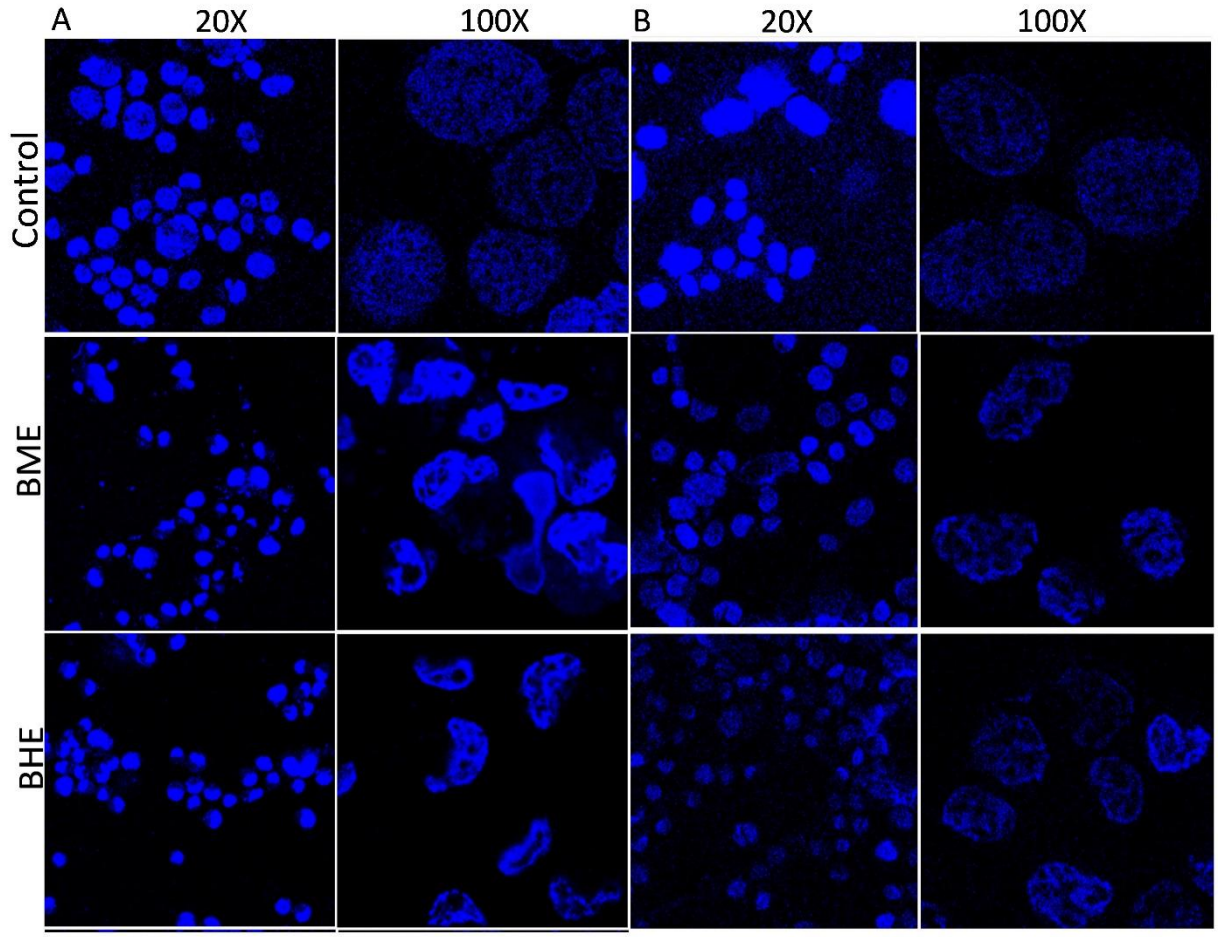


**Figure 4.28** Effect of *B. frutescens* extracts on apoptosis induction potential in breast cancer cells. (A) and (B) Confocal microscopy was used to show the effect of *B. frutescens* extracts on nuclear morphology of MDA-MB-231 and T47D breast cells respectively using Hoechst 33342 dye at sub $IC_{50}$ concentration. BHE= *B. frutescens* hexane extract; BME= *B. frutescens* methanol extract.

should be noted that KU treated T47D cells showed a lesser reduction in survivin expression in comparison to KU treated MDA-MB-231 cells in 48h treatment.

KU treatment showed a significant increase of caspase 3 mRNA levels (≈5.5 and ≈4.2 fold) in MDA-MB-231 cells in 24h and 48h treatment respectively at $IC_{50}$ concentration **(Figure 4.30 A)**. However, in T47D cells KU exerts 1.5 and 2.2 fold increase in caspase 3 mRNA levels in 24h and 48h treatment respectively at $IC_{50}$ concentration. **(Figure 4.30 A)**.

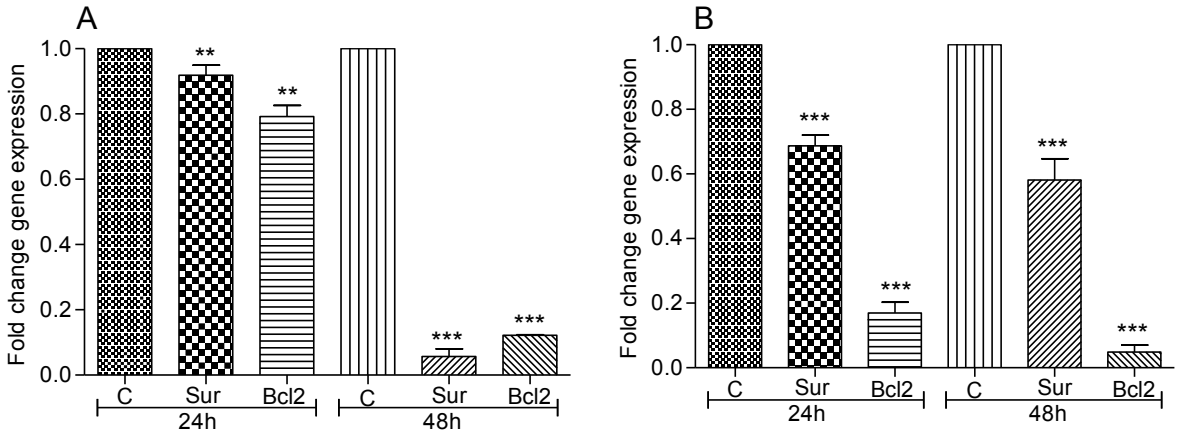


**Figure 4.29** Effect of Kurarinone on mRNA levels of survivin and Bcl2 markers in human breast cancer cells at $IC_{50}$ concentration in 24, and 48h treatment. (A) and (B) mRNA levels of survivin and Bcl-2 in Kurarinone treated MDA-MB-231 and T47D cells respectively. Results are expressed as mean±SD of the three replicates. ***P<0.0005 vs. control. **P<0.0005 vs. control.

Western blot analysis showed reduced procaspase 3 protein levels in KU treated MDA-MB-231 cells in comparison to non-treated breast cancer cells **(Figure 4.30 B)**. This suggests that procaspase 3 converted to active caspase 3 (cleaved caspase 3) which initiates apoptosis in KU treated breast cancer cells.

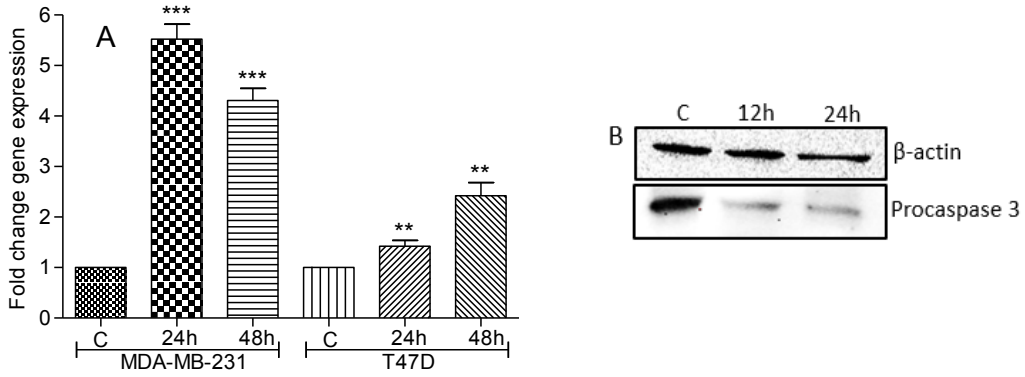


**Figure 4.30** Effect of Kurarinone on mRNA levels of caspase 3 markers in human breast cancer cells at $IC_{50}$ concentration in 24, and 48h treatment. (A) mRNA levels of caspase 3 in Kurarinone treated MDA-MB-231 and T47D breast cancer cells.
Effect of Kurarinone on procaspase 3 protein expression was studied in MDA-MB-231 cells using western blot technique. The cell samples were collected after 12 and 24 h Kurarinone treatment at $IC_{50}$ concentration. (B) Procaspase 3 protein expression in Kurarinone treated MDA-MB-231 cells. β-actin was used as an internal control. Results are expressed as mean±SD of the three replicates. ***P<0.0005 vs. control. **P<0.0005 vs. control.

We quantified the apoptosis induction ability of KU (at sub $IC_{50}$ and $IC_{50}$ concentration) in 12 h treatment MDA-MB-231 breast cells using Annexin-V/PI double staining assay. The result showed that KU has little impact on late apoptosis (4.7-5.9%) at both sub $IC_{50}$ and $IC_{50}$ concentration. KU treatment increased the early apoptotic MDA-MB-231 cell population from 16.2% to 18.1% at sub $IC_{50}$ and $IC_{50}$ concentration respectively**.** It should be noted that KU treatment at sub $IC_{50}$ and $IC_{50}$ in 12h showed 3%-3.1% breast cancer cell necrotic population.

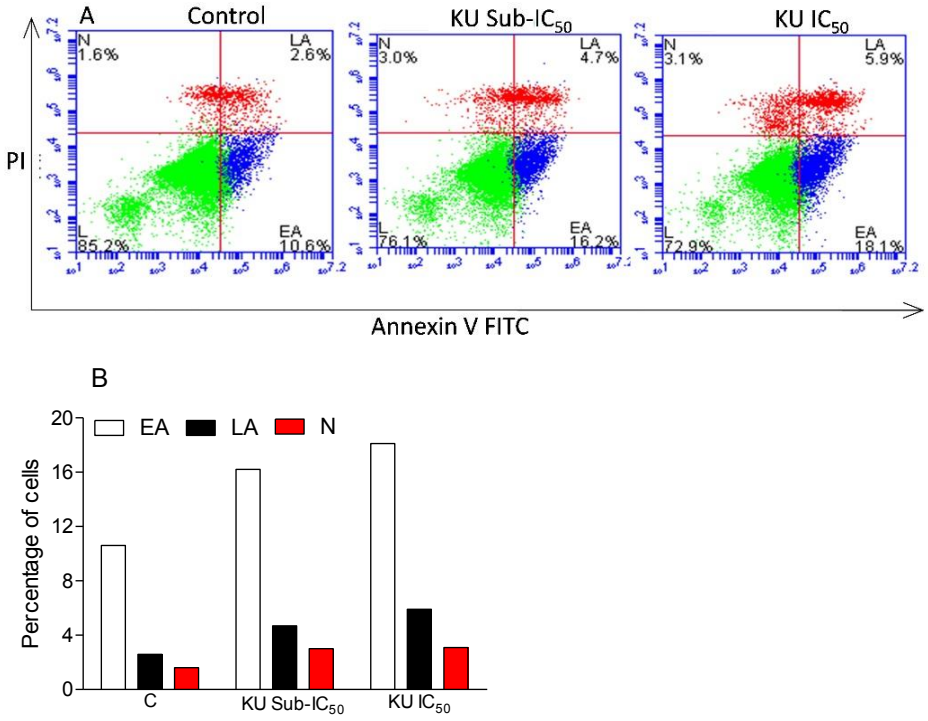


**Figure 4.31** Effect of Kurarinone on apoptosis of breast cancer cells. Flow cytometry technique was used to quantify the Kurarinone apoptosis induction potential in breast cancer cells. (A) Kurarinone induced apoptotic cell death in MDA-MB-231 breast cancer cells at sub $IC_{50}$ and $IC_{50}$ concentration in 12h treatment. (B) Percentage representation of early apoptotic, late apoptotic and necrotic cell population in Kurarinone treated MDA-MB-231 cells in comparison to non-treated cells. PI-H=Propidium iodide-height; EA=Early apoptosis; LA=late apoptosis; N=Necrosis; C=Control.

To confirm the existence of apoptotic cells in Kurarinone treated MDA-MB-231 and T47D cells, treatment was performed at sub $IC_{50}$ concentration for the respective cells for 16h at 37°C. The result showed a significant decrease in fluorescence intensity of MDA-MB-231 and T47D treated cells by about 7 and 1.3 fold respectively in comparison to respective non-treated cells **(Figure 4.31 A-B).** 20X magnification

pictures were used for the graphical representation of the effect of Hoechst 33342 dye in treated cells.

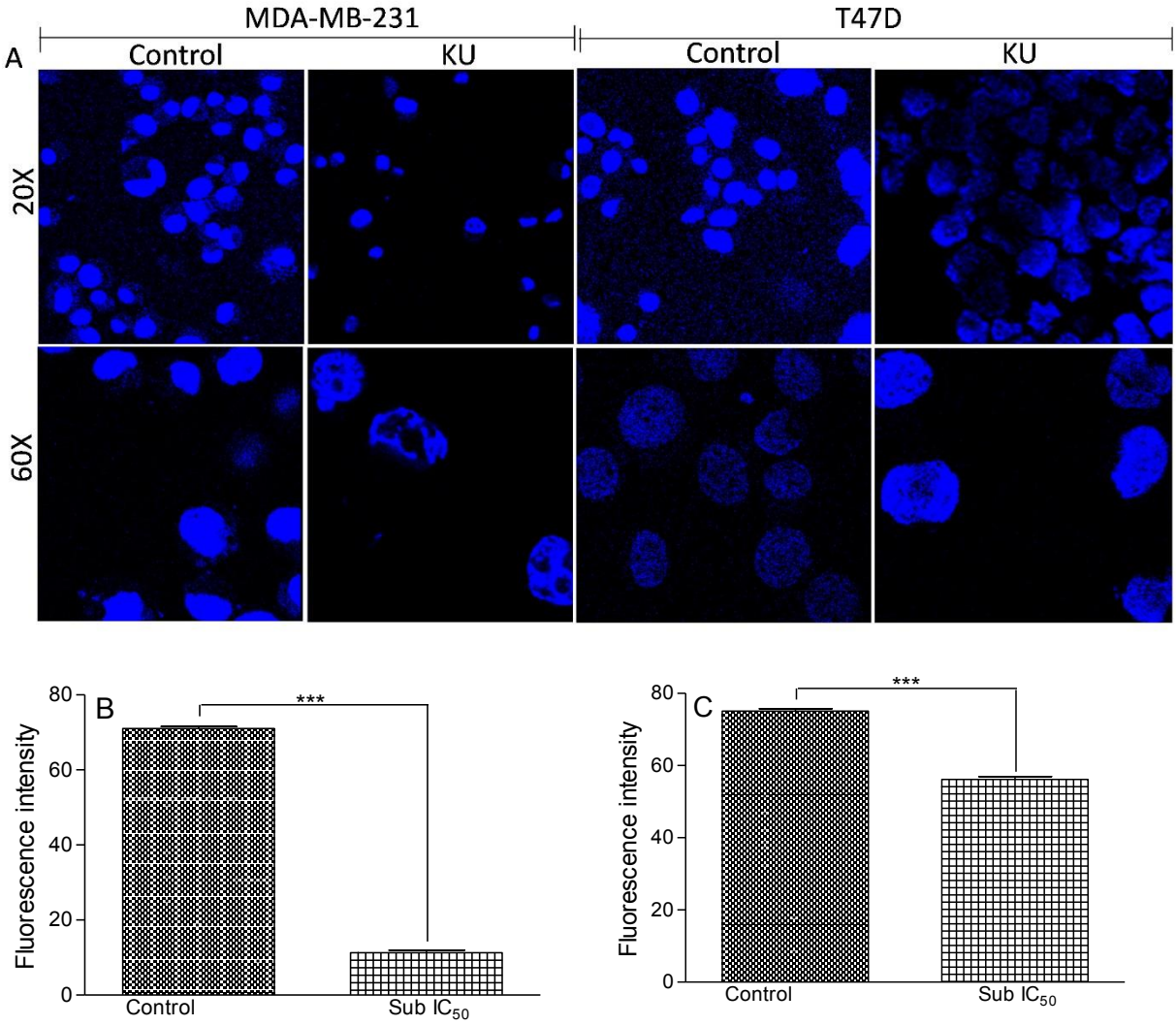


**Figure 4.32** Effect of Kurarinone on apoptotic induction potential in breast cancer cells. (A) Confocal microscopy was used to show the effect of Kurarinone on nuclear morphology of MDA-MB-231 and T47D breast cells using Hoechst 33342 dye at sub $IC_{50}$ concentration. (B) and (C) Graphical representation of fluorescence intensity of 20X magnification image in MDA-MB-231 and T47D cells respectively. Results are expressed as mean±SD of the three replicates. ***P<0.0005 vs. control.

At 20X resolution, the nuclei of apoptotic cells were condensed and fragmented as revealed by the Hoechst 33342 nuclear-staining dye **(Figure 4.32 B-C).** At higher resolution (60X magnification), the deformed shape of the nucleus was found in the treated cells compared to control cells **(Figure 4.32 A).**

CB treatment (24h) significantly lowers the mRNA levels of survivin and Bcl2 in both MDA-MB-231 and T47D cells **(Figure 4.33 A-B)**.

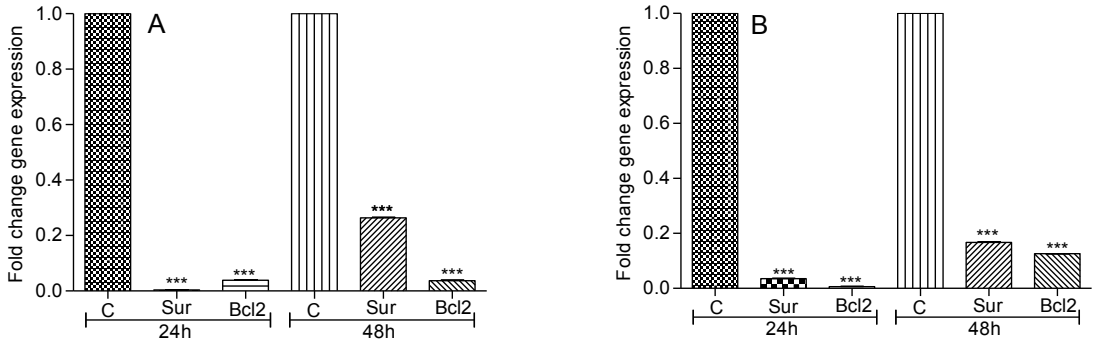


**Figure 4.33** Effect of CB on mRNA levels of survivin and Bcl2 markers in human breast cancer cells at $IC_{50}$ concentration in 24, and 48h treatment. (A) and (B) mRNA levels of survivin and Bcl-2 in CB treated MDA-MB-231 and T47D cells respectively. Results are expressed as mean±SD of the three replicates. ***P<0.0005 vs. control.

After 48h CB treatment at $IC_{50}$ concentration, both survivin and Bcl-2 mRNA levels were significantly decreased in both test cells **(Figure 4.33 A-B)**. It should be mentioned that T47D cells treated with CB treated showed less reduction of Bcl-2 expression in contrast to MDA-MB-231 cells in 48h treatment.

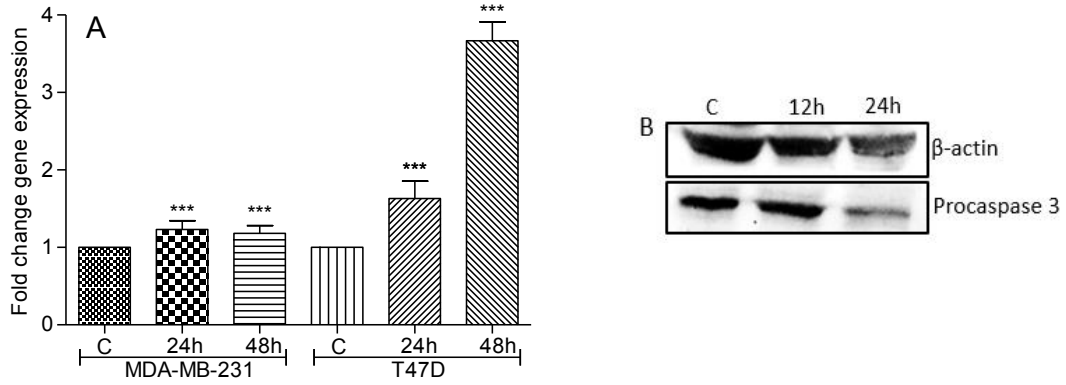


**Figure 4.34** Effect of CB on caspase 3 markers in human breast cancer cells at $IC_{50}$ concentration in different time interval treatment. (A) mRNA levels of caspase 3 in CB treated MDA-MB-231 and T47D breast cancer cells. Effect of CB on procaspase 3 protein expression was studied in MDA-MB-231 cells using western blot technique. The cell samples were collected after 12 and 24h CB treatment at $IC_{50}$ concentration. (B) Procaspase 3 protein expression in CB treated MDA-MB-231 cells. β-actin was used as an internal control. Results are expressed as mean±SD of the three replicates. ***P<0.0005 vs. control.

CB treatment significantly increased the levels of caspase 3 mRNA in MDA-MB-231 cells in 24h and 48h treatment respectively **(Figure 4.34 A)**. However, in T47D cells CB exerts 0.6 and 2.6 fold increase of caspase 3 mRNA levels in 24h and 48h treatment respectively **(Figure 4.34 A)**. Western blot results showed increased levels of procaspase 3 proteins in CB treated MDA-MB-231 cells in contrast to non-treated breast cancer cells in 12 h treatment **(Figure 4.34 B)**. In 24h, CB treated MDA-MB-231 cells showed reduced expression of procaspase 3 which suggests that procaspase 3 converted to active caspase 3 (cleaved caspase 3) which initiates apoptosis in CB treated breast cancer cells.

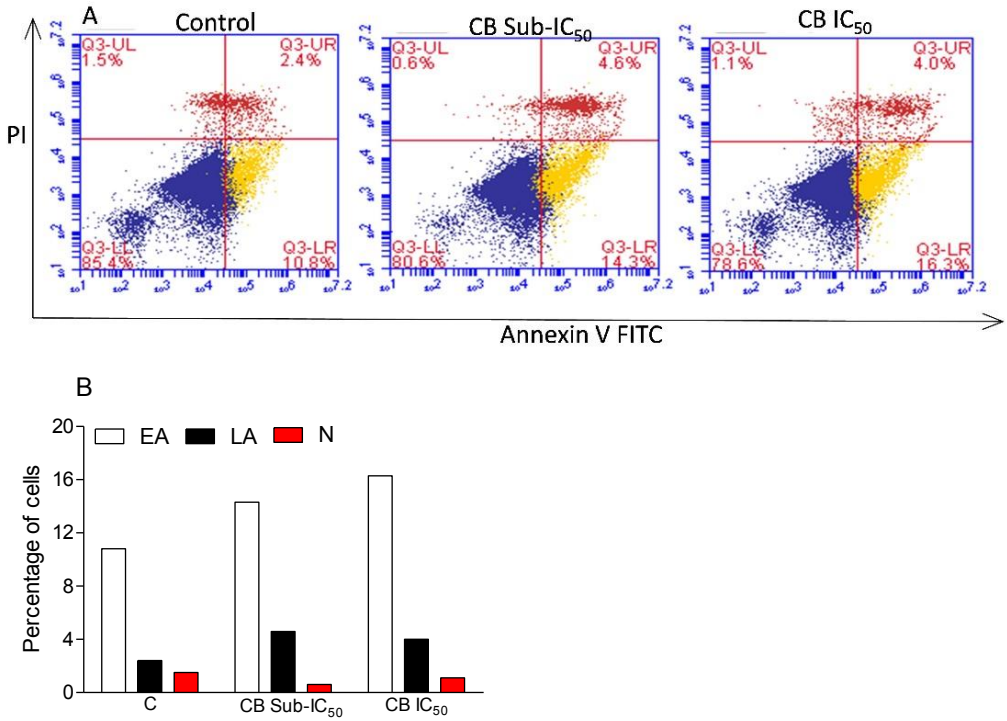


**Figure 4.35** Effect of CB on apoptosis of breast cancer cells. Flow cytometry technique was applied to quantify the CB apoptosis induction potential in breast cancer cells. **(A)** CB induced apoptotic cell death in MDA-MB-231 breast cancer cells at sub $IC_{50}$ and $IC_{50}$ concentration in 12h treatment. **(B)** A percentage representation of early apoptotic, late apoptotic and necrotic cell population in CB treated MDA-MB-231 cells in comparison to non-treated cells. PI=Propidium iodide; EA=Early apoptosis; LA=late apoptosis; N=Necrosis; C=Control.

We quantified apoptosis-inducing potential of CB after 12h treatment in MDA-MB-231 breast cells by performing Annexin-V/PI double staining assay. The result pointed out that CB has a remarkable effect on late apoptosis (4-4.6%) at both $IC_{50}$ and sub $IC_{50}$

concentrations. CB treatment increased early apoptosis in MDA-MB-231 cells by ≈14.3% to ≈16.3% at sub $IC_{50}$ and $IC_{50}$ concentration respectively **(Figure 4.35 A-B).**

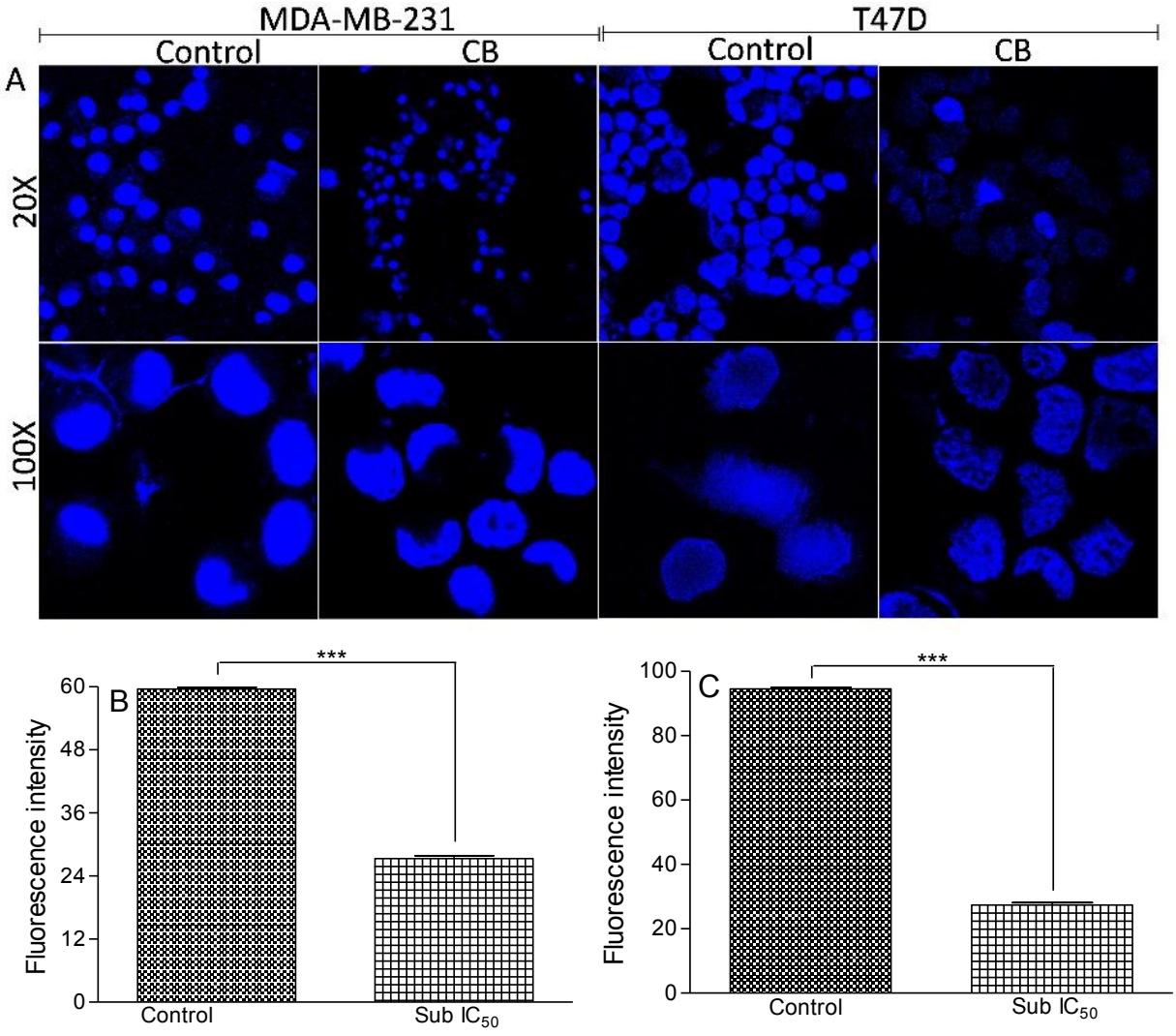


**Figure 4.36** Apoptotic induction potential of 3-O-(E)-p-Coumaroylbetulinic acid (CB) on in breast cancer cells. (A) Confocal microscopy was applied to demonstrate the effect of CB on the nuclear morphology of breast cancer cells (MDA-MB-231 and T47D) using Hoechst 33342 dye at sub $IC_{50}$ concentration. (B) and (C) Graphical representation of fluorescence intensity of 20X magnification image in MDA-MB-231 and T47D cells respectively.

To find the existence of apoptotic cells in CB treated MDA-MB-231 and T47D cells, the treatment was done at sub $IC_{50}$ concentration and incubated for 16h at room temperature. Results revealed a significant decrease in fluorescence intensity was observed in MDA-MB-231 (≈2.18 fold) and T47D cells (≈3.45 fold) in comparison to respective non-treated cells **(Figure 4.36 B-C).** 20X magnification pictures were taken

for the graphical representation of the effect of Hoechst 33342 dye in treated cells. At 20X resolution, Hoechst 33342 nuclear-staining showed condensed and fragmented nuclei of apoptotic cells (**Figure 4.36 A).** At higher resolution (100X magnification), the deformed shape of the nucleus was appeared in the treated cells in contrast to control cells **(Figure 4.36 A).**

## 4.6 Notch signaling inhibition potential of identified/lead natural products at mRNA, protein and promoter level

*In silico* study showed Ɣ-secretase binding potential in *B. frutescens* phytochemicals, KU and CB **(Figure 4.2, 4.4, and 4.5)**. Thus, we tried to study the role of these lead natural products/phytochemicals on the notch signaling pathway in breast cancer cells. The notch signaling pathway was studied at mRNA (Hes1 and Hey1), protein (Hes1, E-cadherin) and promoter (notch promoter) level. In order to elucidate the inhibitory potential of lead compounds/extract on Ɣ-secretase mediated notch signaling pathway inhibition, we assessed the notch promoter activity to check whether NICD is produced or not in the presence of test samples.

Inhibition of Ɣ-secretase enzyme by inhibitors stops NICD production and thereby decrease downstream transcription of notch targeted genes. Standard notch signaling and Ɣ-secretase inhibitor DAPT were taken as control. BME extract significantly reduced Hey1 mRNA levels (2.5 and 5 fold) in T47D cancer cells at 24h and 48h treatment **(Figure 4.37 D)**. BME treatment (at $IC_{50}$ concentration) significantly reduced the Hes1 and Hey1 mRNA levels in MDA-MB-231 and T47D cells in 24h treatment **(Figure 4.37 C-D)**. Comparatively less effect of BME treatment was found on Hes1 and Hey1 mRNA levels in MDA-MB-231 cells in 48h treatment **(Figure 4.37 C)**.

In comparison to BME extract, BHE treatment showed less potential to decrease the mRNA levels of Hes1 and Hey1 in MDA-MB-231 and T47D cells in 24h and 48h treatment **(Figure 4.37 E-F)**. Western blot analysis showed suppressed Hes1 and Hes1 protein levels and increased E-cadherin protein levels in BME treated MDA-MB-231 cells at $IC_{50}$ concentration in time dependent manner **(Figure 4.37 G)**.

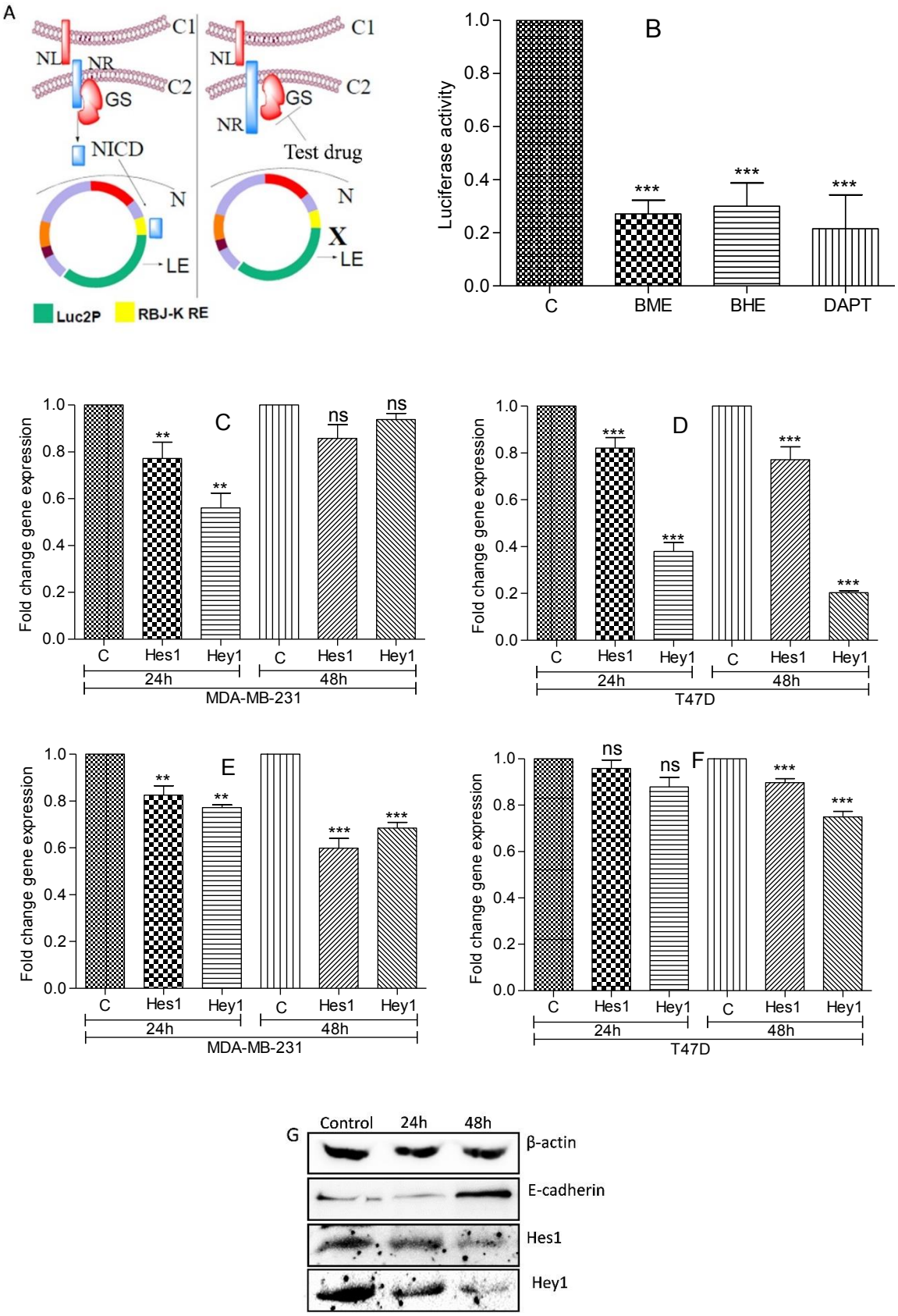
A
C1
NL
NR
C2
GS
NICD
N
LE
Luc2P
RBJ-K RE
Test drug
X
B
Luciferase activity
1.0
0.8
0.6
0.4
0.2
0.0
***
C
BME
BHE
DAPT
C
Fold change gene expression
**
ns
Hes1
Hey1
24h
48h
MDA-MB-231
D
***
T47D
E
F


G
Control
24h
48h
β-actin
E-cadherin
Hes1
Hey1

**Figure 4.37** Notch signaling pathway inhibitory potential in *B. frutescens* extracts against breast cancer cells. Notch dual-luciferase promoter assay was used to study the notch signaling pathway inhibition by BHE and BME at the promoter level. (A) The left and right panel shows activation and inhibition of the notch signaling pathway respectively. In the left panel, NICD is produced by notch-ligand interaction and activation of Ƴ-secretase enzyme. Interaction of NICD to RBJ-K RE sequence (notch promoter sequence) initiates luciferase gene expression. The right panel shows inhibition of luciferase gene expression in the presence of *B. frutescens* phytochemicals which inhibits Ƴ-secretase mediated NICD production. (B) Inhibitory potential of BME and BHE ($IC_{50}$ concentration) extracts and standard notch inhibitor DAPT (20 µM) on notch promoter using dual luciferase assay. HEK293 cells were used for the experiment and luminescence was recorded on GloMax 20/20 Luminometer.
RT-PCR technique was used to show the effect of *B. frutescens* extracts on mRNA levels of notch responsive genes (*HES1* and *HEY1*) in MDA-MB-231 and T47D cells. The cells were treated at $IC_{50}$ concentration for 24 and 48h. (C) and (D) mRNA levels of Hes1 and Hey1 in BME treated MDA-MB-231 and T47D breast cancer cells respectively. E) and F) mRNA levels of Hes1 and Hey1 in BHE treated MDA-MB-231 and T47D breast cancer cells respectively.
Effect of *B. frutescens* on E-cadherin, Hes1 and Hey1 protein expression was studied in MDA-MB-231 cells using the western blot technique. The cell samples were collected after 24 and 48h BME treatment at $IC_{50}$ concentration. (D) E-cadherin, Hes1 and Hey1 protein expression in BME treated MDA-MB-231 cells. β-actin was used as an internal control.
Results are expressed as mean±SD of the three replicates. ***P<0.0005 vs. control; **P<0.005 vs. control. NL=Notch ligand; NR=Notch receptor; C1=Cell membrane of cell 1; C2=Cell membrane of cell 2; GM=Gamma secretase; NICD=Notch intracellular cleaved domain; N=Nucleus; LE=Luciferase expression.

Luciferase gene transcription was significantly decreased in BME, BHE and DAPT treated transfected-HEK293 cells. BME (at $IC_{50}$ concentration), BHE (at $IC_{50}$ concentration), and DAPT (20 µM) treatment showed 3.7, 3.33, and 5 fold downregulation of luciferase gene expression in 24h respectively **(Figure 4.37 B).**

The mRNA levels of notch responsive (*HES1* and *HEY1*) genes in KU treated MDA-MB-231 and T47D breast cancer cells were measured. In 24h, KU treatment significantly reduced the Hes1 and Hey1 mRNA levels in MDA-MB-231 and T47D cells **(Figure 4.38 A-B).** KU treatment significantly reduced Hes1 and Hey1 mRNA levels in T47D cancer cells at 24h and 48h **(Figure 4.38 B).** In 48h treatment, KU treated MDA-MB-231 cells showed a significant reduction in *HES1* gene expression (≈5 fold) in comparison to 24h treated (≈1.25 fold) MDA-MB-231 cells.

Western blot analysis showed suppressed Hes1 protein levels in KU treated (at $IC_{50}$ concentration) MDA-MB-231 cells in comparison to non-treated breast cancer cells at 24h and 48h time interval **(Figure 4.38 D)**.

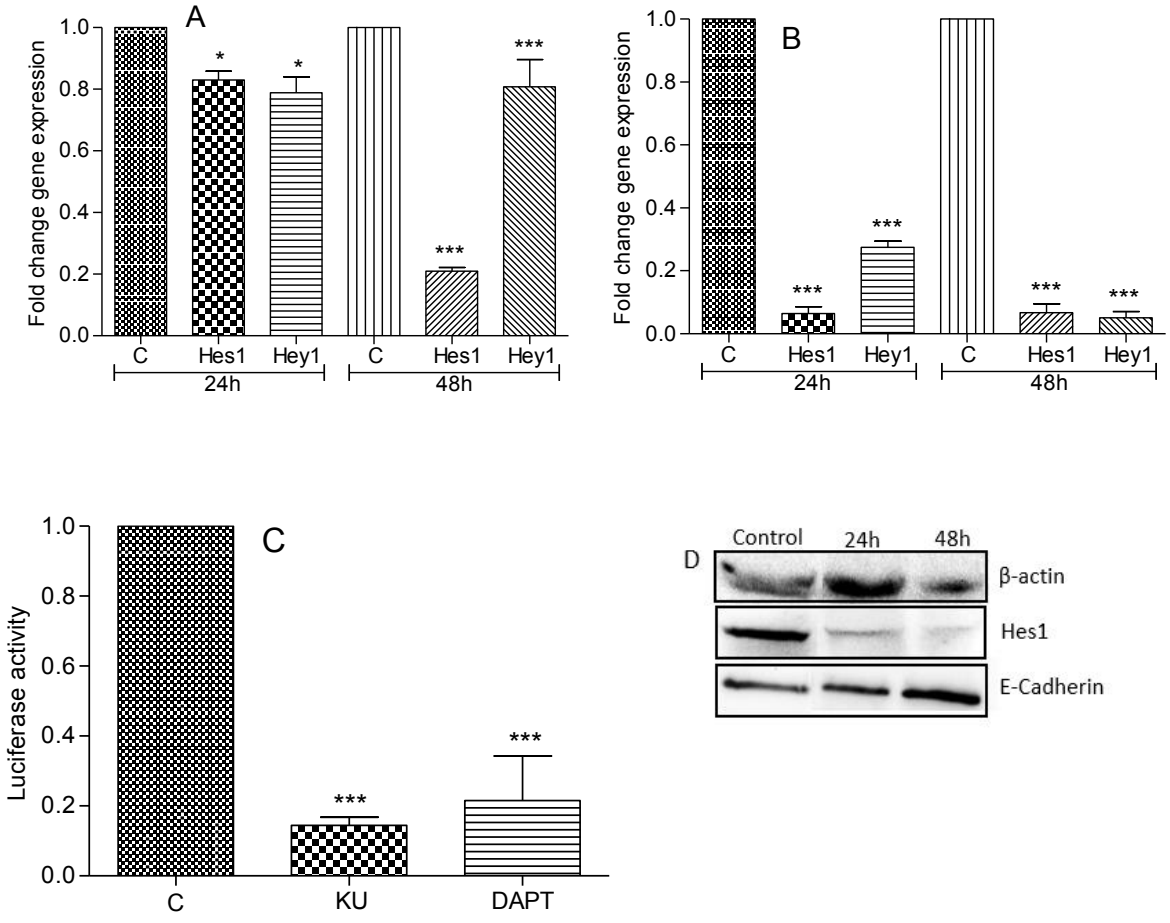


**Figure 4.38** Notch signaling pathway inhibitory potential in Kurarinone against breast cancer cells.
RT-PCR technique was used to show the effect of Kurarinone on mRNA levels of *HES1* and *HEY1* notch responsive genes in human breast cancer cells at $IC_{50}$ concentration in 24 and 48h treatment. (A) and (B) mRNA levels of Hes1 and Hey1 in KU treated MDA-MB-231 and T47D breast cancer cells respectively.
Notch dual-luciferase promoter assay was used to study the notch signaling pathway inhibition by Kurarinone at the promoter level. (C) Inhibitory potential of Kurarinone ($IC_{50}$ concentration) and standard notch inhibitor DAPT (20 μM) on notch promoter using dual luciferase assay.
Effect of Kurarinone on Hes1 and E-cadherin protein expression was studied in MDA-MB-231 cells using the western blot technique. The cell samples were collected after 24 and 48h Kurarinone treatment at $IC_{50}$ concentration. (D) Hes1 and E-cadherin protein expression in Kurarinone treated MDA-MB-231 cells. β-actin was used as an internal control.
Results are expressed as mean±SD of the three replicates. ***P<0.0005 vs. control; *P<0.05 vs. control.

Moreover, KU treatment (at $IC_{50}$ concentration) in breast cancer cells showed time-dependent increased expression of E-cadherin protein **(Figure 4.38 D).** Luciferase gene transcription was significantly decreased in KU and DAPT treated transfected-HEK293 cells. KU and DAPT treatment showed about 10 and 5 fold downregulation of luciferase gene expression in 24h respectively at $IC_{50}$ concentration **(Figure 4.38 C).**

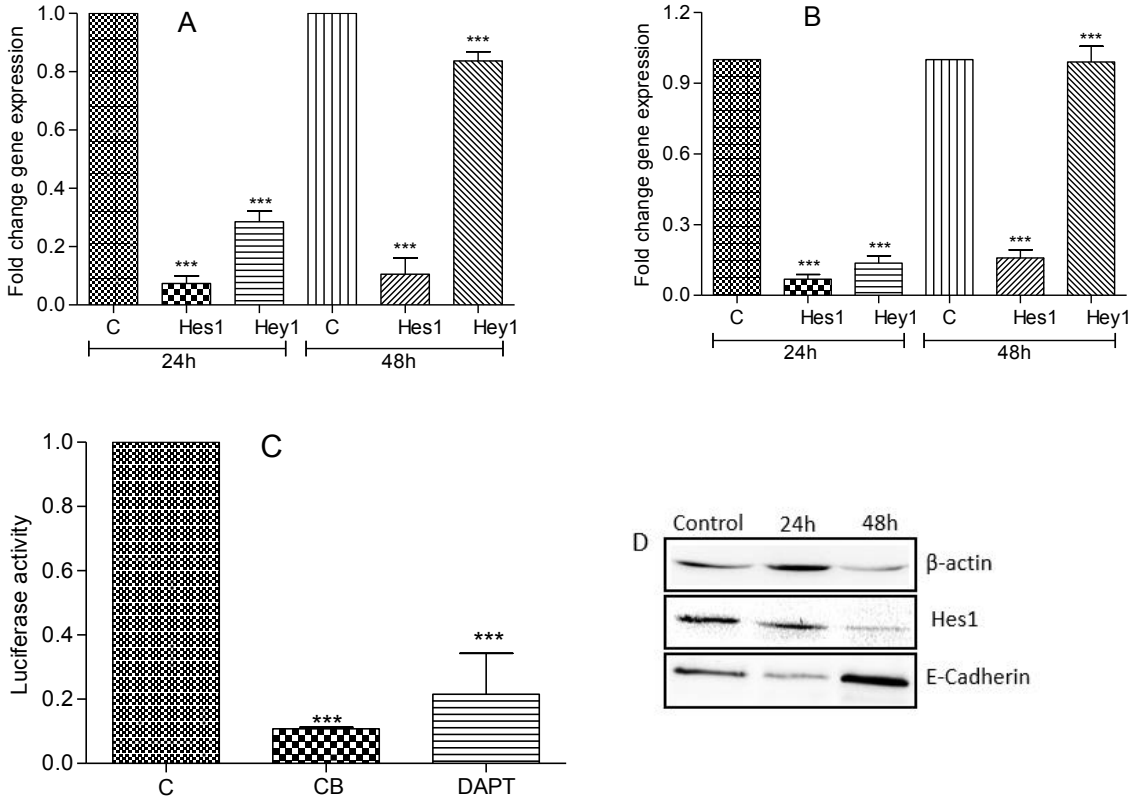


**Figure 4.39** Notch signaling pathway inhibitory potential in 3-O-(E)-p-Coumaroylbetulinic acid (CB) against breast cancer cells.
RT-PCR technique was applied to demonstrate the effect of CB on mRNA levels of *HES1* and *HEY1* notch responsive genes in human breast cancer cells at $IC_{50}$ concentration in 24 and 48h treatment. (A) and (B) mRNA levels of Hes1 and Hey1 in CB treated MDA-MB-231 and T47D breast cancer cells respectively.
Notch dual-luciferase promoter assay was applied to demonstrate the notch signaling pathway inhibition by CB at the promoter level. (C) Inhibitory potential of CB ($IC_{50}$ concentration) and standard notch inhibitor DAPT (20 µM) on notch promoter using dual luciferase assay. HEK293 cells were used for the experiment and luminescence was recorded on GloMax 20/20 Luminometer.
Effect of CB on Hes1 and E-cadherin protein expression was studied in MDA-MB-231 cells using the western blot technique. The cell samples were collected after 24h and 48h CB treatment at $IC_{50}$ concentration. (D) Hes1 and E-cadherin protein expression in CB treated MDA-MB-231 cells. β-actin was used as an internal control.
Results are expressed as mean±SD of the three replicates. ***P<0.0005 vs. control.

The mRNA levels of notch responsive (*HES1* and *HEY1*) genes in breast cancer cells (MDA-MB-231 and T47D) were studied at $IC_{50}$ concentrations of CB. In 24h, CB treatment significantly lowered the mRNA expression of Hes1 and Hey1 in both MDA-MB-231 and T47D cells **(Figure 4.39 A-B).** CB treatment highly reduced Hes1 mRNA levels in both cells (MDA-MB-231 and T47D) at 24h and 48h treatment **(Figure 4.39 A-B).** In 48h treatment, CB treated MDA-MB-231 and T47D cells showed less reduction

in *HEY1* gene expression in comparison to 24h treated breast cancer cells. Western blot analysis showed suppressed Hes1 protein levels in CB treated MDA-MB-231 cells in contrast to non-treated breast cancer cells at $IC_{50}$ concentration in time dependent manner **(Figure 4.39 D)**.

Moreover, CB treatment (at $IC_{50}$ concentrations) induced the E-cadherin protein expression in MDA-MB-231 cells in a time-dependent manner **(Figure 4.39 D)**. Transcription of the luciferase gene was significantly reduced in DAPT and CB treated transfected-HEK293 cells. DAPT (20 µM) and CB (at $IC_{50}$ concentration) treatment showed 5 and 10 fold downregulation of luciferase gene expression respectively after 24h treatment **(Figure 4.39 C).**

## 4.7 Effects of identified/lead natural products on mammosphere

Effect of lead natural products was studied on mammosphere for their notch signaling inhibition potential, sphere formation reduction potential and stemness, self-renewal potential reduction at morphological and molecular levels. For mammosphere related studies, we selected MCF-7 cells as literature revealed that this breast cancer cells forms true mammosphere in comparison to other breast cancer cells.

### 4.7.1 Mammosphere formation reduction potential

MCF-7 mammosphere formation inhibitory potential of Kurarinone (KU) and 3-O-(E)-p-Coumaroylbetulinic acid (CB) was studied using mammosphere formation assay. Mammosphere formation (MCF-7) inhibitory potential of Kurarinone (KU) was performed at different concentrations (10-100 µM) in 96h treatment. Phase-contrast images revealed that KU treatment reduced the mammosphere size at dose-dependent manner in 96h treatment in comparison to non-treated group **(Figure 4.41 B)**. Phase-contrast observation also revealed that the morphology was drastically changed at different concentrations of treatment. Effect of CB on mammosphere formation was examined at two concentrations (10 µM and 100 µM) in 96h treatment. CB reduced mammosphere size and altered morphology at 100 µM concentration in 96h treatment

in comparison to non-treated group as revealed by phase-contrast microscopic images **(Figure 4.42 B)**.

### 4.7.2 Notch signaling inhibition potential at mRNA and protein levels

Gamma secretase mediated notch signaling inhibition potential of KU and CB was studied at mRNA and protein levels in MCF-7 cells mammosphere. *HES1* and *HEY1* notch targeted genes were studied at mRNA levels. Hes1, Hey1 and E-cadherin proteins were studied at protein levels in CB and KU treated mammosphere. KU treatment at $IC_{50}$ concentration showed ≈100 and ≈10 fold reduction in Hes1 and Hey1 mRNA levels respectively at 96h treatment in mammosphere (**Figure 4.40 A)**. KU treatment at $IC_{50}$ concentration reduced Hes1, Hey1 protein levels and enhanced E-cadherin protein levels in mammosphere at 96h treatment **(Figure 4.40 B)**. CB treatment at $IC_{50}$ concentration showed ≈5.2 and ≈1.58 fold reduction in Hes1 and Hey1 mRNA levels respectively at 96h treatment in mammosphere (**Figure 4.40 C)**. CB treatment at $IC_{50}$ concentration reduced Hes1, Hey1 protein levels and increased E-cadherin protein levels in mammosphere at 96h treatment **(Figure 4.40 D)**.

### 4.7.3 Effect of lead natural phytochemicals on self-renewal and stemness reduction potential at mRNA and protein levels in MCF-7 mammosphere

To find out the potential of KU and CB on stemness and self-renewal properties of MCF-7 mammosphere. The MYC, SOX2, CD44, OCT4, NANOG and EPCAM were studied at mRNA levels. Further, c-MYC, SOX2 and CD44 protein were studied in mammosphere to establish the self-renewal and stemness properties reduction potential of KU and CB. In 96h KU treatment, stemness and self-renewal properties in mammosphere was significantly reduced. The mRNA expression of MYC, OCT4, SOX2, NANOG, CD44, and EPCAM were ≈25, ≈2.08, ≈1.28, ≈1.29, ≈33.33, and ≈7.14 fold respectively in KU treated (at $IC_{50}$ concentration) mammosphere at 96h treatment **(Figure 4.41 C)**. Western blot analysis showed suppressed c-MYC, SOX2, and CD44

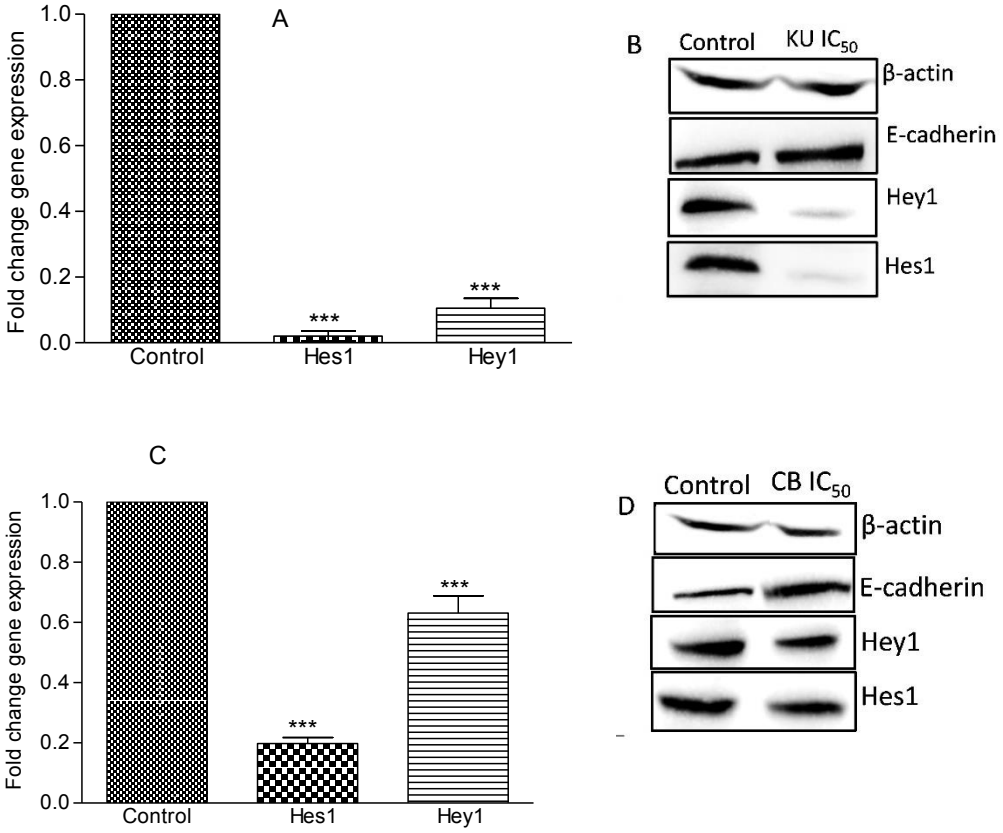


**Figure 4.40** Notch signaling inhibitory potential of Kurarinone and 3-O-(E)-p-Coumaroylbetulinic acid (CB) in treated cancer stem-like cells.
RT-PCR and western blot technique was applied to demonstrate the effect of KU and CB on mRNA and protein levels of notch responsive gene expression in mammosphere cells at $IC_{50}$ concentration in 96h treatment. For western blot analysis, the cell samples were collected after 96h KU and CB treatment at $IC_{50}$ concentration. (A) and (B) Notch responsive gene expression at mRNA (*HEY1* and *HES1*) and protein (Hey1, Hes1, and E-cadherin) levels in KU treated mammosphere cells. (C) and (D) Notch responsive gene expression at mRNA (*HEY1* and *HES1*) and protein (Hey1, Hes1, and E-cadherin) levels in CB treated mammosphere cells. β-actin was used as an internal control. Results are expressed as mean±SD. ***P<0.0005 vs. control.

protein levels in KU treated mammosphere in comparison to non-treated mammosphere **(Figure 4.41 D)**. In 96h CB treatment, stemness and self-renewal properties in mammosphere was significantly reduced. The mRNA expression of MYC, OCT4, SOX2, NANOG, CD44, and EPCAM were ≈33.33, ≈1.29, ≈1.17, ≈1.06, ≈50 and ≈100 fold respectively in CB treated (at $IC_{50}$ concentration) mammosphere at 96h treatment **(Figure 4.42 C)**. Western blot analysis showed suppressed c-MYC, SOX2, and CD44 protein levels in CB treated mammosphere in comparison to non-treated mammosphere **(Figure 4.42 D)**.

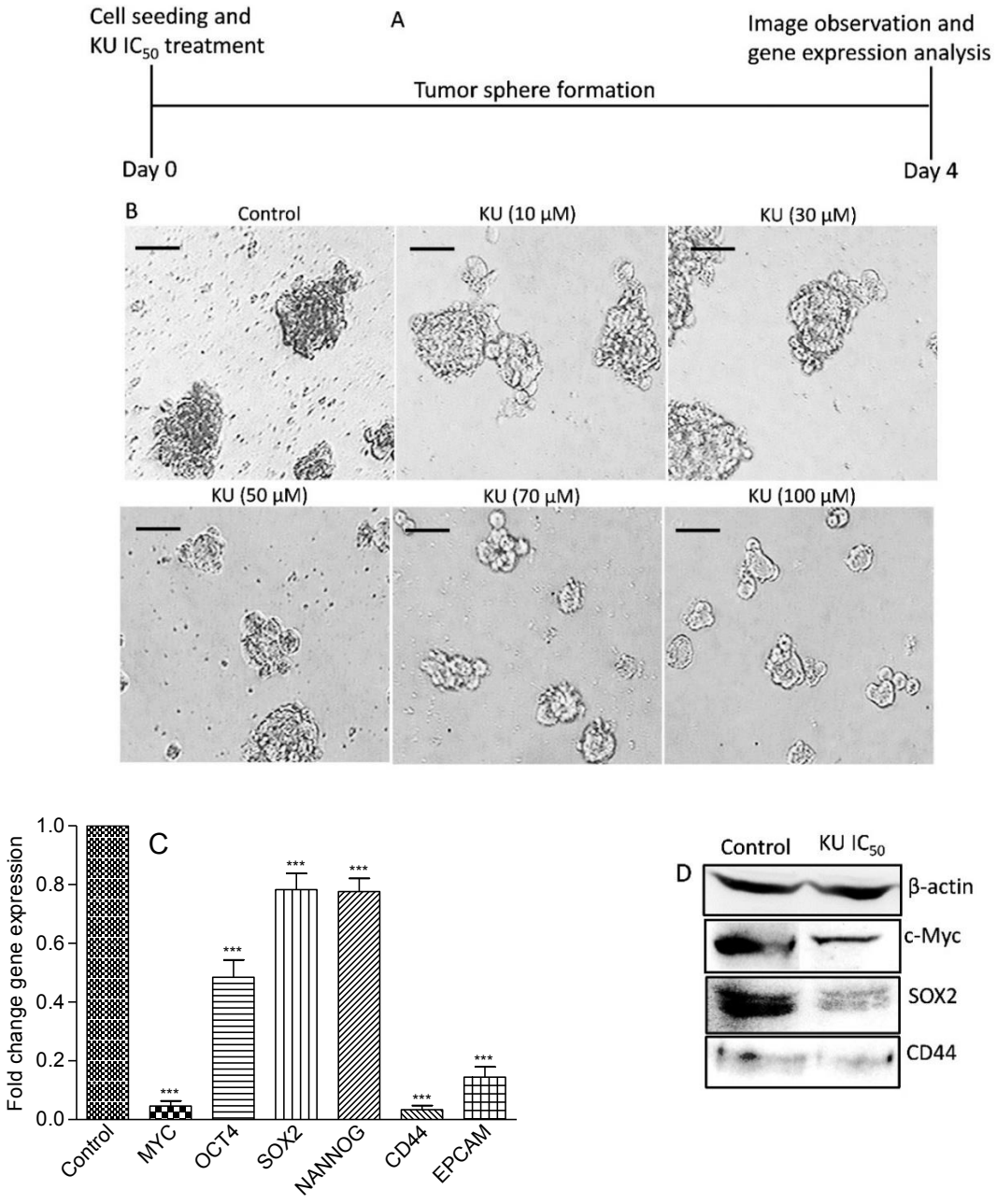


**Figure 4.41** Effect of Kurarinone on mammosphere formation, stemness and self-renewal inhibitory potential of Kurarinone in mammosphere at $IC_{50}$ concentration in 96h treatment. (A) Time schedule of the experiment. (B) Breast cancer cells (MCF-7) were cultured to form mammosphere for four days with initial treatment at different concentrations (10-100 µM) to form spheres in ultra-low attachment surface plates. Phase-contrast images of tumorspheres were taken at 10X resolution.

RT-PCR technique was applied to demonstrate the effect of KU on mRNA levels of self-renewal and stemness related gene expression in mammosphere cells at $IC_{50}$ concentration in 96h treatment. (C) Self-renewal and stemness related gene expression at mRNA (*MYC, OCT4, SOX2, NANOG, CD44*, and *EPCAM*) levels in KU treated mammosphere cells.

Western blot technique was applied to demonstrate the effect of KU on self-renewal and stemness related protein levels in mammosphere cells at $IC_{50}$ concentration in 96h treatment. For western blot analysis, the cell samples were collected after 96h KU treatment at $IC_{50}$ concentration. (D) Self-renewal

and stemness related protein (c-Myc, SOX2, and CD44) levels in KU treated mammosphere cells. β-actin was used as an internal control. Results are expressed as mean±SD. ***P<0.0005 vs. control.

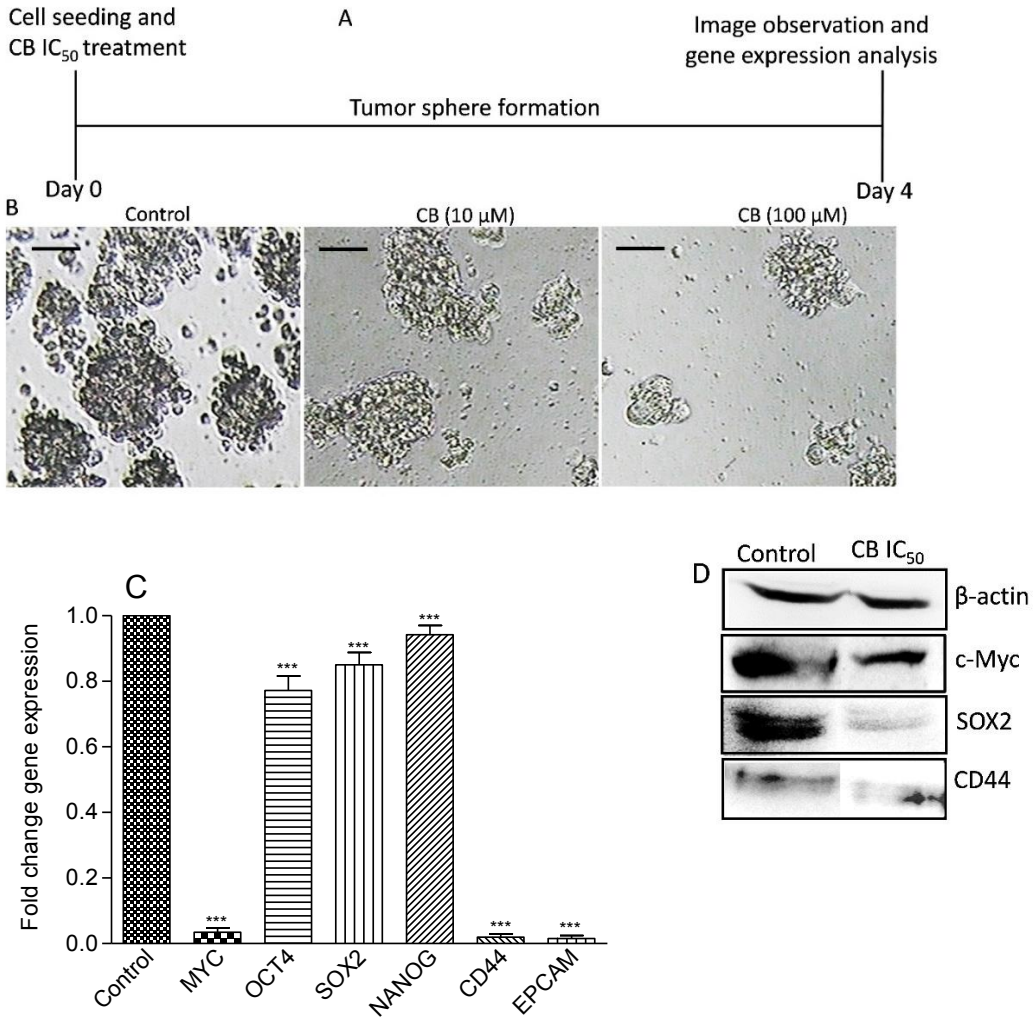


**Figure 4.42** Effect of 3-O-(E)-p-Coumaroylbetulinic acid (CB) on mammosphere formation, stemness and self-renewal inhibitory potential of CB in mammosphere at $IC_{50}$ concentration in 96h treatment. (A) Time schedule of the experiment. (B) Breast cancer cells (MCF-7) were cultured to form mammosphere for four days with initial treatment at two concentrations (10 μM and 100 μM) to form spheres in ultra-low attachment surface plates. Phase-contrast images of tumorspheres were taken at 10X resolution.
RT-PCR technique was applied to demonstrate the effect of CB on mRNA levels of self-renewal and stemness related gene expression in mammosphere cells at $IC_{50}$ concentration in 96h treatment. (C) Self-renewal and stemness related gene expression at mRNA (*MYC, OCT4, SOX2, NANOG, CD44*, and *EPCAM*) levels in CB treated mammosphere cells.
Western blot technique was applied to demonstrate the effect of CB on self-renewal and stemness related protein levels in mammosphere cells at $IC_{50}$ concentration in 96h treatment. For western blot analysis, the cell samples were collected after 96h CB treatment at $IC_{50}$ concentration. (D) Self-renewal and stemness related protein (c-Myc, SOX2, and CD44) levels in CB treated mammosphere cells. β-actin was used as an internal control. Results are expressed as mean±SD. ***P<0.0005 vs. control.

# Chapter 5
# Discussion

# 5. Discussion

Breast cancer is the most common type of cancer among women and the major cause of cancer-related deaths in women. The poor response rates and considerable toxicity of existing chemotherapy treatments have led to searches for other alternative therapies. The notch signaling pathway plays an important in cell proliferation and apoptosis in breast cancer progression. In the present study, an attempt was made to identify and validate the natural notch signaling pathway (ϒ-secretase) inhibitor using *in silico* and *in vitro* approach. The anti-cancer efficacy and notch signaling inhibitory potential of lead phytochemicals/natural products were *in vitro* studied in breast cancer cells and mammosphere.

*Bulbine frutescens* is a medicinal plant but very little is known about this plant to date. Some of the pharmacological activities such as anti-HIV and glutathione S-transferase inhibitory potential has been reported (Shikalepo et al. 2018)**.** The literature revealed the presence of pharmacologically active phytochemicals in *B. frutescens* plant (Tambama et al. 2014)**.** Kurarinone (KU) is a flavonoid found in *Sophora flavescens* (Fabaceae) plant and well known for its anticancer activity against gastric, cervical and non-small cell lung cancer cells by regulating JAK/STAT, NFκB and ERK pathways. 3-O-(E)-p-Coumaroylbetulinic acid (CB) is a terpenoid isolated from the leaves and twigs of *Strychnos vanprukii* Craib (Loganiaceae).

We studied the anticancer potential of *B. frutescens*, Kurarinone and CB and assessed notch signaling inhibitory potential in triple-negative (MDA-MB-231) and $ER^+/PR^+$ (T47D) breast cancer cells. We tried to deduce the possible anticancer mode of action in MDA-MB-231 and T47D breast cancer cells. These two cells are different in terms of aggressiveness, prognosis, and drug susceptibility toward chemotherapy. TNBC and luminal breast cancer cells show a difference in prognosis extent and chemotherapy response (Isakoff, 2010)**.** *In vitro* anticancer screening of the *B. frutescens* methanolic (BME) and hexane (BHE) extracts, Kurarinone and CB showed significant anticancer potential against the test cell lines in concentration and time-dependent manner at low $IC_{50}$ values **(Figure 4.12-4.14)**.

BME and BHE treatment showed dose and time-dependent cytotoxicity in breast cancer cells **(Figure 4.12)**. *B. frutescens* methanolic extract was more cytotoxic than hexane extract against both test cell lines at 24h treatment **(Figure 4.12)**. The methanolic extract showed 2.69 and 1.89 times less $IC_{50}$ than hexane extract against MDA-MB-231 and T47D cells at 24h treatment respectively **(Figure 4.12)**. The difference in anticancer potential of the methanolic and hexane extracts of *B. frutescens* might be attributed to the differential occurrence of phytochemicals present in the respective extract **(Figure 4.1, Table 4.1).** Kurarinone showed potential anticancer efficacy against MDA-MB-231 and T47D cell lines at 0.43-3.42 µM in 24, 48 and 72h treatment **(Figure 4.13 C-H).** KU showed about a similar degree of toxicity ($IC_{50}$ 1.64-1.93 µM) in MDA-MB-231 and T47D breast cancer cells in 48h treatment. KU showed better cytotoxicity ($IC_{50}$ ≈0.4332 µM) against T47D cell lines in 72h treatment. The study showed that MDA-MB-231 cells are less susceptible to kaempferol than T47D cells (Kim et al. 2008). The study reported that luteolin (2-[3,4-dihydroxyphenyl]-5,7-dihydroxy-4-chromenone), a naturally occurring flavonoid, possess anticancer activity against breast cancer cells (Cook, 2018). Similarly, our results showed that KU has better potential against T47D cells in comparison to MDA-MB-231 breast cancer cells. In *in vitro* anticancer screening, CB showed significant anticancer activity against MDA-MB-231 and T47D cell lines at 0.99-5.88 µM in 24, 48 and 72h treatment **(Figure 4.14 C-H).** CB showed better cytotoxicity ($IC_{50}$ ≈0.99 µM) against T47D cell lines in 72h treatment. A study showed that MDA-MB-231 cells are less susceptible to monoterpenes (limonene, perillyl alcohol, and perillic acid) than T47D cells (Bardon et al. (1998). Our results also indicated that CB has better anticancer activity against T47D cells in contrast to MDA-MB-231 breast cancer cells. The presence of anticancer potential in *B. frutescens* extracts, KU and CB motivated us to investigate its mechanism of action in breast cancer cells.

Downregulation of the notch signaling pathway is a novel strategy to target breast cancer aggressiveness and proliferation. Thus, we investigated the lead phytochemicals/natural products notch signaling inhibition potential in breast cancer and mammosphere. Dual-Luciferase Reporter Assay was used to assess the notch promoter inhibitory potential of test samples. The result indicates that *B. frutescens*

phytochemicals inhibited activation of notch promoter activity in extract-treated HEK293 transfected cells **(Figure 4.37 A-B)**. *B. frutescens* extract treatment (BME and BHE) downregulated notch targeted genes (*Hes1* and *Hey1*) at mRNA level in breast cancer cells **(Figure 4.37 C-F)** in a time-dependent manner. Further, *B. frutescens* methanolic extract lowered notch treated genes (*Hes1* and *Hey1*) at protein levels in a time-dependent manner **(Figure 4.37 G)**. Thus *B. frutescens* methanolic extract have the potential to downregulate the notch signaling pathway at the promoter level. Our *in silico* study revealed that lead phytochemicals from *B. frutescens* extract (Bulbineloneside D) interact with the Ɣ-secretase protein in a similar way as the known standard notch inhibitor (DAPT). Moreover, the interaction of Bulbineloneside D with the two additional residues (Ala80 and Leu81) provided stable binding (hydrophobic interaction) with the protein in comparison to DAPT **(Figure 4.2)**. Various studies also showed that flavonoids such as epigallocatechin, quercetin and ginsenoside decline the notch signaling in cancer cells (Lee et al. 2013; Chen et al. 2016; Wang et al. 2015). Dual-Luciferase Reporter Assay showed that KU has significant notch promoter inhibitory potential in HEK293 transfected cells **(Figure 4.38 C)**. Gene (*HES1* and *HEY1*) and protein (Hes1) expression analysis showed time-dependent notch signaling pathway inhibition in KU treated breast cancer cells. Studies reported that natural terpenoids such as oleanolic acid (Xu et al. 2018), oridonin (Dong et al. 2014), celastrol (Wang et al. 2010), lutein (Li et al. 2018), and ginsenoside Rb1 (Wang et al. 2015) declines the Notch signaling in cancer cells. CB inhibited notch promoter activation in treated HEK293 transfected cells at $IC_{50}$ concentration **(Figure 4.39 C)**. Gene and protein expression analysis showed the time-dependent downregulation of *HES1* and *HEY1* genes in CB treated T47D breast cancer cells. Thus CB has the potential to downregulate the Notch signaling pathway at the promoter level **(Figure 4.39).**

*In silico* study demonstrated that KU and CB interact with the Ɣ-secretase protein in a similar way as the known standard notch inhibitor (DAPT). Moreover, the interaction of KU with one additional residue Thr58 provided stable binding (hydrogen interaction) with the protein in comparison to DAPT. It may be inferred that Kurarinone and CB have the potential to inhibit NICD formation by targeting Ɣ-secretase enzyme **(Figure 4.4).**

Notch signaling has been shown to promote EMT of cancer cells. Studies reported that inhibiting ϒ-secretase enzyme induces the E-cadherin expression and suppresses the epithelial-mesenchymal transition. Similarly, our *in silico* and *in vitro* study also showed that *B. frutescens,* KU and CB inhibits notch signaling pathway **(Figure 4.2, 4.4, 4.5, 4.37-4.39)**. Moreover, western blot analysis of test sample treated MDA-MB-231 cells showed induced E-cadherin expression which indicates EMT suppression in MDA-MB-231 cells.

The cell cycle is a highly regulated process by which a cell grows and proliferates. It is divided into different phases G1, S, G2/M. Entry and exit of cells (known as checkpoints) through each phase is highly regulated by the up and down expression of various proteins/transcription factors. Cancer cells escape these checkpoints by deregulated expression of key molecules (such as p21, CDK4 and CyclinD1) and proliferate continually. The p21 (ubiquitous inhibitor of cyclin-dependent kinases), cyclin D1 and CDK4 (phosphorylate key cell cycle proteins) controls cell cycle at G1-S phase transition (Lange et al. 2009; Waga et al. 1994; Xiong et al. 1993)**.** Notch signaling cascade regulates cell cycle by modulating the expression of cyclin D1, CDK4 and p21 levels in cancer cells (Dai et al. 2015)**.** Chemotherapeutic drugs are known to inhibit cancer cell proliferation by arresting the cells in a definite phase and thereby restrict tumor growth. Phytochemicals such as EGCG, kaempferol, cyanidin-3-glucoside, glycyrrhetinic acid, quercetin and ginsenoside exerts growth-inhibitory effects through modulation of cell cycle-related proteins such as CDK4, cyclin D1 and p21 (Liang et al. 1999; Cho and Park, 2013; Chen et al. 2005; Zhu et al. 2015; Zhou et al. 2016; Li et al. 2018). Natural monoterpenes exert growth-inhibitory effects through modulation of cell cycle-related proteins such as CDK4, cyclin D1 and p21 (Bardon et al. 2002). Our results showed that *B. frutescens* extracts have the potential to arrest breast cancer cells in the G1 phase of the cell cycle (**Figure 4.15**). BME and BHE extract upregulated p21 expression and downregulated cyclin D1 and CDK4 at mRNA levels in breast cancer cells **(Figure 4.16)**. KU also arrests breast cancer cells in G1 and G2/M cell cycle phases in 24 and 48h respectively **(Figure 4.17)**. KU increased p21 and decreased cyclin D1 and CDK4 at mRNA level in MDA-MB-231 and T47D cells **(Figure 4.17 I-K).** KU also suppressed the cyclin D1 protein expression at protein

levels in MDA-MB-231 breast cancer cells. In 48h treatment, CB arrests breast cancer cells in the G1 cell cycle phase **(Figure 4.18)**. CB increased p21 and decreased cyclin D1 and CDK4 at mRNA level in both cells (MDA-MB-231 and T47D) **(Figure 4.18 G-I).** CB also suppressed the cyclin D1 expression at protein levels in MDA-MB-231 cells. Thus, the present study indicates test sample has the ability to induce cell cycle arrest by inhibiting the Notch signaling pathway in breast cancer cells.

Apoptosis is a hallmark of cancer and is associated with the normal developmental process. It is also known as programmed cell death by which a cell destroys itself without harming the nearby cells. Apoptosis is a highly regulated phenomenon executed by a fine balance of proapoptotic and anti-apoptotic proteins. In cancer cells, this balance disrupts and the cells escape from apoptosis. Chemotherapeutic drugs reverse this condition in cancer cells by up expressing pro-apoptotic protein (such as caspase 3) and down expressing anti-apoptotic proteins (such as survivin and Bcl2). Decreased expression of caspase 3 and increased levels of anti-apoptotic protein (survivin and Bcl-2) is found in breast cancer cells (Xue et al. 2012)**.** In the present study, apoptosis induction potential of test samples (BME, BHE, KU and CB) was studied at biochemical, mRNA and protein levels in breast cancer cells.

The test sample treatment increased the cleaved caspase 3 fragment levels, suppressed Bcl-2 and survivin expression at mRNA level. Additionally, annexin V FITC and PI dual staining also confirmed the apoptotic induction potential in the sample treated triple-negative breast cancer cells **(Figure 4.27 A-B, 4.31 A-B, 4.35 A-B).** Increased levels of procaspase 3 protein in treated (12h treatment) MDA-MB-231 cells substantiate the apoptotic induction potential in BME, BHE, KU and CB at test concentration **(Figure 4.26 B).** The present study corroborates with the other findings which show increased procaspase 3 protein levels in anticancer drug-treated breast cancer cells (Li et al. 2019)**.** Further, the apoptosis induction potential of test samples was confirmed by confocal microscopy. Test extract/phytochemicals treatment destroyed the nuclear membrane, initiated cell shrinkage and membrane blebbing in treated breast cancer cells **(Figure 4.28)**. Similarly, a previous study showed the formation of apoptotic bodies, nuclei condensation and fragmentation into segregated bodies in drug-treated cancer cells (Rahman et al. 2013)**.**

Apoptosis induction potential in natural occurring flavonoids and terpenoids such as 18-beta-glycyrrhetinic acid, cyanidin-3-glucoside, kaempferol, ginsenoside, quercetin 3-(6-O-acetyl-beta-glucoside), epigallocatechin-3-gallate, naringenin, and vitexin in treated cancer cells has been reported previously (Haghshenas et al. 2014; Chen et al. 2005; Kim et al. 2013; Nag et al. 2012; Rong et al. 2000; Wu et al. 2019; Ahamad et al. 2014; Zhang et al. 2018; Liu et al. 2012).

Notch targeted genes are known to regulate apoptosis by modulating the activity/expression of caspase 3, survivin and Bcl2 proteins in breast cancer cells (Sun et al. 2018)**.** Chen et al. (2016) reported that notch signaling upregulates survivin expression and thereby inhibits apoptosis in cancer cells (Chen et al. 2016). Studies showed that treatment with phytochemical/extract downregulates the notch signaling pathway and increases apoptotic: non-apoptotic protein ratio in breast cancer cells (Xia et al. 2017; Varghese et al. 2018; Xu et al. 2018; Liu et al. 2012). The present finding suggested that CB induced apoptosis by downregulating survivin and Bcl-2 levels and upregulating cleaved caspase 3 levels in both cells (MDA-MB-231 and T47D). Thus, it may be inferred that the test samples have notch signaling inhibition mediated apoptotic potential against breast cancer cells.

Reactive oxygen species are directly linked with the progression and aggressiveness of cancer. Cancer cells upregulate their antioxidant defense system to mitigate the adverse effect of elevated ROS levels up to a limit. Moreover, the energy requirement is also high in cancer cells which necessitate the presence of healthy mitochondria. Thus anticancer drugs that generate an excess of ROS and disrupt the structural integrity of mitochondria in cancer cells are of greater importance nowadays (Boland et al. 2013)**.** Excessive ROS production and alteration in mitochondrial membrane potential is associated with apoptosis initiation in breast cancer cells (Boland et al. 2013)**.** The present study showed that BME extract induced 4.5 and 6.5 times ROS production in T47D and MDA-MB-231 cells respectively in comparison to non-treated cells. On the contrary, both extracts showed greater mitochondrial membrane potential damage in T47D breast cells. Both, fluorescence spectroscopy and confocal microscopy techniques confirmed excessive ROS production and mitochondria membrane potential alteration in extract-treated breast cancer cells **(Figure 4.19, and**

**4.22)**. Several studies reported that natural phytochemicals such as glychionide-A, naringenin, myricetin and chrysin inhibit cancer cell proliferation via modulation of ROS and mitochondrial membrane potential (Yu et al. 2019; Park et al. 2018; Park et al. 2018; Park et al. 2018). The present study showed that KU treatment-induced ≈3 and ≈2 times more ROS production in MDA-MB-231 and T47D cells respectively in comparison to non-treated cells. KU showed similar mitochondrial membrane potential damage in both MDA-MB-231 and T47D cells. Fluorescence spectroscopy and confocal microscopy techniques confirmed increased ROS levels and altered membrane potential in KU treated MDA-MB-231 and T47D cells **(Figure 4.20, and 4.23).** Thus the study establishes that KU has the potential to kill cancer cells in ROS dependent manner. Moreover, KU targets cancer cells mitochondria to induce apoptosis. A study reported that natural terpenes inhibit cancer cell proliferation via modulation of ROS and MMP (Singh et al. 2012). The present study showed that CB treatment-induced very less ROS production in both cells (MDA-MB-231 and T47D) in contrast to non-treated cells. CB showed similar MMP damage in both cells (MDA-MB-231 and T47D). Fluorescence spectroscopy and confocal microscopy techniques established increased ROS levels and altered membrane potential in CB treated MDA-MB-231 and T47D cells **(Figure 4.21, and 2.24).** Thus the study established that CB has the potential to kill cancer cells in ROS dependent manner. Moreover, CB targets cancer cells mitochondria to induce apoptosis. Overall, the study indicates that the test samples exert their cytotoxic effect by enhancing the ROS production and disrupting MMP in breast cancer cells.

Mammosphere formation assays are broadly used to test stem cell activity in tissues, tumors and cell lines (Iglesias et al. 2013). Mammosphere is widely linked with the notch signaling pathway which facilitates uncontrolled cellular progression and tumor aggressiveness. Choi et al. (2018) reported that triterpene isolated from *Aronia melanocarpa* reduces the mammosphere formation potential and stemness. Another study demonstrated by Jadaun et al. (2019) established that Pinostrobin (flavanone) suppressed the sphere formation potential *in vitro*. A gamma-secretase inhibitor (MRK003) inhibits the Notch signaling pathway and reduces stem-like cells population

of breast cancer and prevents mammosphere formation (Grudzien et al. 2010). In the present study, KU and CB reduce the mammosphere (MCF-7) formation potential.

Stemness property in cancer cells reflects their potential to resist chemotherapy and maintain lineage differentiation in tumor thus promoting cancer formation and growth. Cancer stem cells interact with their environment to maintain a balance between quiescence, proliferation, and regeneration. Stem cells constitute a very small population in given tumor tissue and are less affected by therapy. These cells are one of the important causes of drug resistance, cancer aggressiveness, and metastasis in breast cancer. Self-renewal is the process by which stem cells divide to make more stem cells, perpetuating the stem cell pool throughout life. Self-renewal is a division with the maintenance of the undifferentiated state. This requires cell cycle control and often maintenance of multipotency or pluripotency, depending on the stem cell (Shenghui et al. 2009). Thus, targeting breast cancer stem cells by therapeutic molecules is a better strategy for the management of breast cancer (Liu and Wicha, 2010). Mammosphere assay is now a day used to study the effect of therapeutic molecules on breast cancer stemness and self-renewal properties (Lombardo et al. 2015). Flavonoids such as quercetin and cyclohexylmethyl are known to inhibit breast cancer cell stemness potential *in vitro* at ≈15.1 µM concentrations (Liao et al. 2013; Wang et al. 2018) by reducing various stemness related markers such as chemokine receptor type 4 (CXCR4), aldehyde dehydrogenase 1A1 (ALDH1A1), epithelial cell adhesion molecule (EpCAM) etc. Natural terpenoids are also known to possess anti-breast cancer stem-like properties. De la Mare et. al. (2013) reported a significant reduction in mammosphere stemness potential at ≈11-23 µM concentration in polyhalogenated monoterpenes isolated from *Plocamium cornutum* (Plocamiaceae). Recently, studies reported self-renewal property reduction potential in phytochemical (mahanine and 3-O-p-coumaroyltormentic acid) treated breast cancer stem-like cells (Choi et al. 2018; Das et al. 2019). In the present study, result showed that Kurarinone (a flavonoid) and CB (terpenoid) have significant stemness and self-renewal reduction potential in breast cancer stem cells (mammosphere) by reducing the associated markers at protein (c-Myc, SOX2 and CD44) and mRNA (c-Myc, SOX2 and CD44, OCT4, NANOG, EPCAM) levels at $IC_{50}$ concentration (3µM and 5 µM respectively).

Notch signaling has been implicated in the regulation of cell-fate decisions such as self-renewal of adult stem cells and differentiation of progenitor cells along a particular lineage. The signaling is involved in mammary stem cell stemness/self-renewal phenomenon. Recently, Cao et al. (2018) demonstrated that quercetin-3-methyl ether suppresses human breast cancer stem cell formation by inhibiting the Notch signaling pathway. Another study performed by Ray et al. (2015) showed that 6-shogaol inhibits breast cancer cells and stem cell-like spheroids by modulating the notch signaling pathway *in vitro.* In the present study, result showed that Kurarinone and 3-O-(E)-p-coumaroylbetulinic acid has significant notch signaling inhibition potential in breast cancer stem cells (mammosphere) by reducing the expression of notch targeted genes at promoter, mRNA (Hes1, Hey1) and protein (Hes1, Hey1 and E-cad) levels at $IC_{50}$ concentration (3µM and 5 µM respectively). Studies showed that in breast cancer stem cells self-renewal/stemness potential increases up to many folds and is positive correlates with the up-regulated notch signaling pathway in these cells (Xiao et al. 2017). Gamma-secretase inhibitors (GSIs) mediated notch signaling downregulation is known to suppress stemness and self-renewal ability in breast cancer stem cells (Grudzien et al. 2009). Thus it might be inferred that Kurarinone and 3-O-(E)-p-coumaroylbetulinic acid reduces self-renewal/stemness potential in breast cancer stem-like cells by targeting the Notch signaling pathway.

# Summary

# 6. Summary

Breast cancer is a devastating disease and responsible for a large number of deaths in women in India and worldwide. Breast cancer stem cells are a small population of cells in breast tumors having the potential to self-renew and are largely involved in drug resistance and disease recurrence. Chemotherapy side effects and higher cost for the disease treatment always needed to explore newer drugs having lesser toxicity and cost-effective. Natural compounds/products are now a day good hope for this persistent problem. The present study was designed to identify (literature-based or using a computer-based approach) the potential anticancer natural products/phytochemicals and to deduce there mode of action in cancer cells and cancer stem-like cells. Literature survey revealed that *Bulbine frutescens* (Asphodelaceae) may be taken as lead anticancer plant product for the present study as its cytotoxic potential in breast cancer cells and breast cancer stem-like cells is still not studied. Further, we identified one flavonoid (Kurarinone) and one terpenoid (3-O-(E)-p-Coumaroylbetulinic acid) by using a computer-based drug discovery approach as novel notch signaling inhibitors. Kurarinone is reported for its anticancer activity in different cancer but its potential against breast cancer is still to be elusive. We hereby first time reporting the pharmacological activity of CB. Effect of the lead product/phytochemical on breast cancer cell proliferation, cell cycle arrest, apoptosis induction at biochemical, mRNA, and protein levels was studied **(Figure 6.1)**. Further, we selected the notch signaling pathway to be studied under the influence of lead product/phytochemical treatment in breast cancer cells and breast cancer stem-like cells (mammosphere) **(Figure 6.2)**. Notch signaling was selected because 1) It regulates cell proliferation, cell cycle and apoptosis in breast cancer cells, 2) It is one of the important signaling responsible for self-renewal property, drug resistance emergence and cancer cell stemness property in breast cancer stem cells.

This is the first report on the therapeutic effect of *B. frutescens,* KU and CB on MDA-MB-231 and T47D breast cancer cells. *B. frutescens* polar (methanolic) and non-polar (hexane) extracts comprise of secondary metabolites having antiproliferative potential at microgram concentrations ($IC_{50}$ 4-12 µg/ml).

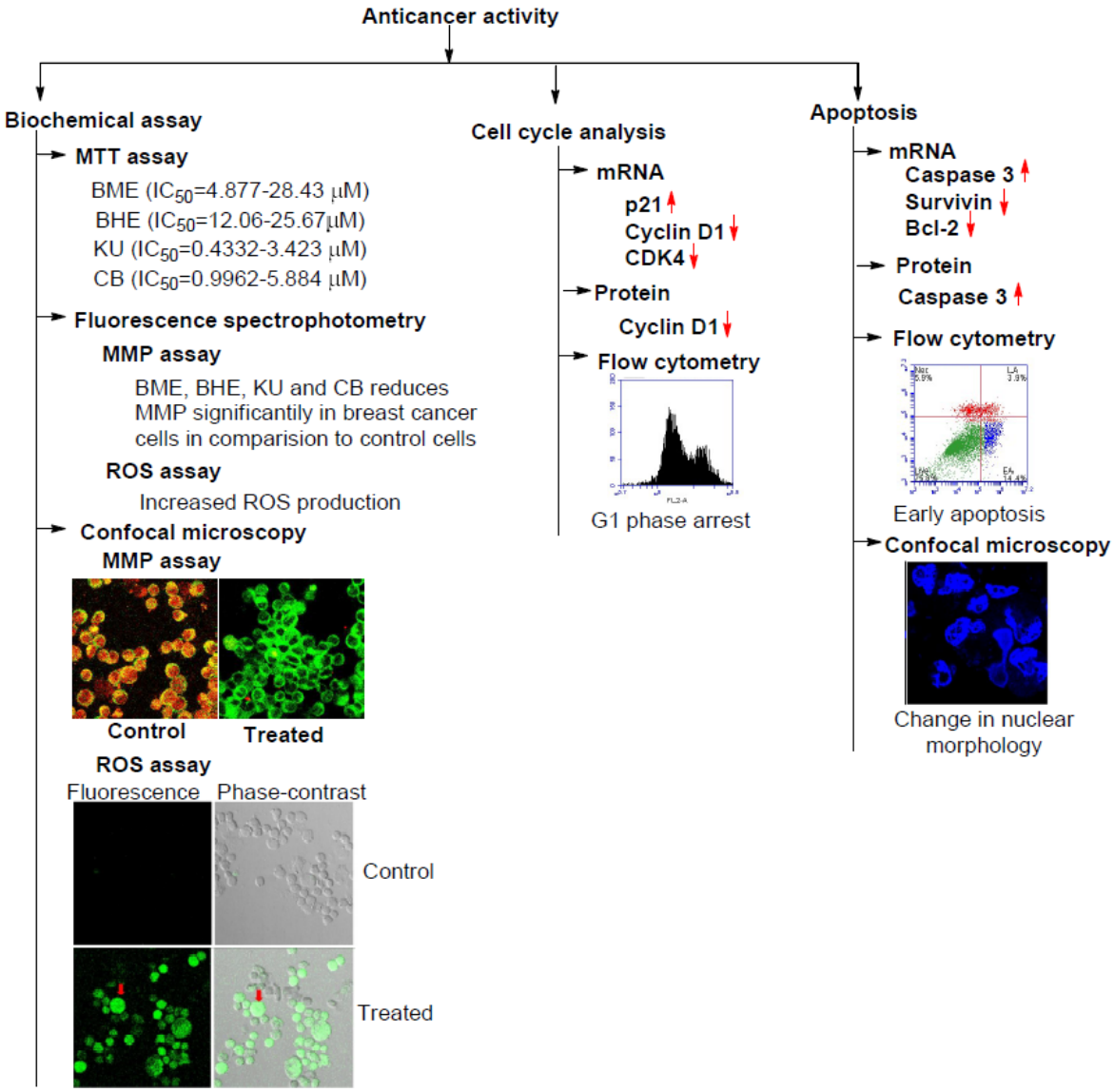


**Figure 6.1** Anticancer screening of *B. frutescens*, KU and CB. The different anticancer assay was performed to evaluate the anticancer potential of *B. frutescens*, KU and CB in MDA-MB-231 and T47D breast cancer cells at a different time interval. MTT assay was performed to calculate the $IC_{50}$ value at 24, 48 and 72h treatment. Fluorescence spectrophotometry technique was used to performed ROS and MMP assay in breast cancer cells at $IC_{50}$ concentration in 48h treatment. Confocal microscopy technique was performed to evaluate the ROS, MMP and nuclear morphology studies in breast cancer cells at the sub-$IC_{50}$ concentration in 16h treatment. Flow cytometry, RT-PCR and western blot technique were performed to evaluate the cell cycle analysis and apoptosis induction potential of *B. frutescens*, KU and CB at $IC_{50}$ concentration in 24 and 48h treatment.

Kurarinone and 3-O-(E)-p-coumaroylbetulinic acid showed potential anticancer activity at micromolar concentrations with low $IC_{50}$ values (0.43-3.42 µM and 0.99-5.88 µM respectively) in 24-72h treated breast cancer cells. Kurarinone showed comparatively better breast cancer cytotoxic potential with lower $IC_{50}$ values (0.4 to 3.4 µM) in the

anticancer screening assay. *B. frutescens*, KU and CB have the potential to induce reactive oxygen species (ROS) and disrupt mitochondria membrane potential (MMP) in triple-negative (MDA-MB-231) and luminal (T47D) breast cancer cells at their respective $IC_{50}$ concentrations. In comparison to pure phytochemicals (KU and CB), *B. frutescens* extracts (BME and BHE) showed better ROS production and MMP disruption potential in test cells. The present study revealed that the test plant product/phytochemicals have early apoptosis induction potential in breast cancer cells at $IC_{50}$ and sub $IC_{50}$ (half of the $IC_{50}$ value) concentrations. At the test concentrations, apoptosis induction potential in flow cytometric assay was in the order of KU>CB>BME>BHE. BME and BME extracts (*B. frutescens* phytochemicals), KU, and CB showed breast cancer cell cycle arrest in G1-phase at $IC_{50}$ concentrations in 24 and 48h treatment. Test samples showed cell cycle arrest in the order of CB>KU> BHE >BME.

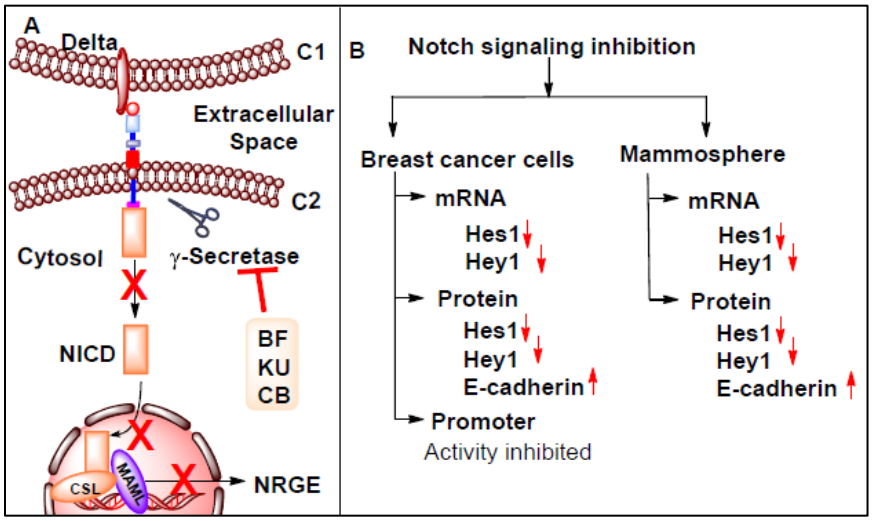


**Figure 6.2** Notch signaling inhibitory potential of KU and CB in breast cancer cells and mammosphere. (A) *B. frutescens*, KU, and CB inhibited the notch signaling cascade in breast cancer cells by targeting gamma-secretase protein and inhibition of NICD formation. (B) RT-PCR and western blot technique were used to assess the mRNA and protein expression of notch responsive gene in breast cancer cells and mammosphere at $IC_{50}$ concentration. Notch promoter activity was evaluated in breast cancer cells at $IC_{50}$ concentration in 24h treatment. C1=Cell membrane of cell 1; C2= Cell membrane of cell 2; BF= *Bulbine frutescens*, KU=Kurarinone; CB= 3-O-(E)-p-Coumaroylbetulinic acid; NRGE= Notch responsive gene expression; CSL=CBF1, Suppressor of Hairless, Lag-1; MAML=Mastermind-like protein 1; NICD=Notch intracellular domain

*In silico* study revealed Bulbineloneside D (phytochemical from *B. frutescens*), KU and CB act as novel ϒ-secretase inhibitor. *In silico* notch signaling pathway (ϒ-secretase)

inhibition potential of KU was further validated by using a computer-based molecular dynamics approach. *B. frutescens*, KU and CB downregulated notch signaling pathway at the promoter, mRNA (Hes1, Hey1) and protein (Hes1, Hey1 and E-cadherin) levels at respective $IC_{50}$ concentrations in breast cancer and breast cancer stem-like cells (mammosphere). Notch promoter inhibition potential of test samples was studied in HEK293 transfected cells and luciferase activity was found in the range of 0.2-0.9. Promoter inhibition potential was in the order of KU>BME>BHE>CB.

Kurarinone and 3-O-(E)-p-Coumaroylbetulinic acid showed noteworthy self-renewal, stemness, and mammosphere formation inhibitory potential by reducing the associated markers at protein (c-Myc, SOX2 and CD44) and mRNA (c-Myc, SOX2 and CD44, OCT4, NANOG, EPCAM) levels at $IC_{50}$ concentration (3 µM and 5 µM respectively).

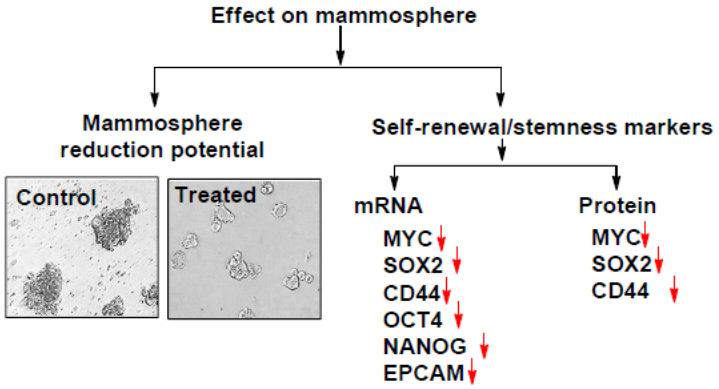


**Figure 6.3** Effect of KU and CB on mammosphere.
Mammosphere reduction potential of KU and CB was performed at $IC_{50}$ concentration in 96h treatment using phase-contrast microscopy. RT-PCR and western blot technique was used to assess the self-renewal and stemness inhibitory potential of KU and CB at $IC_{50}$ concentration in 96h treatment.

Further in-depth study is required to validate the *in vivo* anticancer potential of *B. frutescens* phytochemicals, KU and CB in order to render its effective therapeutic strategy against breast cancer. Limited availability of anticancer drugs and natural occurrence of *B. frutescens*, KU and CB make it a robust choice for future research endeavors.

# References/Bibliography

# 7. References/Bibliography


Abegaz, B. M., Bezabih, M., Msuta, T., Brun, R., Menche, D., Mühlbacher, J., & Bringmann, G. (2002). Gaboroquinones A and B and 4 '-O-demethylknipholone-4 '-O-β-d-glucopyranoside, phenylanthraquinones from the roots of *Bulbine frutescens*. *Journal of Natural Products, 65*(8), 1117-1121.

Ahamad, M. S., Siddiqui, S., Jafri, A., Ahmad, S., Afzal, M., & Arshad, M. (2014). Induction of apoptosis and antiproliferative activity of naringenin in human epidermoid carcinoma cell through ROS generation and cell cycle arrest. *PloS One*, *9*(10), 1-8.

Alotaibi, M. R., Hassan, Z. K., Al-Rejaie, S. S., Alshammari, M. A., Almutairi, M. M., Alhoshani, A. R., Alanazi, W. A., Hafez, M. M., & Al-Shabanah, O. A. (2018). Characterization of apoptosis in a breast cancer cell line after IL-10 silencing. *Asian Pacific Journal of Cancer Prevention, 19*, 777-783.

American Cancer Society. Breast Cancer Facts & Figures 2019. https://www.cancer.org/research/cancer-facts-statistics/breast-cancer-facts-figures.html

Ashfaq, U. A., Mumtaz, A., ul Qamar, T., & Fatima, T. (2013). MAPS Database: Medicinal plant activities, phytochemical and structural database. *Bioinformation, 9*(19), 993-995.

Bachmeier, B. E., Mirisola, V., Romeo, F., Generoso, L., Esposito, A., Dell'Eva, R., Blengio, F., Killian, P. H., Albini, A., & Pfeffer, U. (2010). Reference profile correlation reveals estrogen-like trancriptional activity of curcumin. *Cellular Physiology and Biochemistry*, *26*(3), 471-482.

Bachmeier, B. E., Mohrenz, I. V., Mirisola, V., Schleicher, E., Romeo, F., Höhneke, C., Jochum, M., Nerlich, A. G., & Pfeffer, U. (2008). Curcumin downregulates the inflammatory cytokines CXCL1 and-2 in breast cancer cells via NFκB. *Carcinogenesis*, *29*(4), 779-789.

Bardon, S., Foussard, V., Fournel, S., & Loubat, A. (2002). Monoterpenes inhibit proliferation of human colon cancer cells by modulating cell cycle-related protein expression. *Cancer Letters*, *181*(2), 187-194.

Bardon, S., Picard, K., & Martel, P. (1998). Monoterpenes inhibit cell growth, cell cycle progression, and cyclin D1 gene expression in human breast cancer cell lines. *Nutrition and Cancer*, *32*(1), 1-7.

Basu, D., Lettan, R., Damodaran, K., Strellec, S., Reyes-Mugica, M., & Rebbaa, A. (2014). Identification, mechanism of action, and antitumor activity of a small molecule inhibitor of hippo, TGF-β, and Wnt signaling pathways. *Molecular Cancer Therapeutics*, *13*(6), 1457-1467.

Beevers, C. S., Chen, L., Liu, L., Luo, Y., Webster, N. J., & Huang, S. (2009). Curcumin disrupts the Mammalian target of rapamycin-raptor complex. *Cancer Research*, *69*(3), 1000-1008.

Belandia, B., Powell, S. M., García-Pedrero, J. M., Walker, M. M., Bevan, C. L., & Parker, M. G. (2005). Hey1, a mediator of notch signaling, is an androgen receptor corepressor. *Molecular and Cellular Biology, 25*, 1425-1436.

Boland, M. L., Chourasia, A. H., & Macleod, K. F. (2013). Mitochondrial dysfunction in cancer. *Frontiers in Oncology*, *3*, 1-28.

Bringmann, G., Mutanyatta-Comar, J., Maksimenka, K., Wanjohi, J. M., Heydenreich, M., Brun, R., Müller, W. E., Peter, M. G., Midiwo, J. O., & Yenesew, A. (2008). Joziknipholones A and B: the first dimeric phenylanthraquinones, from the roots of *Bulbine frutescens*. *Chemistry–A European Journal, 14*(5), 1420-1429.

Bruno, A., Siena, L., Gerbino, S., Ferraro, M., Chanez, P., Giammanco, M., Gjomarkaj, M., & Pace, E. (2011). Apigenin affects leptin/leptin receptor pathway and induces cell apoptosis in lung adenocarcinoma cell line. *European Journal of Cancer*, *47*(13), 2042-2051.

Butler, M. S. (2004). The role of natural product chemistry in drug discovery. *Journal of Natural Products*, *67*(12), 2141-2153.

Cao, L., Yang, Y., Ye, Z., Lin, B., Zeng, J., Li, C., Liang, T., Zhou, K., & Li, J. (2018). Quercetin-3-methyl ether suppresses human breast cancer stem cell formation by inhibiting the Notch1 and PI3K/Akt signaling pathways. *International Journal of Molecular Medicine*, *42*(3), 1625-1636.

Charpentier, M. S., Whipple, R. A., Vitolo, M. I., Boggs, A. E., Slovic, J., Thompson, K. N., Bhandary, L., & Martin, S. S. (2014). Curcumin targets breast cancer stem–like cells with microtentacles that persist in mammospheres and promote reattachment. *Cancer Research, 74*(4), 1250-1260.

Chen, A., Xu, J., & Johnson, A. C. (2006). Curcumin inhibits human colon cancer cell growth by suppressing gene expression of epidermal growth factor receptor through reducing the activity of the transcription factor Egr-1. *Oncogene*, *25*(2), 278-287.

Chen, C., Shen, G., Hebbar, V., Hu, R., Owuor, E. D., & Kong, A. N. T. (2003). Epigallocatechin-3-gallate-induced stress signals in HT-29 human colon adenocarcinoma cells. *Carcinogenesis*, *24*(8), 1369-1378.

Chen, P. N., Chu, S. C., Chiou, H. L., Chiang, C. L., Yang, S. F., & Hsieh, Y. S. (2005). Cyanidin 3-glucoside and peonidin 3-glucoside inhibit tumor cell growth and induce apoptosis *in vitro* and suppress tumor growth *in vivo*. *Nutrition and Cancer, 53*(2), 232-243.

Chen, X., Dong, X. S., Gao, H. Y., Jiang, Y. F., Jin, Y. L., Chang, Y. Y., Chen, L. Y., & Wang, J. H. (2016). Suppression of HSP27 increases the anti-tumor effects of quercetin in human leukemia U937 cells. *Molecular Medicine Reports*, *13*(1), 689-696.

Chen, X., Duan, N., Zhang, C., & Zhang, W. (2016). Survivin and tumorigenesis: molecular mechanisms and therapeutic strategies. *Journal of Cancer*, *7*(3), 314-323.

Cho, H. J., & Park, J. H. Y. (2013). Kaempferol induces cell cycle arrest in HT-29 human colon cancer cells. *Journal of Cancer Prevention, 18*(3), 257-263.

Cho, Y., Lee, H. W., Kang, H. G., Kim, H. Y., Kim, S. J., & Chun, K. H. (2015). Cleaved CD44 intracellular domain supports activation of stemness factors and promotes tumorigenesis of breast cancer. *Oncotarget, 6*(11), 8709-8721.

Choi, H., Kim, S. L., Kim, J. H., Deng, H. Y., Yun, B. S., & Lee, D. S. (2018). Triterpene acid (3-Op-coumaroyltormentic acid) isolated from aronia extracts inhibits breast cancer stem cell formation through downregulation of c-Myc protein. *International Journal of Molecular Sciences*, *19*(9), 1-16.

Choi, H., Kim, S. L., Kim, J. H., Deng, H. Y., Yun, B. S., & Lee, D. S. (2018). Triterpene acid (3-Op-coumaroyltormentic acid) isolated from aronia extracts inhibits breast cancer stem cell formation through downregulation of c-Myc protein. *International Journal of Molecular Sciences, 19*(9), 1-16.

Chung, C. S., Jiang, Y., Cheng, D., & Birt, D. F. (2007). Impact of adenomatous polyposis coli (APC) tumor supressor gene in human colon cancer cell lines on cell cycle arrest by apigenin. *Molecular Carcinogenesis*, *46*(9), 773-782.

Cook, M. T. (2018). Mechanism of metastasis suppression by luteolin in breast cancer. *Breast Cancer: Targets and Therapy*, *10*, 89-100.

Cragg, G. M., & Newman, D. J. (2001). Natural product drug discovery in the next millennium. *Pharmaceutical Biology*, *39*(sup1), 8-17.

Cragg, G. M., Newman, D. J., & Snader, K. M. (1997). Natural products in drug discovery and development. *Journal of Natural Products*, *60*(1), 52-60.

Da Rocha, A. B., Lopes, R. M., & Schwartsmann, G. (2001). Natural products in anticancer therapy. *Current Opinion in Pharmacology*, *1*(4), 364-369.

Dai, M. Y., Fang, F., Zou, Y., Yi, X., Ding, Y. J., Chen, C., Tao, Z. Z., & Chen, S. M. (2015). Downregulation of Notch1 induces apoptosis and inhibits cell proliferation and metastasis in laryngeal squamous cell carcinoma. *Oncology Reports*, *34*(6), 3111-3119.

Darzynkiewicz, Z., & Juan, G. (1997). DNA content measurement for DNA ploidy and cell cycle analysis. *Current Protocols in Cytometry, 1*, 7-5.

Das, M., Kandimalla, R., Gogoi, B., Dutta, K. N., Choudhury, P., Devi, R., Dutta, P. P., Talukdar, N. C., & Samanta, S. K. (2019). Mahanine, A dietary phytochemical, represses mammary tumor burden in rat and inhibits subtype regardless breast cancer progression through suppressing self-renewal of breast cancer stem cells. *Pharmacological Research*, *146,* 1-13.

De la Mare, J. A., Sterrenberg, J. N., Sukhthankar, M. G., Chiwakata, M. T., Beukes, D. R., Blatch, G. L., & Edkins, A. L. (2013). Assessment of potential anti-cancer stem cell activity of marine algal compounds using an in vitro mammosphere assay. *Cancer cell international, 13*(1), 1-14.

Dickson, B. C., Mulligan, A. M., Zhang, H., Lockwood, G., O'Malley, F. P., Egan, S. E., & Reedijk, M. (2007). High-level JAG1 mRNA and protein predict poor outcome in breast cancer. *Modern Pathology*, *20*(6), 685-693.

Dong, Y., Zhang, T., Li, J., Deng, H., Song, Y., Zhai, D., Peng, Y., Lu, X., Liu, M., Zhao, Y., & Yi, Z. (2014). Oridonin inhibits tumor growth and metastasis through anti-angiogenesis by blocking the Notch signaling. *PLoS One*, *9*(12), 1-20.

Dontu, G., Jackson, K. W., McNicholas, E., Kawamura, M. J., Abdallah, W. M., & Wicha, M. S. (2004). Role of Notch signaling in cell-fate determination of human mammary stem/progenitor cells. *Breast Cancer Research*, *6*(6), R605-R615.

El-Alfy, T. S., Ezzat, S. M., Hegazy, A. K., Amer, A. M., & Kamel, G. M. (2011). Isolation of biologically active constituents from *Moringa peregrina* (Forssk.) Fiori.(family: Moringaceae) growing in Egypt. *Pharmacognosy Magazine*, *7*(26), 109-115.

Epstein, J., Docena, G., MacDonald, T. T., & Sanderson, I. R. (2010). Curcumin suppresses p38 mitogen-activated protein kinase activation, reduces IL-1β and matrix metalloproteinase-3 and enhances IL-10 in the mucosa of children and adults with inflammatory bowel disease. *British Journal of Nutrition*, *103*(06), 824-832.

Essa, M. M., Akbar, M., & Guillemin, G. (2016). The benefits of natural products for neurodegenerative diseases. *The Advances in Neurobiology, 12,* 293-306.

Farnie, G., Clarke, R. B., Spence, K., Pinnock, N., Brennan, K., Anderson, N. G., & Bundred, N. J. (2007). Novel cell culture technique for primary ductal carcinoma in situ: role of Notch and epidermal growth factor receptor signaling pathways. *Journal of the National Cancer Institute*, *99*(8), 616-627.

Ferreira, C. V., Justo, G. Z., Souza, A. C., Queiroz, K. C., Zambuzzi, W. F., Aoyama, H., & Peppelenbosch, M. P. (2006). Natural compounds as a source of protein tyrosine phosphatase inhibitors: application to the rational design of small-molecule derivatives. *Biochimie*, *88*(12), 1859-1873.

Fornelli, F., Leone, A., Verdesca, I., Minervini, F., & Zacheo, G. (2007). The influence of lycopene on the proliferation of human breast cell line (MCF-7). *Toxicology In Vitro*, *21*(2), 217-223.

Gabor, M., & Eperjessy, E. (1966). Antibacterial effect of fisetin and fisetinidin. *Nature*, *212*, 1273.

García-Zaragoza, E., Pérez-Tavarez, R., Ballester, A., Lafarga, V., Jiménez-Reinoso, A., Ramírez, Á., Murillas, R., & Gallego, M. I. (2012). Intraepithelial paracrine Hedgehog signaling induces the expansion of ciliated cells that express diverse progenitor cell markers in the basal epithelium of the mouse mammary gland. *Developmental Biology*, *372*(1), 28-44.

Globocan 2018: India Factsheet, Globocan 2018. http://cancerindia.org.in/globocan-2018-india-factsheet/

Gopalakrishnan, A., Xu, C. J., Nair, S. S., Chen, C., Hebbar, V., & Kong, A. N. T. (2006). Modulation of activator protein-1 (AP-1) and MAPK pathway by flavonoids in human prostate cancer PC3 cells. *Archives of Pharmacal Research*, *29*(8), 633-644.

Grudzien, P., Lo, S., Albain, K. S., Robinson, P., Rajan, P., Strack, P. R., Golde, T. E., Miele, L., & Foreman, K. E. (2010). Inhibition of Notch signaling reduces the stem-like population of breast cancer cells and prevents mammosphere formation. *Anticancer Research*, *30*(10), 3853-3867.

Grudzien, P., Strack, P., Golde, T., Miele, L., & Foreman, K. E. (2009). Inhibition of Notch signaling reduces the stem-like cell population in T47D breast cancer cells and prevents mammosphere formation. *Anticancer Research, 30*(10), 3853-3867.

Haghshenas, V., Fakhari, S., Mirzaie, S., Rahmani, M., Farhadifar, F., Pirzadeh, S., & Jalili, A. (2014). Glycyrrhetinic acid inhibits cell growth and induces apoptosis in ovarian cancer a2780 cells. *Advanced Pharmaceutical Bulletin, 4*, 437-441.

Hastak, K., Agarwal, M. K., Mukhtar, H., & Agarwal, M. L. (2005). Ablation of either p21 or Bax prevents p53-dependent apoptosis induced by green tea polyphenol epigallocatechin-3-gallate. *The Federation of American Societies for Experimental Biology Journal*, *19*(7), 789-791.

Hoensch, H. P., & Oertel, R. (2011). Emerging role of bioflavonoids in gastroenterology: Especially their effects on intestinal neoplasia. *World Journal of Gastrointestinal Oncology*, *3*(5), 71-74.

Huebner, R. J., & Ewald, A. J. (2014). Cellular foundations of mammary tubulogenesis. *Seminars in Cell & Developmental Biology, 31*, 124-131.

Hunter, T. (2000). Signaling--2000 and beyond. *Cell*, *100*(1), 113-127.

Hunter, T. (2007). The age of crosstalk: phosphorylation, ubiquitination, and beyond. *Molecular Cell*, *28*(5), 730-738.

Iglesias, J. M., Beloqui, I., Garcia-Garcia, F., Leis, O., Vazquez-Martin, A., Eguiara, A., Cufi, S., Pavon, A., Menendez, J. A., Dopazo, J., & Martin, A. G. (2013). Mammosphere formation in breast carcinoma cell lines depends upon expression of E-cadherin. *PloS One*, *8*(10), 1-12.

Isakoff, S. J. (2010). Triple negative breast cancer: role of specific chemotherapy agents. *Cancer Journal*, *16*(1), 53-61.

Jadaun, A., Sharma, S., Verma, R., & Dixit, A. (2019). Pinostrobin inhibits proliferation and induces apoptosis in cancer stem-like cells through a reactive oxygen species-dependent mechanism. *RSC Advances*, *9*(21), 12097-12109.

Jafari, N., Zargar, S. J., Yassa, N., & Delnavazi, M. R. (2016). Induction of apoptosis and cell cycle arrest by *Dorema glabrum* root extracts in a gastric adenocarcinoma (AGS) cell line. *Asian Pacific Journal of Cancer Prevention, 17*, 5189-5193.

Janbandhu, V. C., Singh, A. K., Mukherji, A., & Kumar, V. (2010). p65 negatively regulates transcription of the cyclin E gene. *Journal of Biological Chemistry, 285*, 17453-17464.

Johnson, S. M., Gulhati, P., Arrieta, I., Wang, X., Uchida, T., Gao, T., & Evers, B. M. (2009). Curcumin inhibits proliferation of colorectal carcinoma by modulating Akt/mTOR signaling. *Anticancer Research*, *29*(8), 3185-3190.

Kamdje, A. H. N., Etet, P. F. S., Vecchio, L., Muller, J. M., Krampera, M., & Lukong, K. E. (2014). Signaling pathways in breast cancer: therapeutic targeting of the microenvironment. *Cellular Signalling*, *26*(12), 2843-2856.

Khan, M. A., Chen, H. C., Wan, X. X., Tania, M., Xu, A. H., Chen, F. Z., & Zhang, D. Z. (2013). Regulatory effects of resveratrol on antioxidant enzymes: a mechanism of growth inhibition and apoptosis induction in cancer cells. *Molecules and Cells*, *35*(3), 219-225.

Khan, N., Afaq, F., Khusro, F. H., Adhami, V. M., Suh, Y., & Mukhtar, H. (2012). Dual inhibition of PI3K/AKT and mTOR signaling in human non-small cell lung cancer cells by a dietary flavonoid fisetin. *International Journal of Cancer*, *130*(7), 1695-1705.

Kim, B. W., Lee, E. R., Min, H. M., Jeong, H. S., Ahn, J. Y., Kim, J. H., Choi, H. Y., Choi, H., Kim, E. Y., Park, S. P., & Cho, S. G. (2008). Sustained ERK activation is involved in the kaempferol-induced apoptosis of breast cancer cells and is more evident under 3-D culture condition. *Cancer Biology & Therapy, 7*(7), 1080-1089.

Kim, E. K., Kim, H. A., Koh, J. S., Kim, M. S., Kim, K. I., Lee, J. I., Moon, N. M., Ko, E., & Noh, W. C. (2011). Phosphorylated S6K1 is a possible marker for endocrine therapy resistance in hormone receptor-positive breast cancer. *Breast Cancer Research and Treatment*, *126*(1), 93-99.

King, C. R., Kraus, M. H., & Aaronson, S. A. (1985). Amplification of a novel v-erbB-related gene in a human mammary carcinoma. *Science*, *229*, 974-977.

Koehn, F. E., & Carter, G. T. (2005). The evolving role of natural products in drug discovery. *Nature Reviews Drug discovery*, *4*(3), 206-220.

Koury, J., Zhong, L., & Hao, J. (2017). Targeting signaling pathways in cancer stem cells for cancer treatment. *Stem Cells International, 2017*, 1-10.

Kumazoe, M., & Tachibana, H. (2016). Anti-cancer effect of EGCG and its mechanisms. *Functional Foods in Health and Disease*, *6*(2), 70-78.

Kuroda, M., Mimaki, Y., Sakagami, H., & Sashida, Y. (2003). Bulbinelonesides A− E, phenylanthraquinone glycosides from the roots of Bulbinella floribunda. *Journal of Natural Products*, *66*(6), 894-897.

Lange, C., Huttner, W. B., & Calegari, F. (2009). Cdk4/cyclinD1 overexpression in neural stem cells shortens G1, delays neurogenesis, and promotes the generation and expansion of basal progenitors. *Cell Stem Cell*, *5*(3), 320-331.

Larsen, C. A., & Dashwood, R. H. (2010). (-)-Epigallocatechin-3-gallate inhibits Met signaling, proliferation, and invasiveness in human colon cancer cells. *Archives of Biochemistry and Biophysics*, *501*(1), 52-57.

Lee, J., Hahm, E. R., & Singh, S. V. (2010). Withaferin A inhibits activation of signal transducer and activator of transcription 3 in human breast cancer cells. *Carcinogenesis*, *31*(11), 1991-1998.

Lee, S. H., Nam, H. J., Kang, H. J., Kwon, H. W., & Lim, Y. C. (2013). Epigallocatechin-3-gallate attenuates head and neck cancer stem cell traits through suppression of Notch pathway. *European Journal of Cancer, 49*(15), 3210-3218.

Leonardi, T., Vanamala, J., Taddeo, S. S., Davidson, L. A., Murphy, M. E., Patil, B. S., Wang, N., Carroll, R. J., Chapkin, R. S., Lupton, J. R., & Turner, N. D. (2010). Apigenin and naringenin suppress colon carcinogenesis through the aberrant crypt stage in azoxymethane-treated rats. *Experimental Biology and Medicine*, *235*(6), 710-717.

Leong, H., Mathur, P. S., & Greene, G. L. (2009). Green tea catechins inhibit angiogenesis through suppression of STAT3 activation. *Breast Cancer Research and Treatment*, *117*(3), 505-515.

Li, J., Wang, Q., Wang, Z., Cui, N., Yang, B., Niu, W., & Kuang, H. (2019). Tetrandrine inhibits colon carcinoma HT-29 cells growth via the Bcl-2/Caspase 3/PARP pathway and G1/S phase. *Bioscience Reports*, *39*(5), 1-12.

Li, K. F., Kang, C. M., Yin, X. F., Li, H. X., Chen, Z. Y., Li, Y., Zhang, Q., & Qiu, Y. R. (2018). Ginsenoside Rh2 inhibits human A172 glioma cell proliferation and induces cell cycle arrest status via modulating Akt signaling pathway. *Molecular Medicine Reports, 17*(2), 3062-3068.

Li, Y., Zhang, Y., Liu, X., Wang, M., Wang, P., Yang, J., & Zhang, S. (2018). Lutein inhibits proliferation, invasion and migration of hypoxic breast cancer cells via downregulation of HES1. *International Journal of Oncology*, *52*(6), 2119-2129.

Liang, Y. C., Lin-Shiau, S. Y., Chen, C. F., & Lin, J. K. (1999). Inhibition of cyclin-dependent kinases 2 and 4 activities as well as induction of cdk inhibitors p21 and p27 during growth arrest of human breast carcinoma cells by (-)-epigallocatechin-3-gallate. *Journal of Cellular Biochemistry, 75*(1), 1-12.

Liao, W. Y., Liaw, C. C., Huang, Y. C., Han, H. Y., Hsu, H. W., Hwang, S. M., Kuo, S. C., & Shen, C. N. (2013). Cyclohexylmethyl flavonoids suppress propagation of breast cancer stem cells via downregulation of NANOG. *Evidence-Based Complementary and Alternative Medicine*, *2013*, 1-14.

Liao, Y. C., Shih, Y. W., Chao, C. H., Lee, X. Y., & Chiang, T. A. (2009). Involvement of the ERK signaling pathway in fisetin reduces invasion and migration in the human lung cancer cell line A549. *Journal of Agricultural and Food Chemistry*, *57*(19), 8933-8941.

Lim, D. Y., & Park, J. H. Y. (2009). Induction of p53 contributes to apoptosis of HCT-116 human colon cancer cells induced by the dietary compound fisetin. *American Journal of Physiology-Gastrointestinal and Liver Physiology*, *296*(5), G1060-G1068.

Lin, J. N., Lin, V. C. H., Rau, K. M., Shieh, P. C., Kuo, D. H., Shieh, J. C., Chen, W. J., Tsai, S. C., & Way, T. D. (2009). Resveratrol modulates tumor cell proliferation and protein translation via SIRT1-dependent AMPK activation. *Journal of Agricultural and Food Chemistry*, *58*(3), 1584-1592.

Ling, G. Q., Chen, D. B., Wang, B. Q., & Zhang, L. S. (2012). Expression of the pluripotency markers Oct3/4, Nanog and Sox2 in human breast cancer cell lines. *Oncology Letters*, *4*(6), 1264-1268.

Liu, S., & Wicha, M. S. (2010). Targeting breast cancer stem cells. *Journal of Clinical Oncology, 28*(25), 4006-4012.

Liu, Y., Whelan, R. J., Pattnaik, B. R., Ludwig, K., Subudhi, E., Rowland, H., Claussen, N., Zucker, N., Uppal, S., Kushner, D. M., Felder, M., Patankar, M. S., & Kapur, A.

(2012). Terpenoids from *Zingiber officinale* (Ginger) induce apoptosis in endometrial cancer cells through the activation of p53. *PloS One*, *7*(12), 1-10.

Lombardo, Y., de Giorgio, A., Coombes, C. R., Stebbing, J., & Castellano, L. (2015). Mammosphere formation assay from human breast cancer tissues and cell lines. J*ournal of Visualized Experiments, 97*, 1-5.

Lombardo, Y., de Giorgio, A., Coombes, C. R., Stebbing, J., & Castellano, L. (2015). Mammosphere formation assay from human breast cancer tissues and cell lines. *Journal of Visualized Experiments*, *97*, 1-5.

Macias, H., & Hinck, L. (2012). Mammary gland development. *Wiley Interdisciplinary Reviews: Developmental Biology*, *1*(4), 533-557.

Markovits, J., Linassier, C., Fossé, P., Couprie, J., Pierre, J., Jacquemin-Sablon, A., Saucier, J. M., Le Pecq, J. B., & Larsen, A. K. (1989). Inhibitory effects of the tyrosine kinase inhibitor genistein on mammalian DNA topoisomerase II. *Cancer Research*, *49*(18), 5111-5117.

Mechoulam, H., & Pierce, E. A. (2005). Expression and activation of STAT3 in ischemia-induced retinopathy. *Investigative Ophthalmology & Visual Science*, *46*(12), 4409-4416.

Mohamed, M. S., Abdelhamid, A. O., Almutairi, F. M., Ali, A. G., & Bishr, M. K. (2018). Induction of apoptosis by pyrazolo [3, 4-d] pyridazine derivative in lung cancer cells via disruption of Bcl-2/Bax expression balance. *Bioorganic & Medicinal Chemistry, 26*, 623-629.

Montales, M. T. E., Rahal, O. M., Kang, J., Rogers, T. J., Prior, R. L., Wu, X., & Simmen, R. C. (2012). Repression of mammosphere formation of human breast cancer cells by soy isoflavone genistein and blueberry polyphenolic acids suggests diet-mediated targeting of cancer stem-like/progenitor cells. *Carcinogenesis, 33*(3), 652-660.

Mosmann, T. (1983). Rapid colorimetric assay for cellular growth and survival: application to proliferation and cytotoxicity assays. *Journal of Immunological Methods*, *65*(1-2), 55-63.

Nag, S. A., Qin, J., Wang, W., Wang, M. H., Wang, H., & Zhang, R. (2012). Ginsenosides as anticancer agents: *in vitro* and *in vivo* activities, structure-activity relationships, and molecular mechanisms of action. *Frontiers in Pharmacology*, *3*, 1-18.

Newman, D. J., & Cragg, G. M. (2007). Natural products as sources of new drugs over the last 25 years. *Journal of Natural Products, 70*(3), 461-477.

Newman, D. J., Cragg, G. M., & Snader, K. M. (2000). The influence of natural products upon drug discovery. *Natural Product Reports*, *17*(3), 215-234.

Newman, D. J., Cragg, G. M., & Snader, K. M. (2003). Natural products as sources of new drugs over the period 1981-2002. *Journal of Natural Products*, *66*(7), 1022-1037.

Osipo, C., Patel, P., Rizzo, P., Clementz, A. G., Hao, L., Golde, T. E., & Miele, L. (2008). ErbB-2 inhibition activates Notch-1 and sensitizes breast cancer cells to a γ-secretase inhibitor. *Oncogene*, *27*(37), 5019-5032.

Osta, W. A., Chen, Y., Mikhitarian, K., Mitas, M., Salem, M., Hannun, Y. A., Cole, D. J., & Gillanders, W. E. (2004). EpCAM is overexpressed in breast cancer and is a potential target for breast cancer gene therapy. *Cancer Research, 64*(16), 5818-5824.

Park, H., Park, S., Bazer, F. W., Lim, W., & Song, G. (2018). Myricetin treatment induces apoptosis in canine osteosarcoma cells by inducing DNA fragmentation, disrupting redox homeostasis, and mediating loss of mitochondrial membrane potential. *Journal of Cellular Physiology*, *233*(9), 7457-7466.

Park, S., Lim, W., Bazer, F. W., & Song, G. (2018). Naringenin suppresses growth of human placental choriocarcinoma via reactive oxygen species-mediated P38 and JNK MAPK pathways. *Phytomedicine*, *50*, 238-246.

Park, W., Park, S., Lim, W., & Song, G. (2018). Chrysin disrupts intracellular homeostasis through mitochondria-mediated cell death in human choriocarcinoma cells. *Biochemical and Biophysical Research Communications*, *503*(4), 3155-3161.

Poltronieri, J., Becceneri, A. B., Fuzer, A. M., Filho, J. C., Martin, A. C., Vieira, P. C., Pouliot, N., & Cominetti, M. R. (2014). [6]-gingerol as a cancer chemopreventive agent: a review of its activity on different steps of the metastatic process. *Mini Reviews in Medicinal Chemistry*, *14*(4), 313-321.

Qurishi, Y., Hamid, A., Majeed, R., Hussain, A., Qazi, A. K., Ahmed, M., Zargar, M. A., Singh, S. K., & Saxena, A. K. (2011). Interaction of natural products with cell survival and signaling pathways in the biochemical elucidation of drug targets in cancer. *Future Oncology*, *7*(8), 1007-1021.

Radtke, F., & Raj, K. (2003). The role of Notch in tumorigenesis: oncogene or tumour suppressor?. *Nature Reviews Cancer*, *3*(10), 756-767.

Rahman, S. A., Nur, S., Abdul Wahab, N., Malek, A., & Nurestri, S. (2013). *In vitro* morphological assessment of apoptosis induced by antiproliferative constituents from the rhizomes of Curcuma zedoaria. *Evidence-Based Complementary and Alternative Medicine*, *2013,* 1-14.

Ravindran, J., Prasad, S., & Aggarwal, B. B. (2009). Curcumin and cancer cells: how many ways can curry kill tumor cells selectively?. *The American Association of Pharmaceutical Scientists Journal*, *11*(3), 495-510.

Ray, A., Vasudevan, S., & Sengupta, S. (2015). 6-Shogaol inhibits breast cancer cells and stem cell-like spheroids by modulation of Notch signaling pathway and induction of autophagic cell death. *PloS One, 10*(9), 1-22.

Raynal, N. J. M., Momparler, L., Charbonneau, M., & Momparler, R. L. (2007). Antileukemic activity of genistein, a major isoflavone present in soy products. *Journal of Natural Products*, *71*(1), 3-7.

Reedijk, M., Odorcic, S., Chang, L., Zhang, H., Miller, N., McCready, D. R., Lockwood, G., & Egan, S. E. (2005). High-level coexpression of JAG1 and NOTCH1 is observed in human breast cancer and is associated with poor overall survival. *Cancer Research*, *65*(18), 8530-8537.

Reedijk, M., Pinnaduwage, D., Dickson, B. C., Mulligan, A. M., Zhang, H., Bull, S. B., O'Malley, F. P., Egan, S. E., & Andrulis, I. L. (2008). JAG1 expression is associated with a basal phenotype and recurrence in lymph node-negative breast cancer. *Breast Cancer Research and Treatment*, *111*(3), 439-448.

Rong, Y. U. A. N., Yang, E. B., Zhang, K., & Mack, P. (2000). Quercetin-induced apoptosis in the monoblastoid cell line U937 *in vitro* and the regulation of heat shock proteins expression. *Anticancer Research, 20*(6B), 4339-4345.

Roy, A. M., Baliga, M. S., & Katiyar, S. K. (2005). Epigallocatechin-3-gallate induces apoptosis in estrogen receptor–negative human breast carcinoma cells via modulation in protein expression of p53 and Bax and caspase-3 activation. *Molecular Cancer Therapeutics*, *4*(1), 81-90.

Samady, L., Dennis, J. J., Budhram-Mahadeo, V., & Latchman, D. S. (2004). Activation of CDK4 gene expression in human breast cancer cells by the Brn-3b POU family transcription factor. *Cancer Biology & Therapy, 3*, 317-323.

Sansone, P., Storci, G., Giovannini, C., Pandolfi, S., Pianetti, S., Taffurelli, M., Santini, D., Ceccarelli, C., Chieco P., & Bonafe, M. (2007). p66Shc/Notch-3 interplay controls self-renewal and hypoxia survival in human stem/progenitor cells of the mammary gland expanded *in vitro* as mammospheres. *Stem Cells*, *25*(3), 807-815.

Scoumanne, A., Cho, S. J., Zhang, J., & Chen, X. (2010). The cyclin-dependent kinase inhibitor p21 is regulated by RNA-binding protein PCBP4 via mRNA stability. *Nucleic Acids Research, 39*, 213-224.

Senft, C., Polacin, M., Priester, M., Seifert, V., Kögel, D., & Weissenberger, J. (2010). The nontoxic natural compound curcumin exerts anti-proliferative, anti-migratory, and anti-invasive properties against malignant gliomas. *BMC Cancer*, *10*(1), 1-8.

Seo, E. J., Wiench, B., Hamm, R., Paulsen, M., Zu, Y., Fu, Y., & Efferth, T. (2015). Cytotoxicity of natural products and derivatives toward MCF-7 cell monolayers and cancer stem-like mammospheres. *Phytomedicine, 22*(4), 438-443.

Sever, R., & Brugge, J. S. (2015). Signal transduction in cancer. *Cold Spring Harbor Perspectives in Medicine, 5*(4), 1-21.

Shenghui, H. E., Nakada, D., & Morrison, S. J. (2009). Mechanisms of stem cell self-renewal. *Annual Review of Cell and Developmental, 25*, 377-406.

Shikalepo, R., Mukakalisa, C., Kandawa-Schulz, M., Chingwaru, W., & Kapewangolo, P. (2018). *In vitro* anti-HIV and antioxidant potential of *Bulbine frutescens* (Asphodelaceae). *Journal of Herbal Medicine*, *12*, 73-78.

Siegel, R., Naishadham, D., & Jemal, A. (2013). Cancer statistics, 2013. *CA: A Cancer Journal for Clinicians*, *63*(1), 11-30.

Sikander, M., Hafeez, B. B., Malik, S., Alsayari, A., Halaweish, F. T., Yallapu, M. M., Chauhan, S. C., & Jaggi, M. (2016). Cucurbitacin D exhibits potent anti-cancer activity in cervical cancer. *Scientific Reports*, *6,* 1-13.

Singh, B. K., Tripathi, M., Chaudhari, B. P., Pandey, P. K., & Kakkar, P. (2012). Natural terpenes prevent mitochondrial dysfunction, oxidative stress and release of apoptotic proteins during nimesulide-hepatotoxicity in rats. *PloS One*, *7*(4), 1-11.

Sridhar, S. S., Hedley, D., & Siu, L. L. (2005). Raf kinase as a target for anticancer therapeutics. *Molecular Cancer Therapeutics*, *4*(4), 677-685.

Sun, Z., Zhou, C., Liu, F., Zhang, W., Chen, J., Pan, Y., Ma, L., Liu, Q., Du, Y., Yang, J., & Wang, Q. (2018). Inhibition of breast cancer cell survival by Xanthohumol via modulation of the Notch signaling pathway *in vivo* and *in vitro*. *Oncology Letters*, *15*(1), 908-916.

Suzuki, R., Takemura, K., Tsutsumi, M., Nakamura, S., Hamajima, N., & Seto, M. (2001). Detection of cyclin D1 overexpression by real-time reverse-transcriptase-mediated quantitative polymerase chain reaction for the diagnosis of mantle cell lymphoma. *The American Journal of Pathology, 159*, 425-429.

Tambama, P., Abegaz, B., & Mukanganyama, S. (2014). Antiproliferative activity of the isofuranonaphthoquinone isolated from *Bulbine frutescens* against jurkat T cells. *BioMed Research International*, *2014*, 1-14.

Tseng, Y. Y., Moriarity, B. S., Gong, W., Akiyama, R., Tiwari, A., Kawakami, H., Ronning, P., Reuland, B., Guenther, K., Beadnell, T. C., & Essig, J. (2014). PVT1 dependence in cancer with MYC copy-number increase. *Nature, 512*(7512), 1-18.

Turktekin, M., Konac, E., Onen, H. I., Alp, E., Yilmaz, A., & Menevse, S. (2011). Evaluation of the effects of the flavonoid apigenin on apoptotic pathway gene expression on the colon cancer cell line (HT29). *Journal of Medicinal Food*, *14*(10), 1107-1117.

Varghese, E., Samuel, S. M., Abotaleb, M., Cheema, S., Mamtani, R., & Büsselberg, D. (2018). The “yin and yang” of natural compounds in anticancer therapy of triple-negative breast cancers. *Cancers, 10*(10), 1-49.

Venkatesh, V., Nataraj, R., Thangaraj, G. S., Karthikeyan, M., Gnanasekaran, A., Kaginelli, S. B., Kuppanna, G., & Basalingappa, K. M. (2018). Targeting Notch signalling pathway of cancer stem cells. *Stem Cell Investigation, 5*, 1-12.

Wadood, A., Ahmed, N., Shah, L., Ahmad, A., Hassan, H., & Shams, S. (2013). In-silico drug design: An approach which revolutionarised the drug discovery process. *OA Drug Design & Delivery*, *1*(1), 1-4.

Waga, S., Hannon, G. J., Beach, D., & Stillman, B. (1994). The p21 inhibitor of cyclin-dependent kinases controls DNA replication by interaction with PCNA. *Nature*, *369*(6481), 574-578.

Wang, A. H., & Zhang, L. S. (2007). Effect of lycopene on the proliferation of MCF-7 and MDA-MB-231 cells. *Journal of Sichuan University, 38*(6), 958-60.

Wang, H., OoKhor, T., Shu, L., Su, Z. Y., Fuentes, F., Lee, J. H., & Tony Kong, A. N. (2012). Plants against cancer: a review on natural phytochemicals in preventing and treating cancers and their druggability. *Anti-Cancer Agents in Medicinal Chemistry*, *12*(10), 1281-1305.

Wang, R., Yang, L., Li, S., Ye, D., Yang, L., Liu, Q., Zhao, Z., Cai, Q., Tan, J., & Li, X. (2018). Quercetin inhibits breast cancer stem cells via downregulation of aldehyde dehydrogenase 1A1 (ALDH1A1), chemokine receptor type 4 (CXCR4), mucin 1 (MUC1), and epithelial cell adhesion molecule (EpCAM). *Medical Science Monitor*, *24*, 412-420.

Wang, W., Zeng, L., Wang, Z. M., Zhang, S., Rong, X. F., & Li, R. H. (2015). Ginsenoside Rb1 inhibits matrix metalloproteinase 13 through down-regulating Notch signaling pathway in osteoarthritis. *Experimental Biology and Medicine*, *240*(12), 1614-1621.

Wang, X., Wu, Q., Yang, X., Zhang, L., Wu, Y., & Lu, C. (2010). Effects of celastrol on grouwth inhibition of U937 leukemia cells through the regulation of the Notchl/NF-KB signaling pathway in vitrol. *Chinese Journal of Cancer*, *29*(4), 385.

Wang, Z., Li, B., Zhou, L., Yu, S., Su, Z., Song, J., Sun, Q., Sha, O., Wang, X., Jiang, W., Willert, K., Wei, L., Carson, D. A., & Lu, D. (2016). Prodigiosin inhibits Wnt/β-catenin signaling and exerts anticancer activity in breast cancer cells. *Proceedings of the National Academy of Sciences*, *113*(46), 13150-13155.

Weng, M. T., Tsao, P. N., Lin, H. L., Tung, C. C., Change, M. C., Chang, Y. T., Wong, J. M., & Wei, S. C. (2015). Hes1 increases the invasion ability of colorectal cancer cells via the STAT3-MMP14 pathway. *PLoS One, 10*, 1-13.

White, R. J., & Reynolds, I. J. (1996). Mitochondrial depolarization in glutamate-stimulated neurons: an early signal specific to excitotoxin exposure. *Journal of Neuroscience*, *16*(18), 5688-5697.

Wlodkowic, D., Skommer, J., & Darzynkiewicz, Z. (2009). Flow cytometry-based apoptosis detection. *Methods in Molecular Biology, 559*, 1-14.

Wu, D., & Yotnda, P. (2011). Production and detection of reactive oxygen species (ROS) in cancers. *Journal of Visualized Experiments*, *57*, 1-4.

Wu, D., Liu, Z., Li, J., Zhang, Q., Zhong, P., Teng, T., Chen, M., Xie, Z., Ji, A., & Li, Y. (2019). Epigallocatechin-3-gallate inhibits the growth and increases the apoptosis of human thyroid carcinoma cells through suppression of EGFR/RAS/RAF/MEK/ERK signaling pathway. *Cancer Cell International, 19*(1), 1-17.

Xia, S., Zhang, X., Li, C., & Guan, H. (2017). Oridonin inhibits breast cancer growth and metastasis through blocking the Notch signaling. *Saudi Pharmaceutical Journal*, *25*(4), 638-643.

Xiao, W., Gao, Z., Duan, Y., Yuan, W., & Ke, Y. (2017). Notch signaling plays a crucial role in cancer stem-like cells maintaining stemness and mediating chemotaxis in renal cell carcinoma. *Journal of Experimental & Clinical Cancer Research*, *36*(1), 1-13.

Xiong, Y., Hannon, G. J., Zhang, H., Casso, D., Kobayashi, R., & Beach, D. (1993). p21 is a universal inhibitor of cyclin kinases. *Nature*, *366*(6456), 701-704.

Xu, Y., Shu, B., Tian, Y., Wang, G., Wang, Y., Wang, J., & Dong, Y. (2018). Oleanolic acid induces osteosarcoma cell apoptosis by inhibition of Notch signaling. *Molecular Carcinogenesis*, *57*(7), 896-902.

Xue, M., Ge, Y., Zhang, J., Wang, Q., Hou, L., Liu, Y., Sun, L., & Li, Q. (2012). Anticancer properties and mechanisms of fucoidan on mouse breast cancer *in vitro* and *in vivo*. *PLoS One*, *7*(8), 1-9.

Ye, Y., Wang, H., Chu, J. H., Chou, G. X., & Yu, Z. L. (2011). Activation of p38 MAPK pathway contributes to the melanogenic property of apigenin in B16 cells. *Experimental Dermatology*, *20*(9), 755-757.

Yu, L., Chen, M., Zhang, R., & Xu, T. (2019). Antitumor effects of glychionide-A flavonoid in human pancreatic carcinoma cells are mediated by activation of apoptotic and autophagic pathways, cell cycle arrest, and disruption of mitochondrial membrane potential. *Medical Science Monitor: International Medical Journal of Experimental and Clinical Research*, *25*, 962-969.

Yu, S., Shen, G., Khor, T. O., Kim, J. H., & Kong, A. N. T. (2008). Curcumin inhibits Akt/mammalian target of rapamycin signaling through protein phosphatase-dependent mechanism. *Molecular Cancer Therapeutics*, *7*(9), 2609-2620.

Zeng, H. L., Han, X. A., Gu, C., Zhu, H. Y., Huang, X. S., Gu, J. Q., Zhong, Q., Liu, G. J., Ming, W. J., & Cai, X. N. (2010). Reactive oxygen species and mitochondrial membrane potential changes in leukemia cells during 6-gingerol induced apoptosis. *Journal of Chinese Medicinal Materials*, *33*(4), 584-587.

Zeng, Q., Li, S., Chepeha, D. B., Giordano, T. J., Li, J., Zhang, H., Polverini, P. J., Nor, J., Kitajewski, J., & Wang, C. Y. (2005). Crosstalk between tumor and endothelial cells promotes tumor angiogenesis by MAPK activation of Notch signaling. *Cancer Cell*, *8*(1), 13-23.

Zhang, G., Li, D., Chen, H., Zhang, J., & Jin, X. (2018). Vitexin induces G2/M-phase arrest and apoptosis via Akt/mTOR signaling pathway in human glioblastoma cells. *Molecular Medicine Reports, 17*(3), 4599-4604.

Zhang, L., & Wang, H. (2015). Multiple mechanisms of anti-cancer effects exerted by astaxanthin. *Marine Drugs*, *13*(7), 4310-4330.

Zhang, Y., Vareed, S. K., & Nair, M. G. (2005). Human tumor cell growth inhibition by nontoxic anthocyanidins, the pigments in fruits and vegetables. *Life Sciences*, *76*(13), 1465-1472.

Zhou, J., Li, L. U., Fang, L. I., Xie, H., Yao, W., Zhou, X., Xiong, Z., Wang, Li., & Luo, F. (2016). Quercetin reduces cyclin D1 activity and induces G1 phase arrest in HepG2 cells. *Oncology Letters, 12*(1), 516-522.

Zhu, J., Chen, M., Chen, N., Ma, A., Zhu, C., Zhao, R., Jiang, M., Zhou, J., Ye, L., Fu, H., & Zhang, X. (2015). Glycyrrhetinic acid induces G1-phase cell cycle arrest in human non-small cell lung cancer cells through endoplasmic reticulum stress pathway. *International Journal of Oncology*, *46*(3), 981-988.